5-2022

Evaluation of Hydrograph Separation Techniques with Uncertain End-Member Composition

Eileen Page Lukens
Utah State University

EVALUATION OF HYDROGRAPH SEPARATION TECHNIQUES WITH UNCERTAIN END-MEMBER COMPOSITION

by

Eileen Page Lukens

A thesis submitted in partial fulfillment
of the requirements for the degree

of

MASTER OF SCIENCE

in

Civil and Environmental Engineering

Approved:

_____	_____
Bethany T. Neilson, Ph.D. Co-Major Professor	Janice Brahney, Ph.D. Co-Major Professor
_____	_____
Caleb Buahin, Ph.D. Committee Member	D. Richard Cutler, Ph.D. Interim Vice Provost of Graduate Studies

UTAH STATE UNIVERSITY
Logan, Utah

2022

ABSTRACT

Evaluation of Hydrograph Separation Techniques with Uncertain End-member Composition

by

Eileen Lukens, Master of Science

Utah State University, 2022

Major Professor: Dr. Bethany T. Neilson
Department: Civil and Environmental Engineering

Hydrograph separation is one of many approaches used to analyze shifts in source water contributions to stream flow resulting from climate change in remote watersheds. Understanding these shifts is vital, as shifts in source water contributions to a stream can shape water management decisions. Because remote watersheds are often inaccessible and have poorly characterized contributing water sources, or end-members, it is critical to understand the implications of using different hydrograph separation techniques in these data-limited environments. To explore the uncertainty associated with different techniques, results from mass balance and end-member mixing analyses were compared using three years of aqueous geochemical data from the East River watershed located in the Elk Mountains of Central Colorado. Solute concentrations of the end-members were characterized by both a limited set of direct chemical measurements of different sources and detailed seasonal instream chemistry to examine the influences of uncertain end-member compositions in a data-limited environment. Annual volumetric end-member

contributions to stream flow had relatively good agreement across separation techniques. Large variations in time were observed in the hydrograph separations depending on the end-member type, and estimated flows varied between the selected solutes. Results highlight the benefits of using multiple hydrograph separation techniques by providing a ‘weight-of-evidence’ approach to environments with limited end-member concentration data.

(123 pages)

PUBLIC ABSTRACT

Evaluation of Hydrograph Separation Techniques with Uncertain End-member Composition

Eileen Lukens

Changes to precipitation and temperature occurring as a result of climate change can influence water sources (such as groundwater or snowmelt) that contribute to stream flow in a watershed. This is significant, as shifts in the amount of water coming from different water sources can shape watershed management decisions. One technique often used to investigate changes in water sources is hydrograph separation, a mathematical tool that allows for the quantification of the amount of water that came from different water sources. However, it can be difficult to perform hydrograph separations in remote watersheds as there may be insufficient infrastructure, i.e. roads or research stations, to facilitate the detailed data collection needed for the application of hydrograph separation techniques. Thus, it is critical to understand how limited data may influence hydrograph separation and our understanding of how watersheds work and if they are changing. To explore uncertainty in the results, two different hydrograph separation methods were compared using geochemical data from the East River watershed located in the Elk Mountains of Central Colorado. Water sources were characterized using a limited set of concentration data collected at a few measurable water sources, and also by concentration data derived from stream chemistry at the outlet of the watershed. Results show that both hydrograph separation techniques gave similar estimate of annual source water contributions to stream flow. Results also indicate that using multiple hydrograph

separation techniques and multiple ways of representing water sources may be useful in remote catchments that have limited data.

ACKNOWLEDGMENTS

First, I want to thank my co-advisors, Dr. Bethany Neilson and Dr. Janice Brahney, for their constant support, guidance, and encouragement. Not only did they help me through my degree, but they also helped me personally through rough times in a global pandemic. I would also like to thank Dr. Caleb Buahin for serving on my committee, for providing feedback, and for teaching me many new skills that I can carry into my future.

I would like to thank everyone in the Neilson Lab and Brahney Bunch including Abbygael Johnson, Abby Englund, Chelsey Cowburn, Patrick Strong, Macy Gustavus, Jiahao Wen, Audree Provard, Sydney Southers, Molly Blakowski, Zhen Xu, Juanma Gonzalez-Olalla, Rachel Watts, Gordon Gianniny, and Mark Devey for their support, friendship, and advice. You are all a joy to be around and made graduate school a blast. Thank you to my lab mates, Hyrum Tennant and Bryce Mihalevich, who not only gave advice many times, but who also provided encouragement, fun conversations, and empathy. A special thank you to my fellow lab mate, Dane Brophy, who shared classes with me, spent late nights working on homework with me, and became a close and dear friend. I would like to thank everyone who guided me in my journey including Susan Durham for statistics advice and help. Furthermore, I want to extend my gratitude to everyone on staff at the Utah Water Research Laboratory who helped me along the way.

Thank you to all the contributors and collaborators who made this study possible, especially Dr. Kenneth Williams. All data used in this paper were collected, analyzed, and made available by the Lawrence Berkeley National Laboratory. This work was funded by the Utah Water Research Laboratory and the U.S. Department of Energy

(DOE) award DE-FOA-0001724. This material is partially based upon work supported through the Lawrence Berkeley National Laboratory's Watershed Function Science Focus Area. The DOE, Office of Science, Office of Biological and Environmental Research funded the work under contract DE-AC02-05CH11231 (Lawrence Berkeley National Laboratory; operated by the University of California). This work was additionally supported by the U.S. National Science Foundation under grant numbers 2043363, 2044051, and 2043150.

Lastly, I would like to express my gratitude to all of my family and friends for their constant support and encouragement. I would especially like to thank my mom, who made sure I took breaks and had adventures along the way. Finally, I want to give a special shout out to my life-long friend, Nora Honeycutt, for their constant support, love, and advice. Without them, I would not be the person I am today.

Eileen Lukens

CONTENTS

LIST OF TABLES

Page

LIST OF FIGURES

Page

INTRODUCTION

The hydrology of high-elevation mountain environments has changed dramatically over the past decade (Hock et al., 2019). April 1st snow water equivalent, an important hydrologic indicator, has been in decline across the western United States in part due to rising global temperatures (Mote et al., 2005; Mote et al., 2018; Huning & AghaKouchak, 2018) and an increase in the fraction of precipitation falling as rain (Hamlet et al., 2005; Knowles et al., 2006). This is significant as a decrease in the fraction of precipitation falling as snow has been identified as one cause of decreased streamflow (Berghuijs et al., 2014; Foster et al., 2016), along with shifts in evaporative losses (Foster et al., 2016). Additionally, the timing of snow derived runoff has been observed to occur earlier than long term averages across western North America (Brahney et al., 2017a; Clow, 2010; Stewart et al., 2005), which has been exacerbated by dust deposition on snow (Painter et al., 2007; Skiles et al., 2012). Earlier snowmelt may cause high elevation reservoirs to exceed storage capacities, forcing early releases (Barnett et al., 2005 & references therein; Kopytkovskiy et al., 2015). This loss of storage as snow and storage within reservoirs means less water during periods of summer drought when water demand is high. This is consequential as agriculture is particularly vulnerable to shifts in snowmelt quantity in the western United States (Qin et al., 2020), where 53% of annual runoff is snow derived (Li et al., 2017). This is even higher in mountainous regions where 70% of annual runoff is snow derived (Li et al., 2017). Changes to the timing, duration, and quantity of snowmelt may also impact sensitive endemic instream biota (Brahney et al., 2020; Brown et al., 2007) and may affect the biodiversity of cold water adapted organisms (Hotaling et al., 2017 & references therein).

Given that shifts in source water contributions to instream flow are influential in the genetic diversity and management of mountain stream systems, techniques to track these changes in remote environments are critical.

Hydrograph separation techniques are often used to separate the chemically distinct source waters (end-members) contributing to instream flow. Traditionally, hydrograph separations are performed using mass balances with one or two chemical or isotopic solutes (see Klaus & McDonnell, 2013; Wels et al., 1991). Another more robust form of hydrograph separation additionally utilizes principal component analysis (PCA) and end-member mixing analysis (EMMA). This second method offers an advantage by employing a larger suite of chemical and isotopic information than a traditional mass balance to separate the end-members (see Bearup et al., 2014; Carroll et al., 2018; Liu et al., 2017). This partitioning of flow into the end-members through hydrograph separation techniques is useful for analyzing changes in the hydrology of mountain catchments. For example, hydrograph separation has been used to track temporal changes in glacial contributions to streamflow (Brahney et al., 2017b), analyze base flow patterns in the Upper Colorado River Basin (Miller et al., 2014), and examine how forest bark beetle infestations affect the local water balance (Bearup et al., 2014). Studies such as these demonstrate the power and versatility of hydrograph separation techniques. Using multiple separation techniques offers both a method of comparison and also a potential 'weight-of-evidence' approach to working in catchments where a single separation technique on its own may not fully characterize the contributing end-members.

Components that contribute to instream flow can generally be categorized into "old" (pre-event) and "new" (event) waters, as summarized by Genereux & Hooper

(1998). Old water is usually described as all water that exists in the watershed before hydrologic perturbation, such as a rainstorm or snowmelt event that generally reaches the stream through subsurface pathways. New water may reach the stream by infiltrating and taking short residence time subsurface pathways or may enter the stream through quick surface pathways (Freeze, 1974). Residence time in the watershed is an important factor as it will affect the chemical signal a packet of water accumulates as it moves towards the stream. Sueker et al., (2000) summarizes this well, describing water that undergoes significant chemical changes as 'reacted' water and water that goes unaltered through the watershed as 'unreacted' water. Thus, instream chemistry represents the complex mix of source waters existing as new and old water and having undergone (or not undergone) a chemical alteration. To parse the contribution of these unique water types to streams, hydrograph separations can be used in tandem with geochemically relevant solute information from the stream and the contributing end-members. For accurate separations, solute concentrations of the contributing end-members should be representative of the end-member throughout the basin. However, detailed spatial and temporal information about end-member solute concentrations are very difficult to establish. As highlighted by Bales et al. (2006), spatially detailed hydrologic observation networks in mountainous environments are often unavailable.

As such, data limitations often affect the number of possible end-members that are identified and how end-member concentrations are characterized. Studies often choose to approach characterizing end-member concentrations one of two ways. Some studies (Jenkins et al., 1994; Liu et al., 2017; Williams et al., 2009) characterize end-member concentrations through detailed temporal and spatial sampling directly from the

source waters. The second way is through a type of ‘hydrologic rationalization’ in which end-member concentrations are characterized solely by instream data during certain flows or at certain locations (Pinder & Jones, 1969, Miller et al.. 2014, and Foks et al., 2019). For example, the stream's chemical composition during periods of low flow is often assigned to a groundwater end-member. Still, other studies use a combination of detailed sampling and hydrologic rationalization to characterize end-member concentrations. For example, James & Roulet (2009) utilized diverse spatial sampling to characterize a concentration range for a new-water end-member. Detailed instream sampling during baseflow along with samples from a single spring in the study area were used to characterize concentrations of an old-water end-member. Many studies have highlighted the issues with using poorly characterized end-member concentrations to perform hydrograph separations (Cayuela et al., 2019; Kiewiet et al., 2020; Penna & Meerveld, 2019), but characterizing end-member concentrations via detailed spatial and temporal sampling is not always possible, particularly in remote catchments. This highlights the need to develop methods to overcome inevitable end-member data limitations.

Understanding the strengths and weaknesses of different hydrograph separation techniques in predicting end-member contributions when end-member information is limited is a critical first step. Therefore, this study focuses on how multiple hydrograph separation techniques compare in their prediction of annual volumetric end-member contributions to rivers with limited end-member data but detailed instream data across multiple years. Of specific interest are 1) the consequences of using different end-member characterizations informed by detailed instream data to address challenges related to spatially limited end-member data with two unique hydrograph separation

techniques and 2) if any general conclusions about catchment hydrology can be made as a result of using multiple separation techniques and a ‘weight-of-evidence’ approach.

METHODS

2.1 Study Area

The experimental watershed is located in the Gunnison National Forest near Gothic, Colorado (Figure 1) and serves as the primary drainage of the main stem East River (ER). The study site includes the Rocky Mountain Biological Laboratory (RMBL) and hosts a diversity of hydrogeochemical studies performed as part of the Lawrence Berkeley National Laboratory (LBNL) Watershed Function Science Focus Area (WFSFA) funded by the U.S. Department of Energy. The headwaters of the ER are in a high-alpine region of the Elk Mountains of Central Colorado at an elevation of 3190 m, and with the confluence of the Taylor River near Almont, Colorado form the Gunnison River at an elevation of 2245 m. The sub-watershed of interest has a drainage area of approximately 85 km^2. The ER represents one of the many small watersheds that drain to the Upper Colorado River Basin (UCRB), a critical water resource for much of the western United States. The ER WFSFA receives 1200 mm yr^{-1} of precipitation (PRISM, 2021) that primarily falls as snow (Hubbard et al. 2018). The ER watershed is generally considered pristine and runoff is composed primarily of snowmelt, rain, and groundwater (Carroll et al., 2018) with little to no human impact in the study area apart from atmospheric deposition events. The arid regions of the southwestern United States have been identified as a likely source of dust deposition in the Colorado Rockies (Lawrence et al. 2010). Dust in the Colorado Rocky Mountains is commonly calcareous (Brahney et al., 2013; Clow et al., 2016) and has been observed to shift snowmelt by one to three weeks earlier than pre-dust loading conditions (Clow et al. 2016; Painter et al., 2010; Skiles et al. 2015). The geology of the area is dominated by Mancos shale of Cretaceous

age with intrusions of Paleogene igneous laccoliths and ore-rich stocks (Hubbard et al. 2018). For additional information about the study site, see Hubbard et al. (2018).

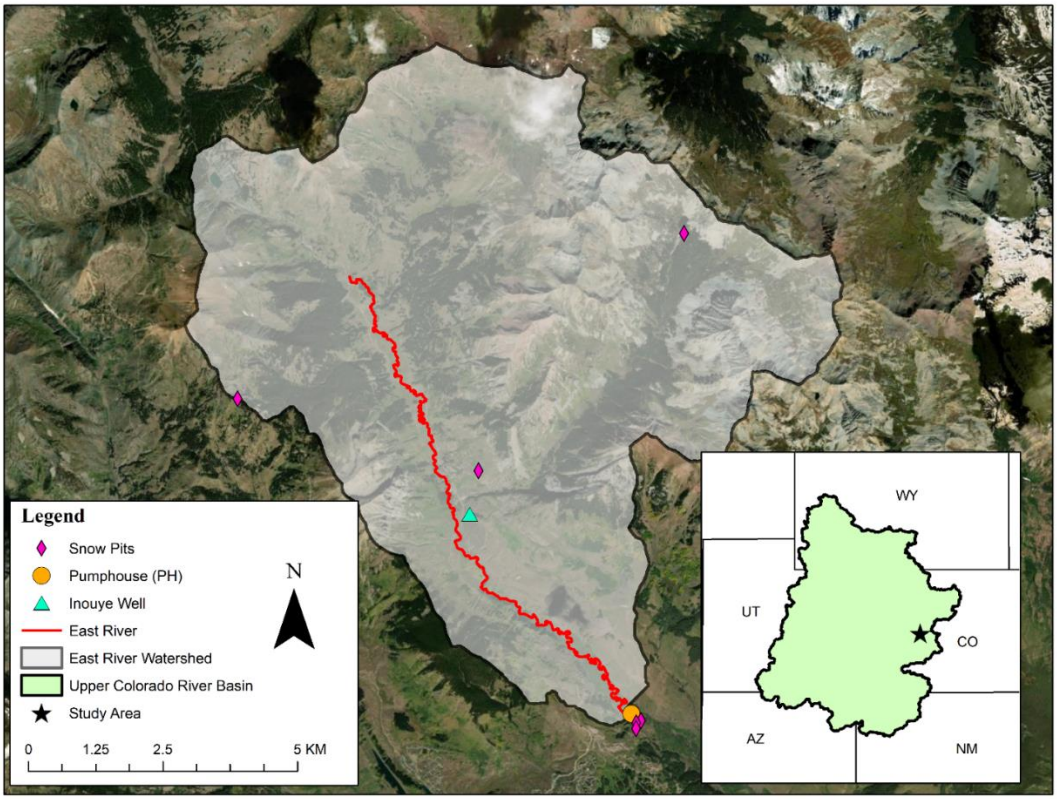

Figure 1. Study area of the East River Basin Located in the Elk Mountains of Central Colorado. Service Layer Credits: Esri, HERE, Garmin, ©OpenStreetMap contributors, and the GIS user Community

2.2 Data Collection

2.2.1 Instream Sampling

Associated with ongoing research as part of the WFSFA, LBNL investigators have been collecting stream discharge and solute data at daily to weekly intervals beginning in May 2014 at one instream monitoring site located at the watershed outlet (Pumphouse (PH), Figure 1). The PH site is located at an elevation of 2760 m and includes an automated water sampler (Model 3700; Teledyne ISCO, NE, USA) to recover stream water samples from a fixed location in the stream channel via a peristaltic pump into uncapped 1 L polyethylene bottles. Geochemical analysis of all water samples

includes cations, trace metals, and anions. Prior to analysis, samples were filtered (Pall, NY, USA; polytetrafluoroethylene: 0.45μm) and stored at 4 C. Anion samples were stored in high-density polyethylene vials with Cl, NO3, and SO4 measured using an ion chromatograph (ICS-2100, Dionex, CA, USA) equipped with AS-18 analytical and guard columns with concentrations determined using factory-provided calibration standards. Cation samples were preserved with trace metal grade 12N HNO3 and analyzed using ion coupled plasma mass spectrometry (Element 2, Thermo Fisher, MA, USA). For this study, only solutes from the 2016, 2017, and 2018 water years (WYs) were used (where the 2016 WY is defined as October 1st, 2015 to September 30th, 2016). The PH site also includes a multi-parameter sonde (EXO2; YSI, Inc.; Yellow Springs, OH, USA) equipped with an EXO conductivity/temperature sensor for measuring the specific conductivity (SC) of stream water at 5-minute intervals over the WY2016-2018 interval.

2.2.2 End-member sampling

Two potential end-members were sampled (snow and deep groundwater). Snow samples were collected from 2017 to 2020 with the majority of samples collected in 2020 at six locations around the basin (Snow pits, Figure 1). Snow pits were dug in open, flat areas with anion, cation, and trace metal concentrations determined by filtering (Pall, NY, USA; polytetrafluoroethylene: 0.45μm) melted samples collected at 10 cm intervals over the pit depth. Pit depths ranged from 67 to 140.5 cm depending upon location. Solute data representative of deep (~60 m) groundwater sourced from Mancos shale bedrock has been monitored weekly to monthly since 2015 at the Inouye Well, which is drilled to a depth of 61 m with water pumped to the ground surface from this depth using a fixed downhole pump. Samples were filtered upon collection and stored at 4C until analysis. For this study, only groundwater samples collected in the 2016 – 2018 WYs were used.

2.3 Hydrograph Separation Approaches

Two methods of hydrograph separation and two characterization methods for end-member concentrations were used to compare volumetric contributions to instream flow using limited end-member data, but detailed instream chemistry data for three water years (WYs). The first hydrograph separation technique used PCA and EMMA. PCA is a statistical tool that uses the variances and co-variances of datasets to highlight collective trends. Through PCA, highly dimensional datasets - such as those produced from a detailed chemical analysis of instream solute samples - are projected into a lower dimensioned mixing space that can then be more easily analyzed. The purpose of this type of analysis is to identify a shared factor (such as an end-member) that may explain trends exhibited in the new mixing space. This can be done using EMMA, which employs a statistical analysis of the mixing space to identify end-members based on instream chemical signals (Christophersen & Hooper 1992) . Since the mixing space consists of projected solute concentration data, it can be used in tandem with flow data in a constrained system of equations to solve for the contributions to instream flow due to each end-member. This approach of using PCA and EMMA for hydrograph separation is herein referred to as the ‘statistically-based approach’. Several important assumptions are made to ensure the validity of this approach. First, EMMA requires the assumption of the conservative (linear) mixing of end-members (Christophersen et al., 1990; Christophersen & Hooper, 1992). In addition, EMMA requires end-members to have a constant composition or the variability in end-member composition must be known through time and/or space. The last requirement is that end-member concentrations must be sufficiently different for at least one solute (Christophersen et al., 1990; Hooper et al., 1990).

The second method of hydrograph separation used was a chemical mass balance. Chemical data are collected to characterize the composition of each of the source waters contributing to the stream. These data, along with instream concentration and discharge data, are then used in a constrained system of equations where mass is conserved to parse the contribution of each source water (Pinder & Jones, 1969). This approach is herein referred to as the 'mass-based' approach. Several assumptions are applied that are similar to those established by Sklash & Farvolden (1979) and those from the statistically-based method of separation. These include: 1) that end-member composition is assumed constant or else the variability in time and/or space is known, 2) solutes mix conservatively, 3) the number of end-members are known, 4) instream concentrations are only composed of waters originating from the identified end-members or else all other waters contributing are considered negligible, and 5) end-member concentrations are sufficiently different for at least one solute.

End-member concentrations were characterized using two methods because of the uncertainties associated with limited measured end-member data. The first characterization of the end-member concentrations was by direct sampling of two potential end-members (groundwater and snowmelt) at a limited number of sites across the basin (Figure 1). The second method of characterizing end-member concentrations was done by inferring potential end-members from instream chemistry during certain flow regimes at certain times of the year at the outlet of the catchment. Hereinafter, end-member concentrations characterized by direct sampling of the source waters will be referred to as 'measured end-member concentrations' and end-member concentrations characterized by instream sampling at the outlet of the catchment during certain flows

and times of the year will be referred to as 'hydrologically rationalized end-member concentrations'. These two characterizations of the concentrations of the end-members have unique ranges and both of these will be discussed in further detail in the following sections.

By using these two hydrograph separation techniques and two different characterizations of the end-members, five types of separations were performed for the 2016, 2017, and 2018 WYs (Figure 2). Each separation offers unique insight into the possible separation of the hydrograph and the associated uncertainties.

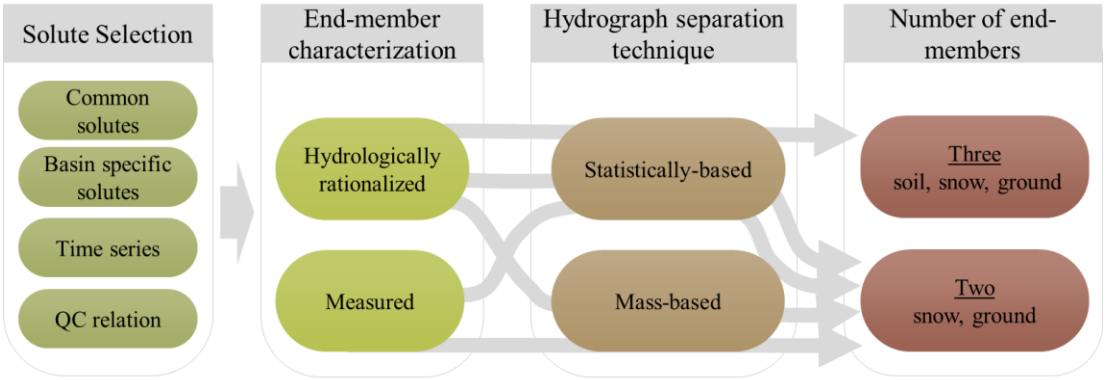

Figure 2. Experimental design matrix for all three water years. In general, solutes were selected for use in the analysis, then an end-member characterization method was chosen. Next, the hydrograph was separated using one of two techniques. Finally, two or three end-members were used to complete the separation. This led to five unique separations being performed, as indicated by the light grey arrows.

2.3.1 Solute Selection

The solutes used in both methods play an essential role in determining the outcome of the hydrograph separation. Different combinations of solutes will yield slightly different answers. Non-conservative solutes or solutes without geochemical relevance to the basin will result in poor separations. Four different methods were used to select the solutes for both analyses: First, commonly used conservative solutes in hydrograph separations were examined. Second, conservative solutes used previously at

this specific study site were examined. Third, the temporal behavior of instream solutes was examined. Fourth, solute behavior in relation to flow was examined. In the statistically-based approach, a posteriori method can also be used to select solutes. This posteriori method involves plotting measured instream concentrations against predicted instream solutes concentrations, calculated from end-member concentrations and fractional flow contributions informed by the statistically-based hydrograph separation. If predictions are sufficient, as evaluated by coefficients of determination and slopes, the solutes can be retained in the analysis. If not, new solutes can be selected.

Commonly used conservative solutes in hydrograph separation methods include calcium, magnesium, potassium, silicon, and sodium, as was done by Wels et al. (1991), Hooper (2003), and Liu et al. (2017). Less commonly used solutes include rubidium, barium, strontium, uranium, and (sometimes) sulfate as was done by Ladouche et al. (2001) and Barthold et al. (2011). A previous study done in ER WFSFA used calcium, uranium, strontium, sulfate, and two stable isotopes to perform their separation in the 2016 WY; but, they suggested that sulfate not be used in future studies in the basin due to observed non-conservative behavior (Carroll et al., 2018).

Time series of solute data were also analyzed (Figures A1-A3). This was helpful for identifying solutes with clear temporal patterns (e.g Ca or Na) and those without clear temporal patterns (e.g. Sn or V). After examining temporal behaviors, the solute's relation to flow was used as the final a priori metric of selection (see, Ladouche et al., 2001; Pinder & Jones, 1969). The linearity of solute concentrations in this study was quantified and classified based on hydrologic responsiveness to changes in flow. High coefficients of determination (R^2), slope, and low root mean square error (RMSE)

produced from the comparison of a linear best-fit on logarithmic discharge – concentration (Q-C) plots were used as indicators for the strength of the relationship (Table 1) (Godsey et al., 2009). If solutes qualified as "Best" or "Moderate" in two of the three categories, they were retained for use in the analysis for that WY (Table A1). This was done to find solutes that mobilize with changes in runoff generation and to highlight seasonal end-members. It is important to note that using Q-C plots to select solutes assumes simple linear mixing of just two end-members. However, since this method of selecting solutes is also highly effective at highlighting solutes that are responsive to changes in end-member contributions that influence instream concentrations, it was used in tandem with the other three methods described previously.

Table 1. Criteria for evaluating Q-C plots. Criteria are relative to the water year. Slopemax and R^2_{max} are the maximums found in a single water year. $RMSE_{min}$ was the minimum for the water year.

Rating	**Slope**	**R^2**	**RMSE**
Best	$\geq 0.7\ \lvert slope_{max} \rvert$	$\geq 0.8\ R^2_{max}$	$\leq 1.2\ RMSE_{min}$
Moderate	$\geq 0.5\ \lvert slope_{max} \rvert$	$\geq 0.7\ R^2_{max}$	$\leq 1.5\ RMSE_{min}$
Poor	$< 0.5\ \lvert slope_{max} \rvert$	$< 0.7\ R^2_{max}$	$> 1.5\ RMSE_{min}$

2.3.2 End-member Characterization

2.3.2.1 Hydrologically Rationalized End-member Concentrations

Given the availability of detailed instream solute data at the outlet of the catchment, three potential end-members (deep groundwater, snowmelt, and soil water) were characterized based on these data. These hydrologically rationalized end-member concentration ranges were chosen to capture the chemical variability instream over time. This characterization of end-member concentration ranges may be helpful indicators of changes in end-member contributions to the stream throughout the year when detailed end-member concentration data are limited or unavailable.

Commonly, deep groundwater concentrations are inferred from instream chemistry during base flow (see James & Roulet, 2009; Miller et al., 2014, Pinder & Jones 1969). As such, solute concentrations during the lowest 5% of discharge were used to represent deep groundwater chemistry. Similarly, solute concentrations during the highest 5% of discharge were used to represent snowmelt when deep groundwater contributions are limited and snowmelt dominates runoff in mountainous systems such as the UCRB. While this characterization of the snowmelt end-member concentrations will not perfectly represent the variability in snow composition, it does provide a reasonable representation of the variability in the integrated snow end-member contributions to instream chemistry. Finally, shallow soil waters were characterized by using the highest 15% of discharge from the summer storm events in August through October. This period was chosen as any deviation in base flow chemistry that late in the water year was likely due to storm events and could represent older and reacted water. It is important to note that characterizing end-member concentrations based on instream chemistry will bias hydrograph separation results to 100% contribution of the defined end-member during the respective flow regimes. To account for variability in the hydrologically rationalized end-member concentrations, a normal distribution was assumed using the mean and standard deviation of each end-member. This distribution was randomly sampled 1000 times to establish a range of possible source compositions for each solute.

2.3.2.2 Measured End-member Concentrations

The second method of characterizing end-member concentrations used measured values. To establish measured end-member concentration ranges for each solute representing two potential end-members (snowmelt and deep groundwater), we created distributions based on a limited number of available solute samples. This provided insight

into acceptable concentration ranges for the two measured and potential end-members. The snowmelt sample size was small (n = 18 – 36) and represented six sample sites from the basin from 2017 to 2020. Because of the small sample size, we established a uniform distribution based on the min and max of the field samples and randomly sampled it 1000 times to get at the possible source concentrations for each solute (Figures A4 – A8). This was done to better represent the uncertainty in the measured end-member concentration for each solute.

The number of measured groundwater samples was spatially limited. The field samples collected from 2016 WY through the 2018 WY (n =122-124) from a single location, the Inouye Well, were nearly normally distributed (Figures A9 – A13). A distribution was generated for each solute based on the distribution inherent to the field samples collected by LBNL and sampled 1000 times to determine possible groundwater compositions. The resulting concentrations from each sampled distribution were then used in the hydrograph separation techniques.

As with hydrologically rationalized end-member concentrations, characterizing end-member concentrations via direct measurements also poses challenges. Acquiring representative source samples can be difficult in mountain environments where there may be significant spatial variation. In addition, end-member concentrations can change significantly while en route to the stream. This is why creating distributions from our limited set of measured data was important to represent uncertainty in end-member composition.

2.3.3 PCA and EMMA

To begin the statistically-based method of hydrograph separation, first the PCA must be performed. Through PCA, stream chemistry is projected into a mixing space (referred to as the *U*-space) defined by the principal components retained for analysis (Equations A1-A3). Determining the number of principal components to retain is significant as the number of end-members is one greater than the number of principal components retained. To do this, $\boldsymbol{X}$ – which represents the standardized matrix containing time series of stream chemistry - is projected into the *U*-space while maintaining the units in the solute space (*S*-space) following (Christophersen & Hooper, 1992; Equation 1)

$$\widehat{\boldsymbol{X}} = \boldsymbol{X}\boldsymbol{V}'(\boldsymbol{V}\boldsymbol{V}')^{-1}\boldsymbol{V} \quad (1)$$

where $\widehat{\boldsymbol{X}}$ is the de-standardized but projected matrix of $\boldsymbol{X}$ that has units equivalent to that of the *S*-space, and $\boldsymbol{V}$ is the eigenvector obtained from the PCA. The residuals (Equation 2) between the modeled stream chemistry in the projected matrix and the measured stream chemistry are calculated as

$$\boldsymbol{E_j} = \widehat{\boldsymbol{X_j}} - \boldsymbol{X_j} \quad (2)$$

where $\boldsymbol{E}$ is the matrix of residuals between the projected jth solutes and the measured jth solutes. Generally, if the modeled data is a good fit to the observed data, the residuals should be identical and normally distributed with a mean of zero and constant variance (Draper & Smith, 1981). If the residuals violate any of these conditions, it suggests that there is a pattern within the data that the model is not capturing. As such, residuals were analyzed using the coefficient of determination (R^2) and relative root mean square error (RRMSE) to evaluate structure and variance. Residuals were also analyzed using p-

values to find significant ($p < 0.05$) linear trends in the residuals and analyzed with quantile-quantile plots to evaluate normality. RRMSE (Equation 3) was calculated as

$$RRMSE = \frac{\sqrt{\frac{\sum \boldsymbol{E_j^2}}{n}}}{\overline{\boldsymbol{X_J}}} \quad (3)$$

where $\overline{\boldsymbol{X_J}}$ represents the average solute concentration and n represents the number of samples. Similar studies have also used R^2 and/or RRMSE (e.g. Ali et al., 2010; Bearup et al., 2014; Carroll et al., 2018) to quantify the residuals (Table A2). These studies were used as a basis for comparison to determine appropriately low R^2 and RRMSE values. Using these metrics, the number of principal components as well as the predicted number of end-members were determined. To complete the analysis, all solutes and end-members were projected into the *U*-space (Equations A4 & A5).

2.4 Hydrograph Separation

2.4.1 Statistical Hydrograph Separation

The final steps of the statistically-based approach result in a set of linear equations, which can then be solved using the constrained least-squares method. A constrained least-squares method was used in order to accommodate end-member concentrations characterized by hydrologic rationalization. To separate the hydrograph, the system of equations (Equation 4) is solved for f , the fraction of instream signal due to each end-member. An example of the system of equations in the instance of three end-members is shown below; but, it can be easily reduced in the instance that only two end-members are found to describe the mixing space.

$$\begin{cases} 1 = f_1 + f_2 + f_3 \\ \boldsymbol{U_1} = \boldsymbol{W_1^1} f_1 + \boldsymbol{W_1^2} f_2 + \boldsymbol{W_1^3} f_3 \\ \boldsymbol{U_2} = \boldsymbol{W_2^1} f_1 + \boldsymbol{W_2^2} f_2 + \boldsymbol{W_2^3} f_3 \end{cases} \quad (4)$$

$$where\ f \quad due\ to\ each\ end-member \geq 0$$

$\boldsymbol{W}$ is known and represents the projected end-member in the *U*-space, with subscripts indicating the principal component and superscripts indicating the identity of the end-member. $\boldsymbol{U}$ represents the projected solutes instream with the subscripts again indicating the corresponding principal component. In instances of just two end-members, the system of equations was reduced accordingly. $\boldsymbol{W}$ was selected from the end-member distributions described previously to solve the system of equations. This was done 1000 times to produce 1000 different solutions to Equation 1. For each iteration, the end-member fraction was multiplied by the stream flow to calculate the flow due to that end-member. This resulted in a separated hydrograph with 1000 possible solutions for each time-step to reflect the uncertainty in end-member concentrations.

2.4.2 Mass Balance Separation

For mass balance separations, the number of end-members and the identity of the end-members are decided a priori. Since the ER is a snow-dominated basin in the UCRB, deep groundwater and snowmelt were two logical choices for end-members. A third end-member was not included in this method of separation, but could be in future studies. To separate the hydrograph using a mass balance, discharge and concentration data were combined in a system of just two equations. The first equation in the system below represents a flow balance where unaltered groundwater and snow water are assumed to mix instantaneously in the water column. This equation (Equation 5) represents a mass balance with a particular solute.

$$\begin{cases} Q_{tot} = Q_{gw} + Q_{sm} \\ C_{tot}Q_{tot} = C_{gw}Q_{gw} + C_{sm}Q_{sm} \end{cases} \quad (5)$$

Q_{tot} is the total instream discharge measured at the Pumphouse, Q_{gw} and Q_{sm} and represent discharges from groundwater and snowmelt. C_{tot} is the concentration instream at the Pumphouse. C_{gw} and C_{sm} are the measured concentrations at the groundwater and snow end-members, respectively. Like the statistical separation, C_{gw} and C_{sm} were selected from the generated distributions described previously for both measured and hydrologically rationalized end-members. The system of equations was solved 1000 times for Q_{gw} and Q_{sm} for each time step to generate 1000 possible solutions of the separated hydrograph.

RESULTS

3.1 Solute Selection

The Q-C plots revealed that the solutes with the strongest relationship to discharge were generally calcium, uranium, and strontium for all years analyzed (Table A1; Figures A14 -A16). Solute correlation with discharge was often inverse with concentration dipping when discharge peaked (Figures A17 – A19). Barium strongly correlated to discharge in both the 2016 and 2018 WYs, and as a result, it was also used in the 2017 WY. Strontium was also used in 2017 WY despite only meeting one out of the two criteria for retention defined in Table 1, given that it met all criteria sufficiently in 2016 WY and 2018 WY. Magnesium correlated strongly with discharge in the 2016 WY and was included for that water year only. Sulfate, a commonly used solute in mixing analyses albeit one that is not conservative, had a strong correlation to discharge; however, previous research by Carroll et al. (2018) has suggested it may not be conservative in this watershed owing to anaerobic forms of microbial reduction, and it was subsequently excluded from this analysis. In summary, the selected solutes used in all years were barium, calcium, strontium, and uranium, with magnesium used only in the 2016 WY.

3.2 End-members

3.2.1 End-member Concentration Distributions

The individual end-member solute concentration distributions that were sampled for hydrograph separation differed based on the method of characterization (hydrologically rationalized or measured). For end-member concentrations characterized by hydrologic rationalization, solute concentrations were randomly sampled from the generated normal distributions described previously. For end-member concentrations

characterized by field measurements, solute concentrations were sampled from generated uniform distributions for the snow end-member (Figures A4-A8). Solute concentrations for the groundwater end-member were sampled from the generated distributions inherent to the field samples of groundwater (Figures A9-A13).

3.2.2 End-member Retention

Following an analysis of the residuals and principal component space, the number of end-members contributing to instream flow was determined. For all water years, the residuals as evaluated by R^2 and RRMSE indicated the retention of two to three principal components (Table 2). The number of end-members is one more than the number of principal components; hence, three to four end-members were predicted. Although R^2 and RRMSE values are reasonable based on accepted ranges in similar studies (Table A2), none of the residuals were normally distributed according to the quantile-quantile plots (Figures A20 – A31). This indicates that there could be aspects of mixing space that are not entirely captured by the solutes included in the analysis. Results from the residuals as evaluated by p-values are variable, but generally agree that four end-members could adequately describe the mixing space. p-values often (although not always) indicated slopes significantly ($p < 0.05$) different that zero for $m \leq 2$, which suggests some remaining pattern in the residuals at low levels of principal component retention. An example of these results for the 2016 WY are shown below for strontium (Figure 3). Overall, R^2 and RRMSE indicated that the calculated principal components adequately described the mixing space for the purposes of this study, but quantile-quantile plots and p-values results vary and suggest that this analysis could be improved in the future, such as by testing different solute combinations in an aim to reduce structure in residuals.

Table 2. The mean RRMSE and R2 for the residuals for each water year. Average values for retaining two to three principal components (m = 2 and m = 3) fit ranges defined by Table A2. Expanded tables which include p values by solutes are available (Tables A3 – A5)

	2015-16 WY		2016-17 WY		2017-18 WY	
m	RRMSE (%)	R^2	RRMSE (%)	R^2	RRMSE (%)	R^2
1	5.6	0.109	9.6	0.233	8.1	0.141
2	4.1	0.057	4.9	0.055	4.8	0.054
3	2.5	0.024	1.8	0.007	1.4	0.010
4	1.1	0.006				

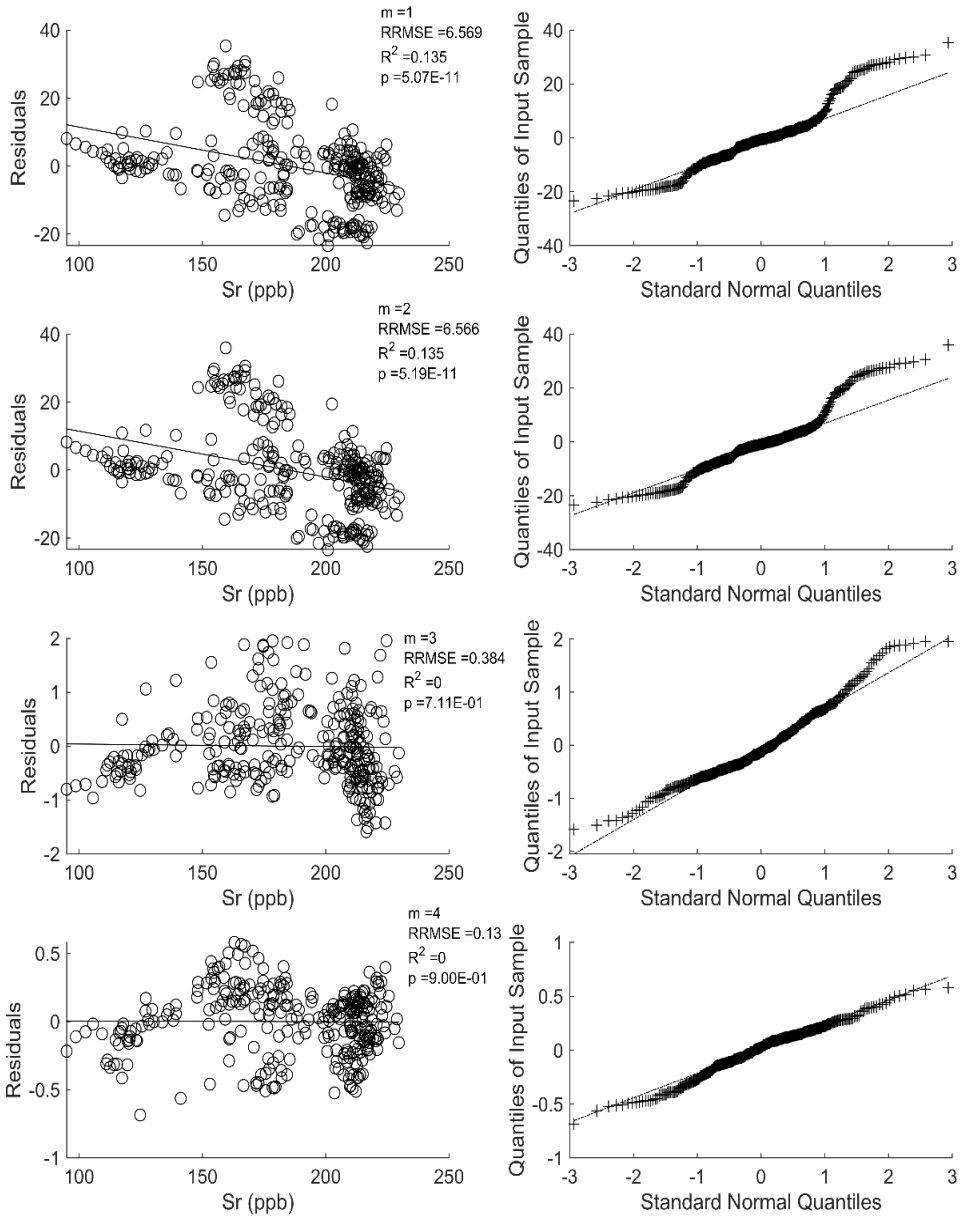

Figure 3. Residuals analysis for the 2016 WY for the solute strontium. Plots on the left show residuals at different numbers (m) of principal component retention and the associated R2, RRMSE. p-values indicate if slope is significantly ($p < 0.05$) different than zero. Open dots represent data points; line evaluates trends in data. Right hand plots assess normality at each level of principal component retention. Plus signs represent the residuals, dashed line represents the theoretical normal distribution residuals would follow if they were normally distributed.

For all water years, similar trends in the projections of solutes into the mixing space (*U*-space) were observed (Figure 4). Projection into the *U*-space indicates that solutes have seasonal variation. The stream signal tends towards the snow end-member during peak runoff and then towards the groundwater end-member during periods of base flow. The collective non-linear shape of the projected solutes in the *U*-space support the findings from the residuals analysis and suggests the existence of more end-members than identified. Thus, based on the collective information from all analyses, three major end-members are likely. Given the ER WFSFA is a snow-dominated basin with seasonal melt, it was safely assumed that groundwater and snow water were two likely contributors to the instream. The possibility of a potential third major end-member (soil water) was tested using hydrologically rationalized end-member concentrations with the statistically-based method of hydrograph separation. However, this was not possible in separations with measured end-member concentrations due to limited end-member data. In summary, instream flow was assumed to be composed of waters originating from two to three end-members, with three end-members being most likely. The implications of potential missing end-members in hydrograph separations done with only two end-members are discussed in more detail in the following sections.

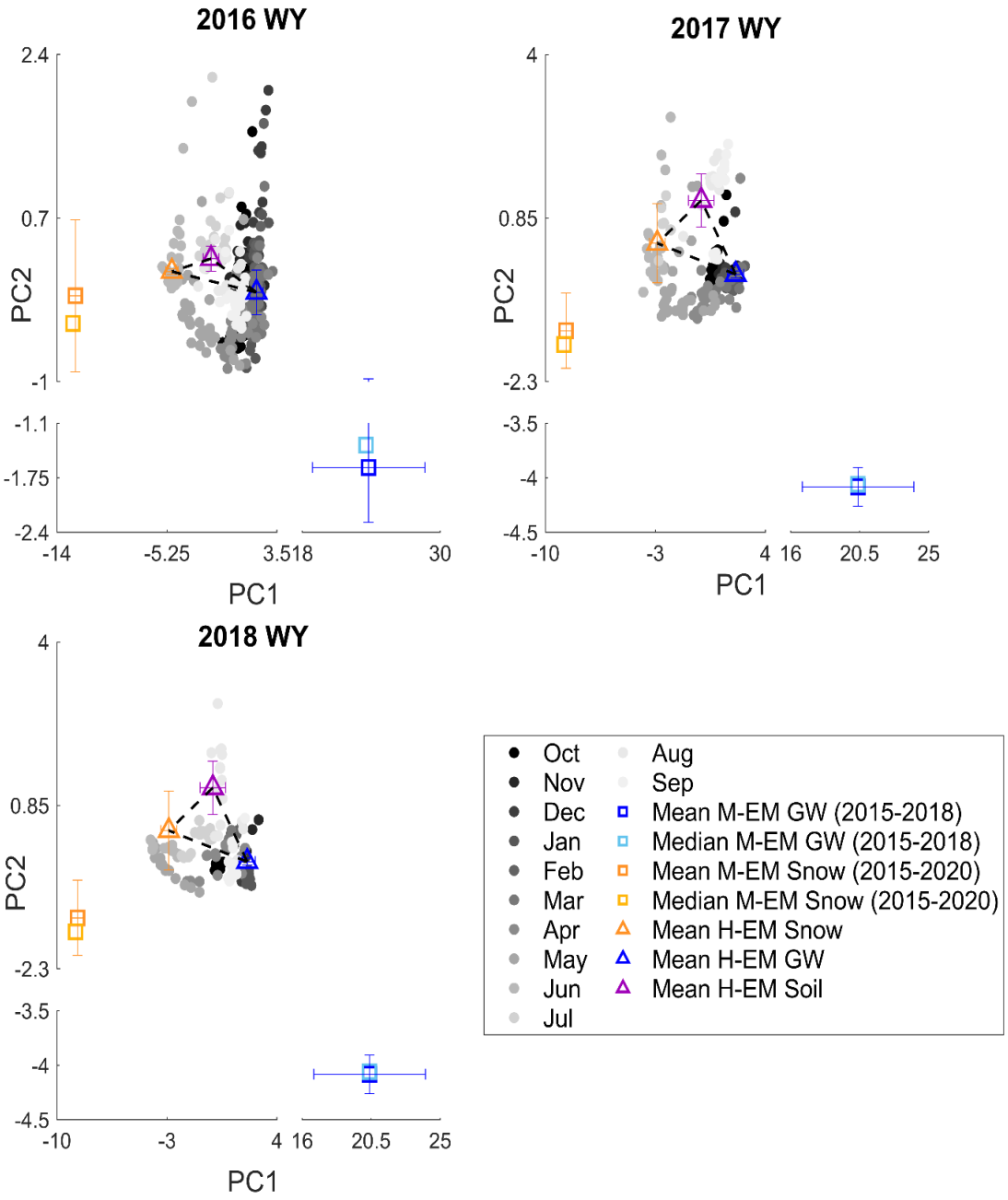

Figure 4. Data projected into the U-space across all WYs as defined by the principal components (PCs). All years include projections using Ba, Mg, Sr, and U. The 2016 WY additionally includes Mg. Error bars represent the standard deviation of the end-member concentrations about the mean. Solutes are in grey. Hydrologically rationalized end-members (H-EM) concentrations are represented by triangles. Measured end-member (M-EM) concentrations are represented by squares.

3.3 Hydrograph Separations

With the solutes and the number of end-members selected, hydrograph separations proceeded. Recall the hydrographs were separated using two different methods with two different end-member characterizations (Figure 2). In addition, both two and three end-member separations were tested.

3.3.1 Statistically-based Hydrograph Separation

3.3.1.1 Three End-members Characterized by Hydrologic Rationalization (3 H-EM)

Using hydrologically rationalized end-member concentrations, a separation was performed to yield a groundwater component, a snow water component, and a soil water component (Figure 5). Error band shows the interquartile range (IQR) that is created by the sampling of the end-member distributions. The initial flush of groundwater generally peaks in May while the snow signal tends to peak in June, with this behavior is generally replicable across water years. In contrast, soil water contributions vary across years. Increases in soil water contributions during June may be related to precipitation events (Figure A32), but direct causation is unclear. Large variations seen in the 2017 WY may be due to using barium even though it lacked a strong relationship with discharge in the 2017 WY. A feature to note in all separations done with hydrologically rationalized end-member concentrations is the short period of time in June where there is no evident contribution of groundwater. This is an artifact of using hydrologically rationalized end-members and will be discussed in detail in the following sections.

3.3.1.2 Two End-members Characterized by Hydrologic Rationalization (2 H-EM)

Using two end-members with hydrologically rationalized concentrations, the hydrograph was separated into a groundwater component and a snow water component (Figure A33). While the discharge contribution of each end-member differs slightly from that of a three end-member separation, the timing of the peak groundwater contribution is

the same. Similar to the separation with three end-members, there is again an artifact from the methodology where groundwater contributions in all water years go to zero for one to two weeks in June.

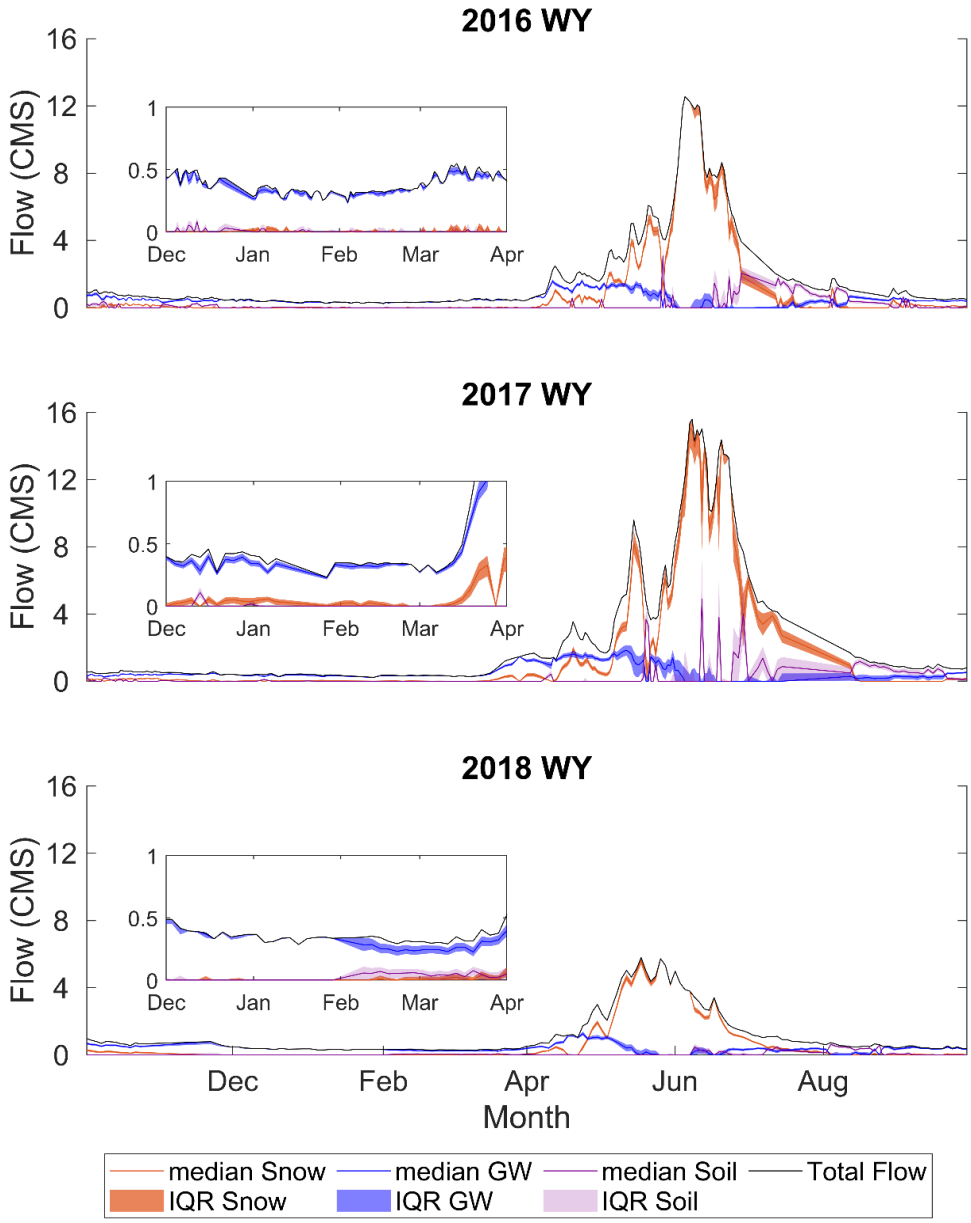

Figure 5. Hydrograph separation of three end-members with hydrologically rationalized concentrations (3 H-EM) using the statistically-based method of separation. Lines indicate median response from 1000 samplings around the mean and standard deviation of the end-member concentrations. The interquartile range (IQR) shaded around the median represents the lower 25th to upper 75th quantiles.

3.3.1.3 Two End-members Characterized by Measurements (2 M-EM)

Using two end-members characterized by measured concentrations rather than the hydrologically rationalized concentrations, there is a difference in the timing of peak groundwater contributions (Figure 6). In this separation, where two measured end-member concentrations are used, groundwater peaks with peak snowmelt rather than before peak snowmelt. This difference in timing is likely due to the two different characterizations of the end-members. In addition, discharge contributions from snow are greater than groundwater contributions at most times of the year. This occurs even when there is no snow in the basin, like during the late summer and early winter months. However, a soil water end-member may help to explain this discrepancy as soil water can enter the stream during these times.

3.3.1.4 Model Evaluation

As stated previously, selected solutes were examined posteriori by comparing predicted versus measured instream concentrations in the statistically-based method. In general, predicted versus measured instream concentrations showed strong relationships across all years as indicated by high R^2 values (Figures A34 – A40). However, separations with measured end-member concentrations showed consistent underestimations of instream concentrations of calcium and barium, and consistent over estimations of strontium (Figures A34 - A35). This is demonstrated well in the 2016 WY (Figure 7). Uranium was well predicted with measured end-member concentrations. Instream concentrations of solutes were well predicted with models using hydrologically rationalized end-member concentrations, which was expected as the hydrologically rationalized end-member concentrations were derived from the stream chemistry (Figure 8; Figures A36 – A40). In general, residuals indicate that most solutes were able to

predict instream concentrations reasonably well (as seen by the relatively normal distribution of the residuals) with the exception of barium in the 2017 WY; however, end-member concentrations characterized by measurements generally over or under predicted instream concentrations in some capacity.

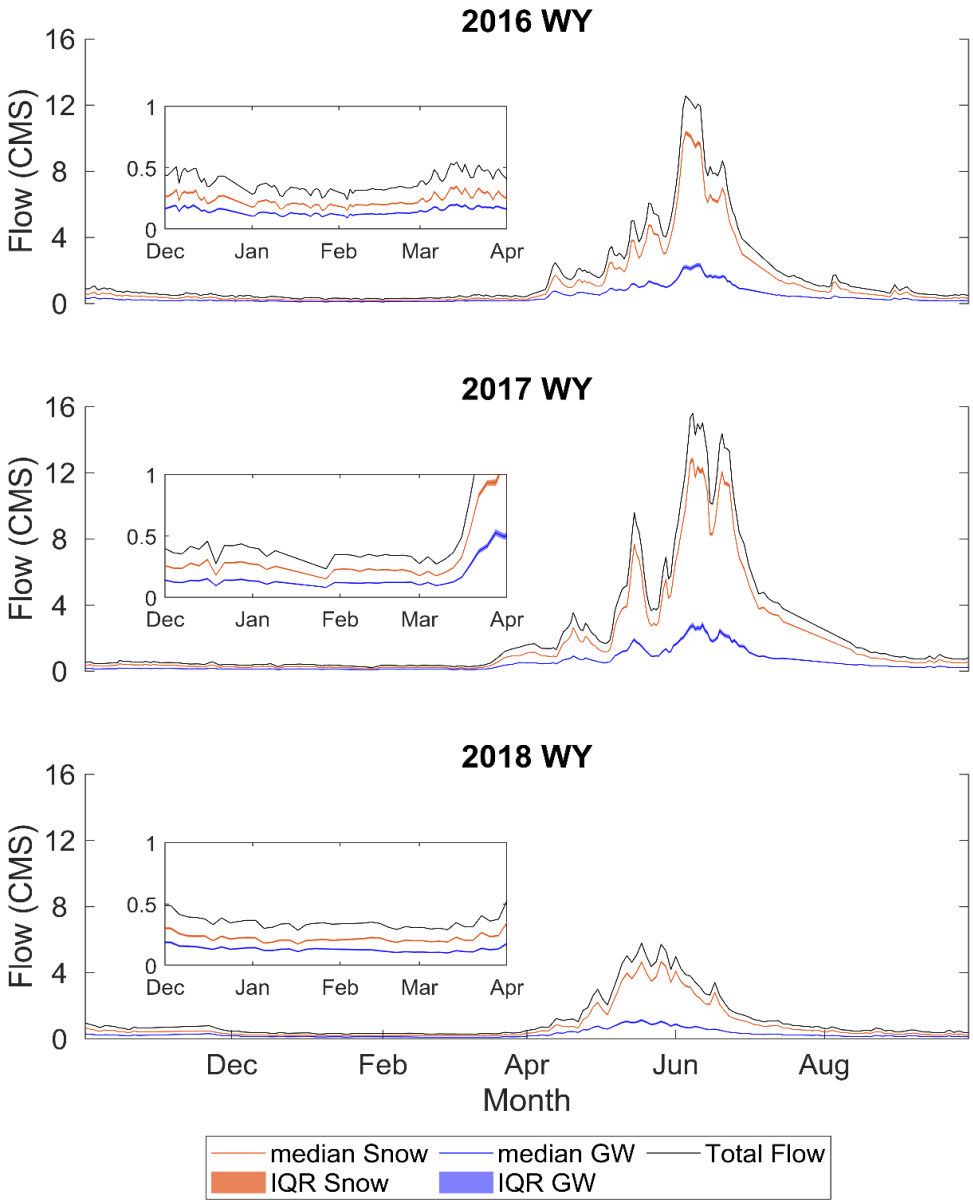

Figure 6. Hydrograph separation of two end-members with measured concentrations (2 M-EM) using the statistically-based method of separation. Lines indicate median response to 1000 samplings of the end-member concentration distributions. The interquartile range (IQR) shaded around the median represents the lower 25th to upper 75th quantiles.

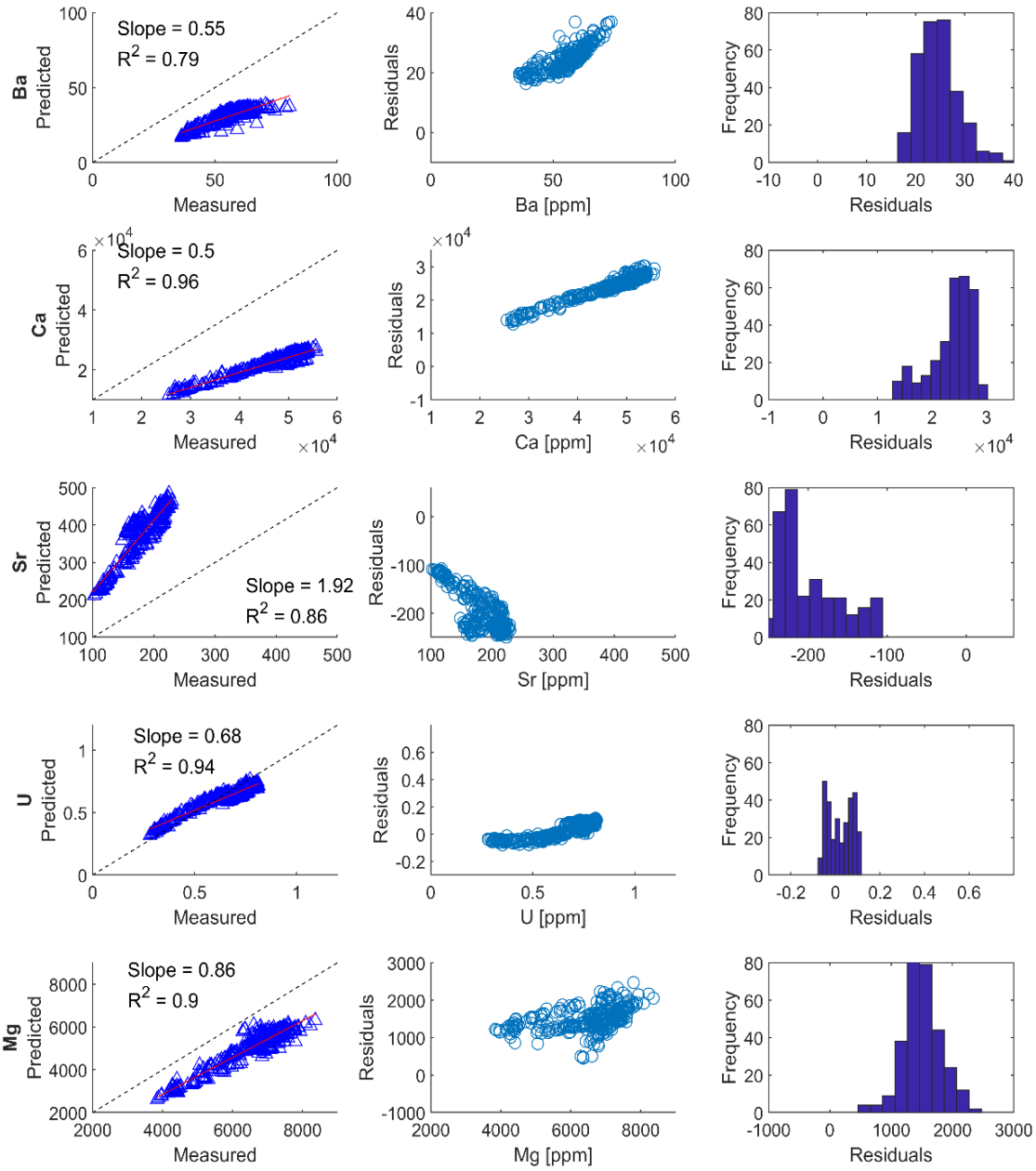

Figure 7. Plots on the left show predicted versus measured concentrations of the instream using 2 end-members characterized by measured concentrations in the 2016 WY. Trends indicated by red line. Dashed lined shows the theoretical perfect predicition of instream concentrations. Middle plots show residuals between predicted and measured instream concentration data. Histogram on the right show the distribution of residuals.

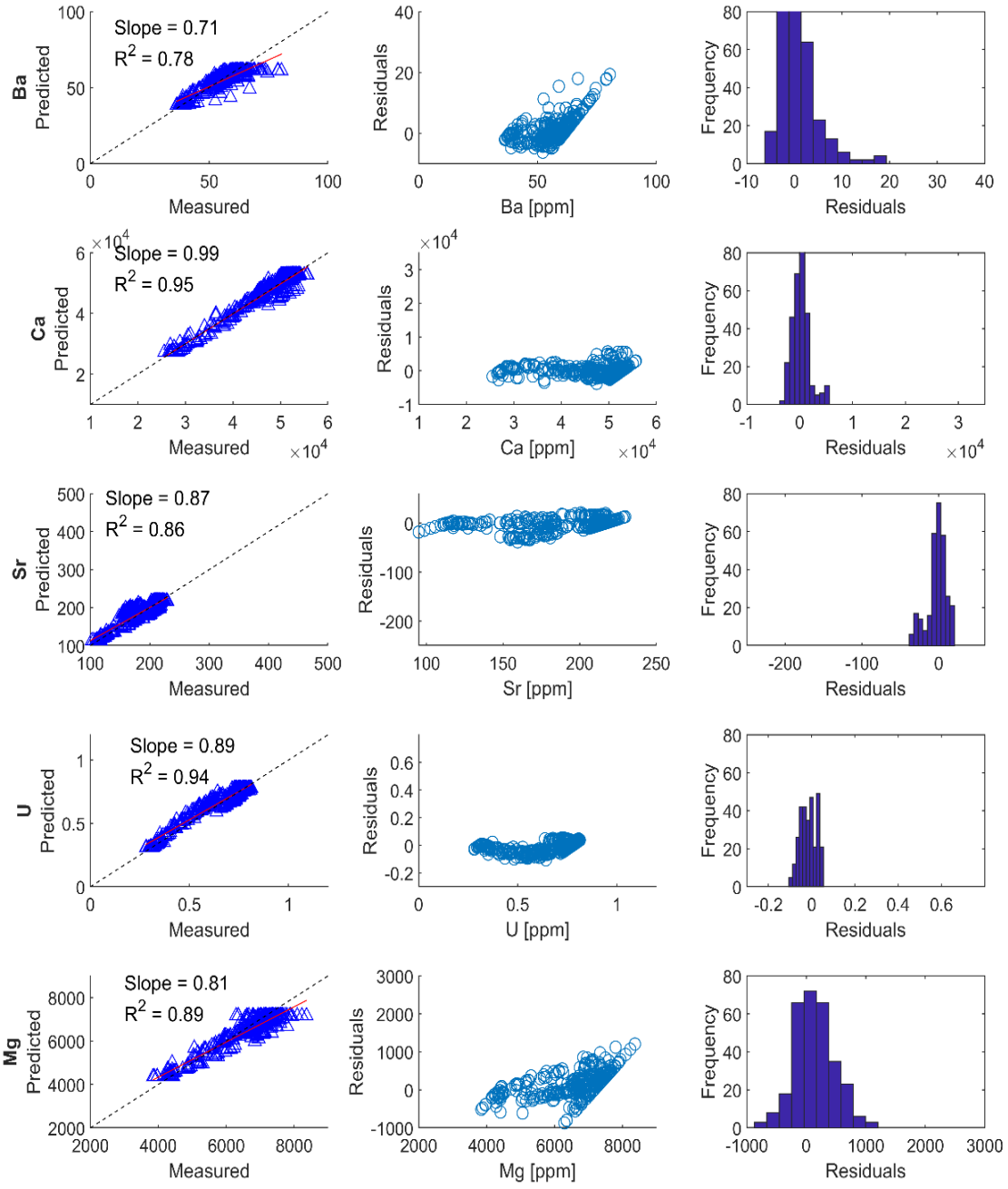

Figure 8. Plots on the left show predicted versus measured concentrations of the instream using two end-members characterized by hydrologic rationalization in the 2016 WY. Trends indicated by red line. Dashed lined shows the theoretical perfect predicition of instream concentrations. Middle plots show residuals between predicted and measured instream concentration data. Histogram on the right show the distribution of residuals.

3.3.2 Mass-based Hydrograph Separation

3.3.2.1 Two End-members Characterized by Hydrologic Rationalization (2 H-EM)

Using two end-members with hydrologically rationalized concentrations in a mass balance separation yielded similar results as the statistically-based method of separation (Figure 9). Again, the timing of peak groundwater contribution is shifted so that it occurs before peak snowmelt, which is an artifact of using hydrologically rationalized end-member concentrations. However, the mass balance method reveals how the separation is affected by different solutes (Figure A41). There is a clear separation of the hydrograph in all water years and good agreement among all solutes with the exception of barium in 2017 WY (Figure A41).

3.3.2.2 Two End-members Characterized by Measurements (2 M-EM)

Similar to a statistical separation of the hydrograph with two end-members with measured concentrations, the mass-based separation method also showed groundwater and snowmelt peaking at the same time. When the median response of all solutes is assessed, the IQR is quite large (Figure A42). However, using the mass-based method, the influence of each solute can be examined (Figures A43). Viewing solutes individually, it is clear that calcium is very different from the other solutes, predicting an almost 50/50 split in the flow contributions of each end-member during the entire water year. When calcium is removed from the analysis (Figure A44), the IQR is greatly decreased and there is a better separation of groundwater and snow water contributions (Figure 10). Again, barium is a poor solute for separation the 2017 WY.

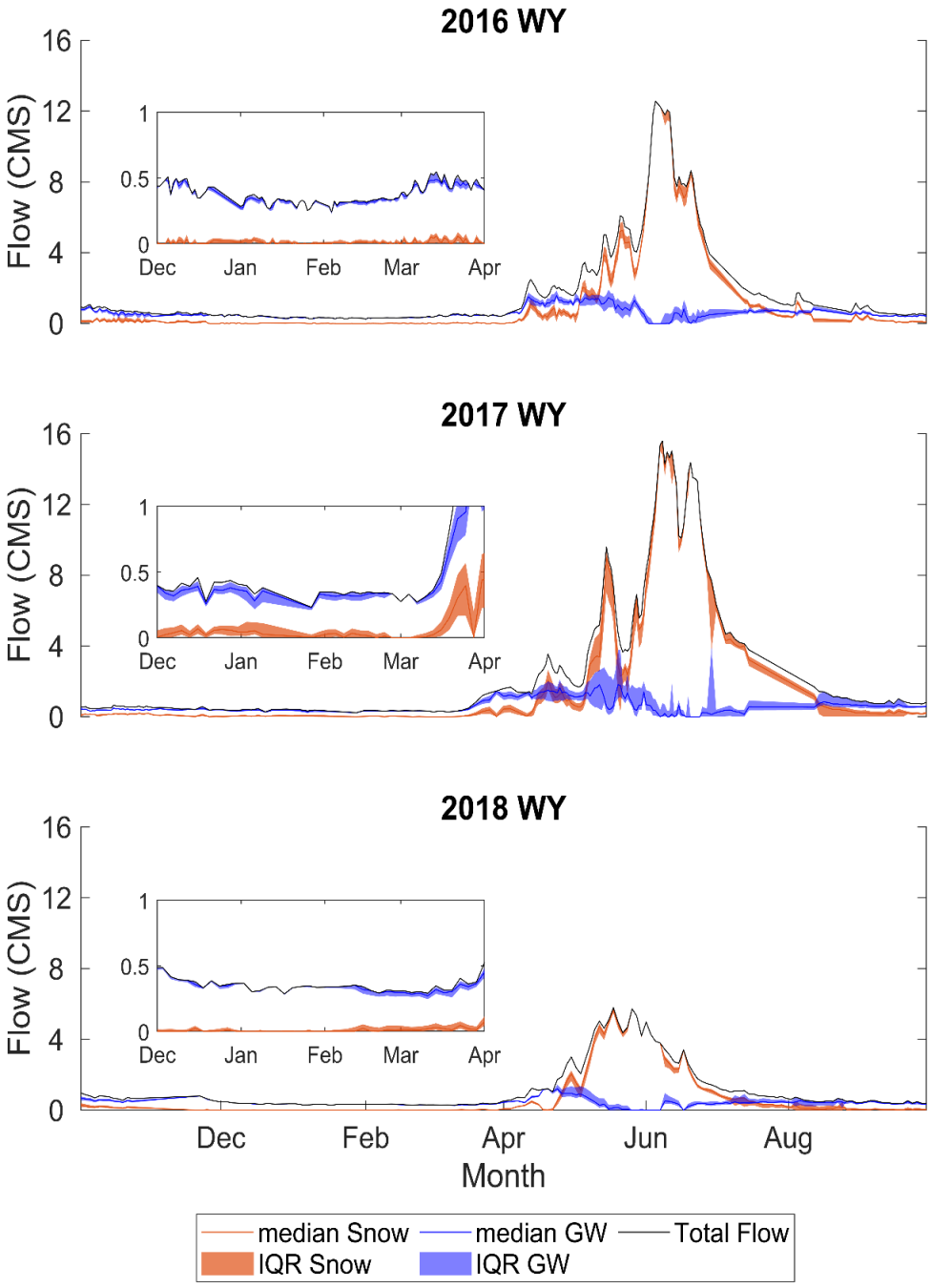

Figure 9. Hydrograph separation of two end-members with hydrologically rationalized concentrations (2 H-EM) using the mass-based method of separation. Lines indicate median response from four solutes (Ba, Ca, Sr, U) where each end-member concentration for each solute was sampled 1000 times. The interquartile range (IQR) shaded around the median represents the lower 25th to upper 75th quantiles.

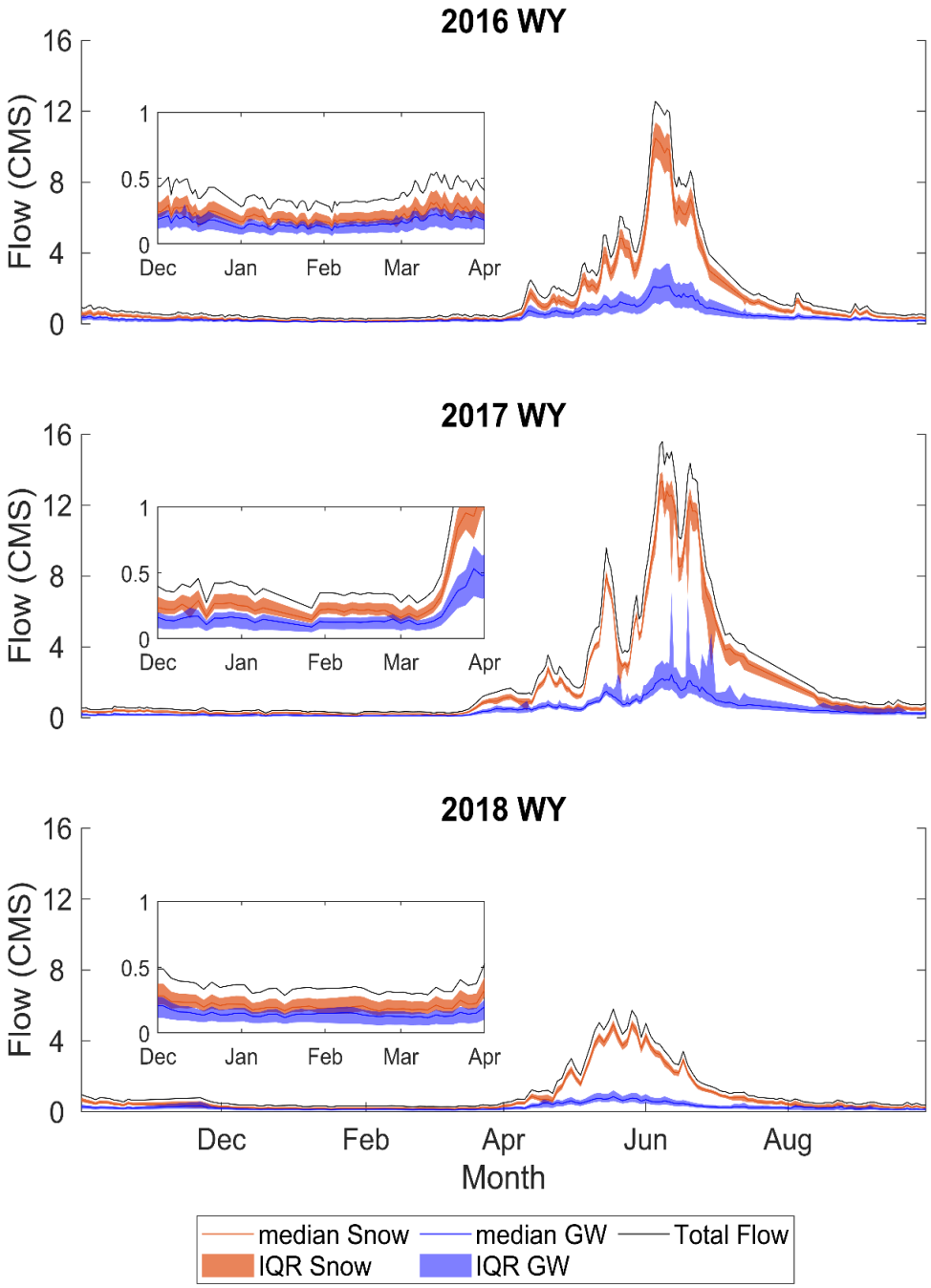

Figure 10. Hydrograph separation of two end-members with measured concentrations (2 M-EM) using the mass-based method of separation. Lines indicate median response from all solutes except calcium where each end-member concentration for each solute was sampled 1000 times. The interquartile range (IQR) shaded around the median represents the lower 25th to upper 75th quantiles

3.4 End-member Fractions of Total Annual Volumes

Since there are several differences in the time series of the separated hydrographs due to the different methods and end-member characterizations, annual volumetric contributions from the end-members to stream flow were used as another method of comparison (Figure 11, Table 3). Across methods, the median percent of total annual volume from groundwater ranged from 21% to 41% from 2016 - 2018 (regardless of the number of end-members or the characterization of the end-members). Median annual groundwater contributions from hydrologically rationalized end-member concentrations ranged from 21% – 41%, while median groundwater contributions estimated from measured end-member concentrations had a slightly smaller range from 22% – 35%. In general, the IQR of the same end-member number and characterization overlap regardless of the method of hydrograph separation. Overall, it appears that the median percent annual volumes of the end-members are similar across hydrograph separation techniques and vary more across end-member characterization. However, there are large variations in the mass-based method of separation depending on the solute used (Figure A45).

Table 3. Median fraction of annual end-member contributions to volume water leaving basin the statistically-based (STAT), mass-based (MB) and end-member (EM) characterizations: measured (M) or hydrologically rationalized (H).

		Snowmelt (%)		Groundwater (%)	
WY	End-Member Characterization	STAT	MB	STAT	MB
2016	3 H-EM	58		27	
	2 H-EM	66	65	34	35
	2 M-EM	75	65	25	35
2017	3 H-EM	67		21	
	2 H-EM	73	75	27	25
	2 M-EM	78	72	22	28
2018	3 H-EM	58		35	
	2 H-EM	59	59	41	41
	2 M-EM	74	69	26	31

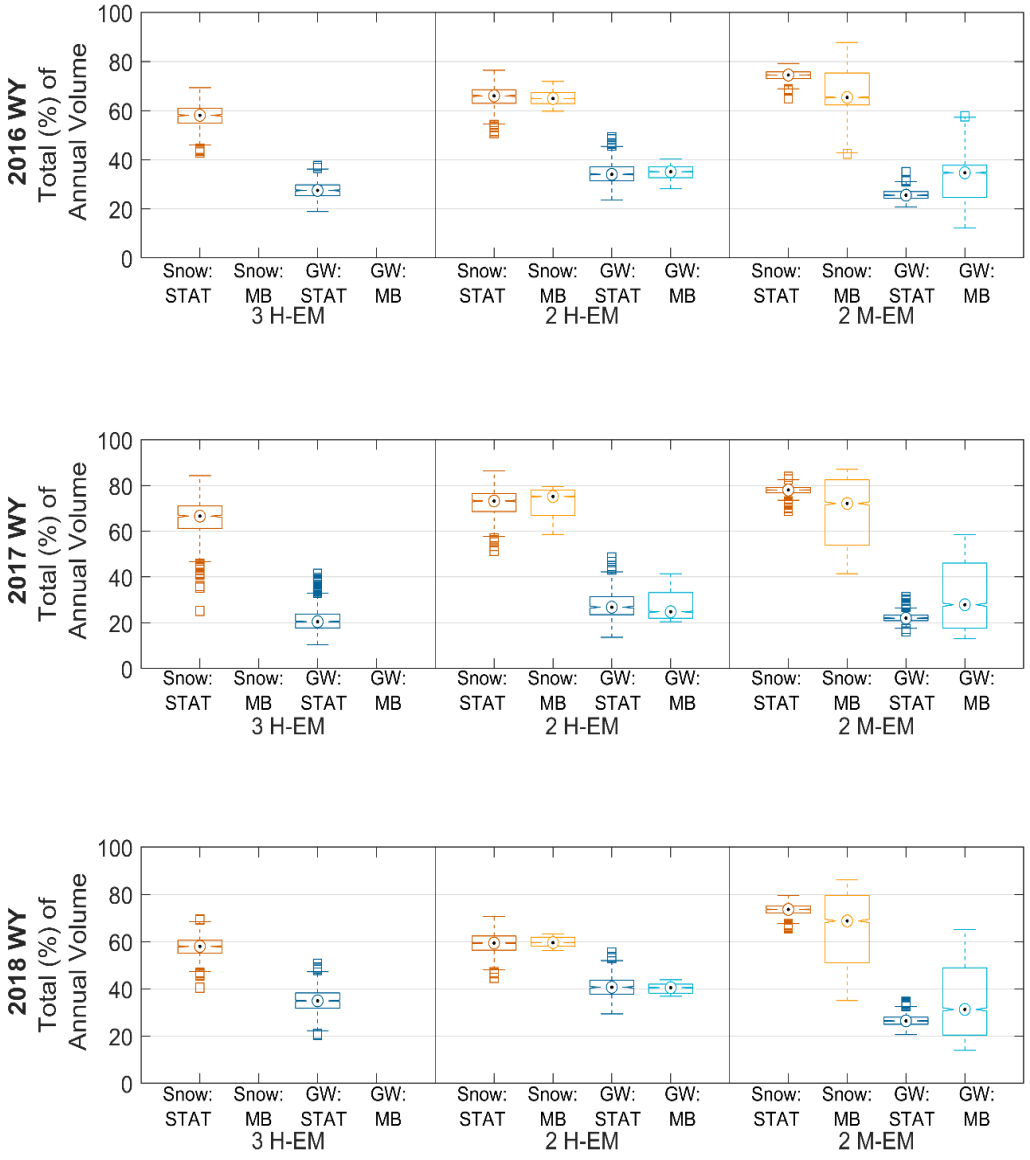

Figure 11. Total percent of the annual volume of water leaving the catchment coming from each end-member – groundwater (GW) or snowmelt (snow)- via statistically-based (STAT) and mass-based (MB) methods of separation with hydrologically rationalized end-members concentration (H-EM) and measured end-member concentrations (M-EM). Targets represent the median, boxes represent the interquartile range (IQR) spanning the 25th to 75th quantiles with error bars representing the minimum and maximum, and boxes representing outliers (1.5IQR). The snow end-member is represented in orange, groundwater in blue. H-EMs show n = 1000 for all years while M-EMs show n = 4000 (n = 5000 for 2016WY only)

DISCUSSION

Hydrograph separations via statistically-based and mass-based methods with two unique end-member characterizations were used to analyze the hydrology of a catchment with limited end-member data but detailed instream data. Results highlight the importance of solute choice as well as end-member retention and characterization in separations. In addition, annual volumes were similar despite differences in timing caused by different end-member characterizations.

4.1 Selected Solutes

Selected solutes influenced results in both statistical and mass-based methods of separation. Although solutes were selected using multiple methods, selection procedures were heavily reliant on the solute's hydrologic responsiveness to flow, which inherently assumes simple mixing of two end-members. In addition, choosing solutes that changed with flow prioritized solutes that mobilized strongly (as opposed to periodically or weakly) with flow. In a detailed end-member mixing study by Barthold et al. (2011), it was found that geochemically similar elements like magnesium and calcium (both of which mobilize fairly well with discharge) could potentially deliver similar information and suggested it may be better to include more minor elements. Thus, our analysis may be flawed in that minor elements that did not mobilize with flow were not included, even though they may have offered a broader perspective of basin hydrology. Limiting the number of solutes could also unintentionally exclude important hydrogeochemical indicators in the watershed.

This is well demonstrated by mass-based separation results wherein two solutes stand out as behaving very differently from the others. The first is calcium in separations

with measured end-member concentrations, which often predicts a 50/50 contribution of end-members at all times of the year across all water years (Figure A43). As a result, when examining the median response from all solutes, including calcium (Figure A42), there is a much larger total IQR than without calcium (Figure 10). Interestingly, in contrast to the analysis with measured end-member concentrations, a mass-based separation with hydrologically rationalized end-member concentrations has a very clear separation using calcium (Figure A41). This variation demonstrated by calcium across end-member characterization is very different from solutes, such as strontium and uranium, that produce clear separations regardless of being derived from measured or hydrologically rationalized end-member concentrations. Barium also tends to act like strontium and uranium in all years except in the 2017 WY. In this year, barium tends to dramatically and rapidly change end-member response (Figures A41 and A44). Although this behavior may be partly due to its weak relationship with discharge in this year (Table A1), it also illustrates why having more solutes may be needed to provide additional information. Perhaps other minor elements would behave similarly and prompt investigation into the presence of additional unidentified end-members, such as ephemeral springs or creeks sporadically discharging to the river after storm periods. Alternatively, the use of additional solutes could highlight non-conservative behaviors or other reactive processes occurring as a package of water travels to the stream. Non-conservative behavior is a critical consideration while examining the separated hydrograph as it could affect the amount of water attributed to an end-member during the water year. All in all, the behaviors demonstrated by individual solutes stress the importance of choosing appropriate solutes that can capture the full basin hydrology,

particularly in environments where sampling is limited. A broader range of conservative solutes based on multiple catchment characteristics (hydrology, geology, atmospheric deposition patterns, etc.) may prove to be beneficial. Future studies will need to explore the solute selection process more deeply and perhaps establish additional methods that can guide researchers to the hydro-geochemically pertinent solutes for their catchment.

4.2 Implications of End-member Characterization and Retention

4.2.1 End-member Characterization

In this study, end-member data was limited. As a result, two methods were used to characterize end-member concentrations: hydrologic rationalization of end-members based on instream chemistry and direct measurement of end-members at the source location. Using these two end-member characterization methods led to several substantial differences in the resulting separated hydrographs.

4.2.1.1 Hydrologically Rationalized End-member Concentrations

Two features were unique to hydrograph separations done with hydrologically rationalized end-member concentrations. The first was a difference in the timing of peak groundwater contributions to earlier in the year than separations performed with measured end-member concentrations (Figures 5 and 9). This is because hydrologically rationalized end-member concentrations are close in magnitude to the instream concentrations. This similarity to instream concentrations makes it so small chemical shifts in the stream can indicate more dramatic shifts in end-member contributions, hence the earlier increase in peak groundwater contribution to the stream as compared to separations performed with measured end-member concentrations. Subsequently, the difference between instream concentrations and measured end-member concentrations is much larger, so small changes in the instream concentration of solutes indicate small

changes in end-member contributions. Hence, only when there are substantial changes in the composition of the stream are dramatic shifts in the contributing end-members indicated.

The other important feature of hydrograph separations done with hydrologically rationalized end-members is the period of zero contribution of groundwater during peak snowmelt. The reason for this is well demonstrated by the principal component mixing space (Figure 4). It is clear that hydrologically rationalized end-member concentrations can overlap with the instream solutes allowing 100% contribution of that end-member to instream flow at a given time of year (Figures 5 & S41). This is a violation of the end-member mixing model assumptions that state end-members must be a convex combination that encompass the solutes in the mixing space (Christophersen & Hooper, 1992; Hooper, 2003; Hooper et al., 1990). Furthermore, the mixing space can be encompassed by any number of end-members, but with hydrologically rationalized end-member concentrations it is very hard to distinguish more than three contributing end-members that can encompass the solutes in the mixing space.

Despite this, hydrologically rationalized end-member concentrations may pose an advantage in data-limited environments. Hydrologically rationalized end-member concentrations – unlike measured end-member concentrations - do not require spatially and temporally uniform end-member data or detailed sampling schemes. Rather, hydrologically rationalized end-member concentrations derived from instream data are able to provide a snapshot of the major end-member contributors to streamflow during the year. Hence in studies where distinctions between more than three end-members are not needed, hydrologically rationalized end-members may offer unique and desirable

benefits such as the reduced sample location requirements (just needing one at the outlet of the catchment).

4.2.1.2 Measured End-member Concentrations

Limited measured end-member concentration data was available for use in the hydrograph separations. This was important, as it gave evidence for the observed solute concentration ranges of the possible end-members. Ideally, the measured composition of an end-member for a hydrograph separation should be representative of the end-member composition for the entire watershed. In this study, a single sampling point at the Inouye Well was used to represent all groundwater regardless of depth or bedrock composition. However, a USGS geologic survey of the area shows a diverse geologic profile (Gaskill et al., 1991) that suggests such spatially limited sampling of the groundwater end-member likely insufficiently captured the range of possible groundwater concentrations within the 85 km^2 basin. Other studies have also noted spatial (Penna & Meerveld, 2019) and temporal (Feng et al., 2002; Liu et al., 2004) variability in end-member composition. Furthermore, the spatial and temporal variability in end-member composition and its effect on the hydrograph has been observed in catchments < 1 km^2 in size (Cayuela et al., 2019; Kiewiet et al., 2020). Studies such as these emphasize the importance of spatially diverse and temporally detailed end-member data for hydrograph separation. However, this is not always possible in remote catchments with limited access, financial, and/or personnel resources and highlights how multiple methods of separation may be useful when detailed end-member data is unavailable.

4.2.2 End-member Retention

With limited end-member data available, this study included two possible end-members with concentrations characterized by field measurements (groundwater and

snowmelt) and three possible end-members with concentrations characterized by hydrologic rationalization (groundwater, snowmelt, and soil water). However, residuals and *U*-space analysis indicated that three to four end-members would best capture basin hydrology (Tables A3 – A5; Figure 4). As such, there is likely an over attribution of flow to the end-members that were available for use in the separations. For example, in separations where just two end-members characterized by measured concentrations are present, snowmelt contributions are predicted even when was no snow was present in the basin like during the late summer (after July) and early fall months (Figures 6 and 10). This over attribution of flow to the snow end-member may have been due to missing end-members in the analysis, such as soil water or rainfall producing overland flow.

4.3 Annual Volumetric End-member Contributions

Across hydrograph separation methods, total percent of annual volume from each end-member was generally similar with median groundwater contributions ranging between 21% and 41% (Table 3; Figure 11). These findings agree reasonably well with other studies of the UCRB. Miller et al. (2014) performed a solute separation across multiple sub-basins in the UCRB finding that annual contributions of base flow to discharge ranged between 21 and 58% in large basins (>1000 km^2). This estimate is expected to be greater as the study areas are much larger. However, there was a study conducted previously in a sub-basin of the ER WFSFA where a hydrologic water budget revealed groundwater contributions ranged from 21 to 52% with an average of 35% (Carroll et al., 2019). Our findings using a limited set of end-member data appears relatively consistent with the much more data-detailed study Carroll et al., (2019) of the same watershed; although, there is variation based on the characterization of the end-member concentrations and the solutes used in the analysis. Overall, these findings seem

to suggest that in the face of limited data, multiple methods of hydrograph separation may be useful in tracking shifts in the hydrology of mountainous and seasonally snow-dominated catchments.

CONCLUSIONS

Using limited end-member data and multiple conservative solutes, two hydrograph separation techniques were compared. Results showed that there can be large temporal differences in the predicted hydrograph based on the characterization of the end-member and solute used. A consequence of using hydrologically rationalized end-member concentrations are periods of time where contributions from an end-member can be zero. However, hydrologically rationalized end-member concentrations only require a single sampling point which could be advantageous in data-limited environments. In addition, annual volumetric contribution of the end-members to instream flow were similar across hydrograph separation methods and provided reasonable annual volumetric estimates of the groundwater end-member. The results suggest that in remote mountainous catchments where data is limited, the use of multiple hydrograph separation techniques could provide valuable information about shifting water resources. This is critical considering the growing significance of water coming from remote catchments and the role such water plays in the security and management of our water future and sensitive mountain ecosystems.

ENGINEERING SIGNIFICANCE

In remote catchments, collecting detailed spatial information about end-member composition is often not possible due to a variety of reasons such as lack of infrastructure (i.e. roads or research stations), dangers in the watershed like avalanches or wildlife, or even lack of regulatory access and permissions from private or government entities to drill monitoring wells on private or publicly owned land. Because of these barriers to collecting detailed end-member data, this study investigated two different hydrograph separation techniques using two unique end-member characterizations in order to explore the uncertainties associated spatially limited end-member data. Studies such as these are beneficial for the management of local and regional watersheds as they give managers the tools to quantify water resources in data-limited environments which is a critical step for protecting ecologically sensitive rivers and local water supplies.

DATA AVAILABILITY

All data used in the analysis are available through the Lawrence Berkley National Laboratory at https://data.ess-dive.lbl.gov/view/doi:10.21952/WTR/1495380 and https://data.ess-dive.lbl.gov/view/doi:10.15485/1668055. Snow pit data from the Lawrence Berkley National Laboratory will be made available after publication of this work (in review) at https://data.ess-dive.lbl.gov/, along with a data package specific to this project.

REFERENCES

Ali, G. A., Roy, A. G., Turmel, M.-C., & Courchesne, F. (2010). Source-to-stream connectivity assessment through end-member mixing analysis. *Journal of Hydrology*, *392*(3), 119–135. https://doi.org/10.1016/j.jhydrol.2010.07.049

Bales, R.C., Molotch, N.P., Painter, T.H., Dettinger, M. D., Rice, R., & Dozier, J. (2006). Mountain Hydrology of the western United States, *Water Resources Research*, 42(8), https://doi.ord/10.1029/2005WR004387

Barnett, T. P., Adam, J. C., & Lettenmaier, D. P. (2005). Potential impacts of a warming climate on water availability in snow-dominated regions. *Nature*, *438*(7066), 303–309. https://doi.org/10.1038/nature04141

Barthold, F. K., Tyralla, C., Schneider, K., Vaché, K. B., Frede, H.-G., & Breuer, L. (2011). How many tracers do we need for end member mixing analysis (EMMA)? A sensitivity analysis. *Water Resources Research*, *47*(8). https://doi.org/10.1029/2011WR010604

Bearup, L. A., Maxwell, R. M., Clow, D. W., & McCray, J. E. (2014). Hydrological effects of forest transpiration loss in bark beetle-impacted watersheds. *Nature Climate Change*, *4*(6), 481–486. https://doi.org/10.1038/nclimate2198

Berghuijs, W. R., Woods, R. A., & Hrachowitz, M. (2014). A precipitation shift from snow towards rain leads to a decrease in streamflow. *Nature Climate Change*, *4*(7), 583–586. https://doi.org/10.1038/nclimate2246

Brahney, J., Ballantyne, A. P., Sievers, C., & Neff, J. C. (2013). Increasing Ca2+ deposition in the western US: The role of mineral aerosols. *Aeolian Research*, *10*, 77–87. https://doi.org/10.1016/j.aeolia.2013.04.003

Brahney, J., Bothwell, M. L., Capito, L., Gray, C. A., Null, S. E., Menounos, B., & Curtis, P. J. (2020). Glacier recession alters stream water quality characteristics facilitating bloom formation in the benthic diatom Didymosphenia geminata. *Science of The Total Environment*, 142856. https://doi.org/10.1016/j.scitotenv.2020.142856

Brahney, J., Menounos, B., Wei, X., & Curtis, P. J. (2017b). Determining annual cryosphere storage contributions to streamflow using historical hydrometric records. *Hydrological Processes*, *31*(8), 1590–1601. https://doi.org/10.1002/hyp.11128

Brahney, J., Weber, F., Foord, V., Janmaat, J., & Curtis, P. J. (2017a). Evidence for a climate-driven hydrologic regime shift in the Canadian Columbia Basin. *Canadian Water Resources Journal / Revue Canadienne Des Ressources Hydriques*, *42*(2), 179–192. https://doi.org/10.1080/07011784.2016.1268933

Brown, L. E., Hannah, D. M., & Milner, A. M. (2007). Vulnerability of alpine stream biodiversity to shrinking glaciers and snowpacks. *Global Change Biology*, *13*(5), 958–966. https://doi.org/10.1111/j.1365-2486.2007.01341.x

Carroll, R. W. H., Bearup, L. A., Brown, W., Dong, W., Bill, M., & Willlams, K. H. (2018). Factors controlling seasonal groundwater and solute flux from snow-dominated basins. *Hydrological Processes*, *32*(14), 2187–2202. https://doi.org/10.1002/hyp.13151

Carroll, R. W. H., Deems, J. S., Niswonger, R., Schumer, R., & Williams, K. H. (2019). The Importance of Interflow to Groundwater Recharge in a Snowmelt-Dominated Headwater Basin. *Geophysical Research Letters*, *46*(11), 5899–5908. https://doi.org/10.1029/2019GL082447

Cayuela, C., Latron, J., Geris, J., & Llorens, P. (2019). Spatio-temporal variability of the isotopic input signal in a partly forested catchment: Implications for hydrograph separation. *Hydrological Processes*, *33*(1), 36–46. https://doi.org/10.1002/hyp.13309

Christophersen, N., & Hooper, R. P. (1992). Multivariate analysis of stream water chemical data: The use of principal components analysis for the end-member mixing problem. *Water Resources Research*, *28*(1), 99–107. https://doi.org/10.1029/91WR02518

Christophersen, N., Neal, C., Hooper, R. P., Vogt, R. D., & Andersen, S. (1990). Modelling streamwater chemistry as a mixture of soilwater end-members—A step towards second-generation acidification models. *Journal of Hydrology*, *116*(1), 307–320. https://doi.org/10.1016/0022-1694(90)90130-P

Clow, D. W. (2010). Changes in the timing of snowmelt and streamflow in Colorado: A response to recent warming. *Journal of Climate*, *23*(9), 2293–2306. USGS Publications Warehouse. https://doi.org/10.1175/2009JCLI2951.1

Clow, D. W., Williams, M. W., & Schuster, P. F. (2016). Increasing aeolian dust deposition to snowpacks in the Rocky Mountains inferred from snowpack, wet deposition, and aerosol chemistry. *Atmospheric Environment*, *146*, 183–194. https://doi.org/10.1016/j.atmosenv.2016.06.076

Davis, J. (2002). *Statistics and Data Analysis in Geology* (3rd ed.). John Wiley & Sons, INC.

Draper, N. R., & Smith, H. (1981). *Applied Regression Analysis* (2nd ed.). John Wiley & Sons, INC.

Feng, X., Taylor, S., Renshaw, C. E., & Kirchner, J. W. (2002). Isotopic evolution of snowmelt 1. A physically based one-dimensional model. *Water Resources Research*, *38*(10), 35-1-35–38. https://doi.org/10.1029/2001WR000814

Foks, S. S., Raffensperger, J. P., Penn, C. A., & Driscoll, J. M. (2019). Estimation of Base Flow by Optimal Hydrograph Separation for the Conterminous United States and Implications for National-Extent Hydrologic Models. *Water*, *11*(8), 1629. https://doi.org/10.3390/w11081629

Foster, L. M., Bearup, L. A., Molotch, N. P., Brooks, P. D., & Maxwell, R. M. (2016). Energy budget increases reduce mean streamflow more than snow–rain transitions: Using integrated modeling to isolate climate change impacts on Rocky Mountain hydrology. *Environmental Research Letters*, *11*(4), 044015. https://doi.org/10.1088/1748-9326/11/4/044015

Freeze, R.A. (1974). Streamflow generation, Rev. Geophys. and Space Physics, 12(4), 627-647.

Gaskill, D. L., Mutschler, F. E., Kramer, J. H., Thomas, J. A., & Zahony, S. G. (1991). *Geologic Map of the Gothic quandrangle (GQ-1689)* [Map]. USGS. https://ngmdb.usgs.gov/Prodesc/proddesc_1199.htm

Genereux, D., & Hooper, R. (1998). *Chapter 10 – Oxygen and Hydrogen Isotopes in Rainfall-Runoff Studies*. https://doi.org/10.1016/B978-0-444-81546-0.50017-3

Godsey, S. E., Kirchner, J. W., & Clow, D. W. (2009). Concentration–discharge relationships reflect chemostatic characteristics of US catchments. *Hydrological Processes*, *23*(13), 1844–1864. https://doi.org/10.1002/hyp.7315

Hamlet, A. F., Mote, P. W., Clark, M. P., & Lettenmaier, D. P. (2005). Effects of Temperature and Precipitation Variability on Snowpack Trends in the Western United States. *Journal of Climate*, *18*(21), 4545–4561. https://doi.org/10.1175/JCLI3538.1

Hock, R., Rasul, C., Adler, C., Cáceres, B., Gruber, S., Hirabayashi, Y., Jackson, M., Kääb, A., Kang, S., Kutuzov, S., Milner, A., Molau, U., Morin, S., Orlove, B., & Steltzer, H. (2019). *High Mountain Areas. In: IPCC Special Report on the Ocean*

and Cryosphere in a Changing Climate. IPCC. https://www.ipcc.ch/srocc/chapter/chapter-2/

Hooper, R. P. (2003). Diagnostic tools for mixing models of stream water chemistry. *Water Resources Research*, *39*(3). https://doi.org/10.1029/2002WR001528

Hooper, R. P., Christophersen, N., & Peters, N. E. (1990). Modelling streamwater chemistry as a mixture of soilwater end-members—An application to the Panola Mountain catchment, Georgia, U.S.A. *Journal of Hydrology*, *116*(1), 321–343. https://doi.org/10.1016/0022-1694(90)90131-G

Hotaling, S., Hood, E., & Hamilton, T. L. (2017). Microbial ecology of mountain glacier ecosystems: Biodiversity, ecological connections and implications of a warming climate. *Environmental Microbiology*, *19*(8), 2935–2948. https://doi.org/10.1111/1462-2920.13766

Hubbard, S. S., Williams, K. H., Agarwal, D., Banfield, J., Beller, H., Bouskill, N., Brodie, E., Carroll, R., Dafflon, B., Dwivedi, D., Falco, N., Faybishenko, B., Maxwell, R., Nico, P., Steefel, C., Steltzer, H., Tokunaga, T., Tran, P. A., Wainwright, H., & Varadharajan, C. (2018). The East River, Colorado, Watershed: A Mountainous Community Testbed for Improving Predictive Understanding of Multiscale Hydrological–Biogeochemical Dynamics. *Vadose Zone Journal*, *17*(1), 180061. https://doi.org/10.2136/vzj2018.03.0061

Huning, L. S., & AghaKouchak, A. (2018). Mountain snowpack response to different levels of warming. *Proceedings of the National Academy of Sciences*, *115*(43), 10932–10937. https://doi.org/10.1073/pnas.1805953115

James, A. L., & Roulet, N. T. (2009). Antecedent moisture conditions and catchment morphology as controls on spatial patterns of runoff generation in small forest catchments. *Journal of Hydrology*, *377*(3), 351–366. https://doi.org/10.1016/j.jhydrol.2009.08.039

Jenkins, A., Ferrier, R. C., Harriman, R., & Ogunkoya, Y. O. (1994). A case study in catchment hydrochemistry: Conflicting interpretations from hydrological and chemical observations. *Hydrological Processes*, *8*(4), 335–349. https://doi.org/10.1002/hyp.3360080406

Kiewiet, L., Meerveld, I. van, & Seibert, J. (2020). Effects of Spatial Variability in the Groundwater Isotopic Composition on Hydrograph Separation Results for a Pre-Alpine Headwater Catchment. *Water Resources Research*, *56*(7), e2019WR026855. https://doi.org/10.1029/2019WR026855

Klaus, J., & McDonnell, J. J. (2013). Hydrograph separation using stable isotopes: Review and evaluation. *Journal of Hydrology*, *505*, 47–64. https://doi.org/10.1016/j.jhydrol.2013.09.006

Knowles, N., Dettinger, M. D., & Cayan, D. R. (2006). Trends in Snowfall versus Rainfall in the Western United States. *Journal of Climate*, *19*(18), 4545–4559. https://doi.org/10.1175/JCLI3850.1

Kopytkovskiy, M., Geza, M., & McCray, J. E. (2015). Climate-change impacts on water resources and hydropower potential in the Upper Colorado River Basin. *Journal of Hydrology: Regional Studies*, *3*, 473–493. https://doi.org/10.1016/j.ejrh.2015.02.014

Ladouche, B., Probst, A., Viville, D., Idir, S., Baqué, D., Loubet, M., Probst, J.-L., & Bariac, T. (2001). Hydrograph separation using isotopic, chemical and hydrological approaches (Strengbach catchment, France). *Journal of Hydrology*, *2*(3–4), 255–274.

Lawrence, C. R., Painter, T. H., Landry, C. C., & Neff, J. C. (2010). Contemporary geochemical composition and flux of aeolian dust to the San Juan Mountains, Colorado, United States. *Journal of Geophysical Research: Biogeosciences*, *115*(G3). https://doi.org/10.1029/2009JG001077

Li, D., Wrzesien, M. L., Durand, M., Adam, J., & Lettenmaier, D. P. (2017). How much runoff originates as snow in the western United States, and how will that change in the future? *Geophysical Research Letters*, *44*(12), 6163–6172. https://doi.org/10.1002/2017GL073551

Liu, F., Conklin, M. H., & Shaw, G. D. (2017). Insights into hydrologic and hydrochemical processes based on concentration-discharge and end-member mixing analyses in the mid-Merced River Basin, Sierra Nevada, California. *Water Resources Research*, *53*(1), 832–850. https://doi.org/10.1002/2016WR019437

Liu, F., Williams, M. W., & Caine, N. (2004). Source waters and flow paths in an alpine catchment, Colorado Front Range, United States. *Water Resources Research*, *40*(9). https://doi.org/10.1029/2004WR003076

Miller, M. P., Susong, D. D., Shope, C. L., Heilweil, V. M., & Stolp, B. J. (2014). Continuous estimation of baseflow in snowmelt-dominated streams and rivers in the Upper Colorado River Basin: A chemical hydrograph separation approach. *Water Resources Research*, *50*(8), 6986–6999. https://doi.org/10.1002/2013WR014939

Mote, P. W., Hamlet, A. F., Clark, M. P., & Lettenmaier, D. P. (2005). Declining Mountain Snowpack in Western North America. *Bulletin of the American Meteorological Society*, *86*(1), 39–50. https://doi.org/10.1175/BAMS-86-1-39

Mote, P. W., Li, S., Lettenmaier, D. P., Xiao, M., & Engel, R. (2018). Dramatic declines in snowpack in the western US. *Npj Climate and Atmospheric Science*, *1*(1), 1–6. https://doi.org/10.1038/s41612-018-0012-1

Painter, T. H., Barrett, A. P., Landry, C. C., Neff, J. C., Cassidy, M. P., Lawrence, C. R., McBride, K. E., & Farmer, G. L. (2007). Impact of disturbed desert soils on duration of mountain snow cover. *Geophysical Research Letters*, *34*(12). https://doi.org/10.1029/2007GL030284

Painter, T. H., Deems, J. S., Belnap, J., Hamlet, A. F., Landry, C. C., & Udall, B. (2010). Response of Colorado River runoff to dust radiative forcing in snow. *Proceedings of the National Academy of Sciences*, *107*(40), 17125–17130. https://doi.org/10.1073/pnas.0913139107

Penna, D., & Meerveld, H. J. (Ilja) van. (2019). Spatial variability in the isotopic composition of water in small catchments and its effect on hydrograph separation. *WIREs Water*, *6*(5), e1367. https://doi.org/10.1002/wat2.1367

Pinder, G. F., & Jones, J. F. (1969). Determination of the ground-water component of peak discharge from the chemistry of total runoff. *Water Resources Research*, *5*(2), 438–445. https://doi.org/10.1029/WR005i002p00438

PRISM Climate Group, Oregon State University, http://prism.oregonstate.edu, created 4 Feb 2021

Qin, Y., Abatzoglou, J. T., Siebert, S., Huning, L. S., AghaKouchak, A., Mankin, J. S., Hong, C., Tong, D., Davis, S. J., & Mueller, N. D. (2020). Agricultural risks from changing snowmelt. *Nature Climate Change*, *10*(5), 459–465. https://doi.org/10.1038/s41558-020-0746-8

Skiles, S. M., Painter, T. H., Belnap, J., Holland, L., Reynolds, R. L., Goldstein, H. L., & Lin, J. (2015). Regional variability in dust-on-snow processes and impacts in the Upper Colorado River Basin. *Hydrological Processes*, *29*(26), 5397–5413. https://doi.org/10.1002/hyp.10569

Skiles, S. M., Painter, T. H., Deems, J. S., Bryant, A. C., & Landry, C. C. (2012). Dust radiative forcing in snow of the Upper Colorado River Basin: 2. Interannual variability in radiative forcing and snowmelt rates. *Water Resources Research*, *48*(7). https://doi.org/10.1029/2012WR011986

Sklash, M. G., & Farvolden, R. N. (1979). The role of groundwater in storm runoff. *Journal of Hydrology*, *43*(1), 45–65. https://doi.org/10.1016/0022-1694(79)90164-1

Stewart, I. T., Cayan, D. R., & Dettinger, M. D. (2005). Changes toward Earlier Streamflow Timing across Western North America. *Journal of Climate*, *18*(8), 1136–1155. https://doi.org/10.1175/JCLI3321.1

Sueker, J. K., Ryan, J. N., Kendall, C., & Jarrett, R. D. (2000). Determination of hydrologic pathways during snowmelt for alpine/subalpine basins, Rocky Mountain National Park, Colorado. *Water Resources Research*, *36*(1), 63–75. https://doi.org/10.1029/1999WR900296

Wels, C., Cornett, R. J., & Lazerte, B. D. (1991). Hydrograph separation: A comparison of geochemical and isotopic tracers. *Journal of Hydrology*, *122*(1), 253–274. https://doi.org/10.1016/0022-1694(91)90181-G

Williams, M. W., Seibold, C., & Chowanski, K. (2009). Storage and release of solutes from a subalpine seasonal snowpack: Soil and stream water response, Niwot Ridge, Colorado. *Biogeochemistry*, *95*(1), 77–94. https://doi.org/10.1007/s10533-009-9288-x

APPENDICES

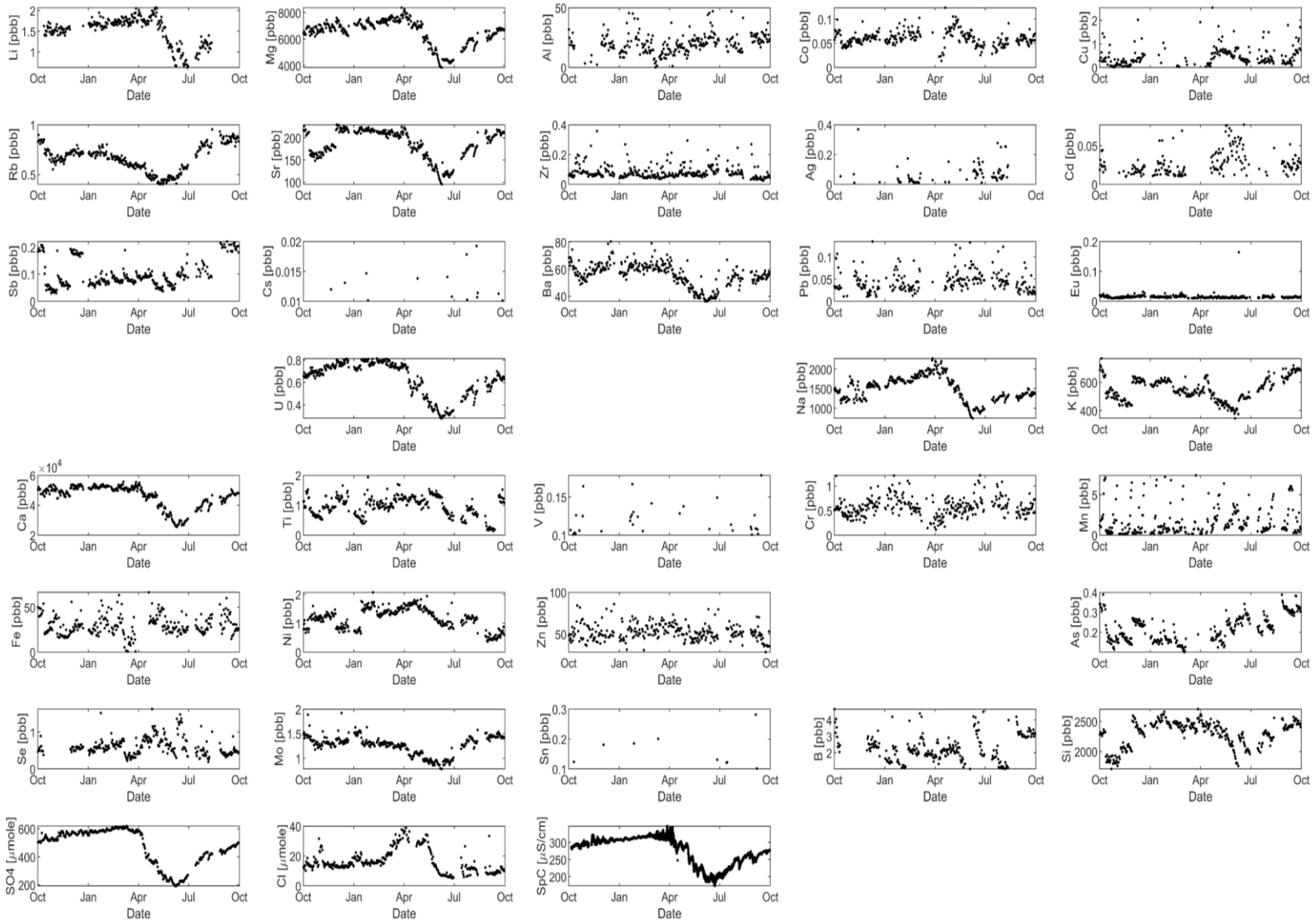

Figure A1. Times series of all solutes analyzed for the 2016 WY

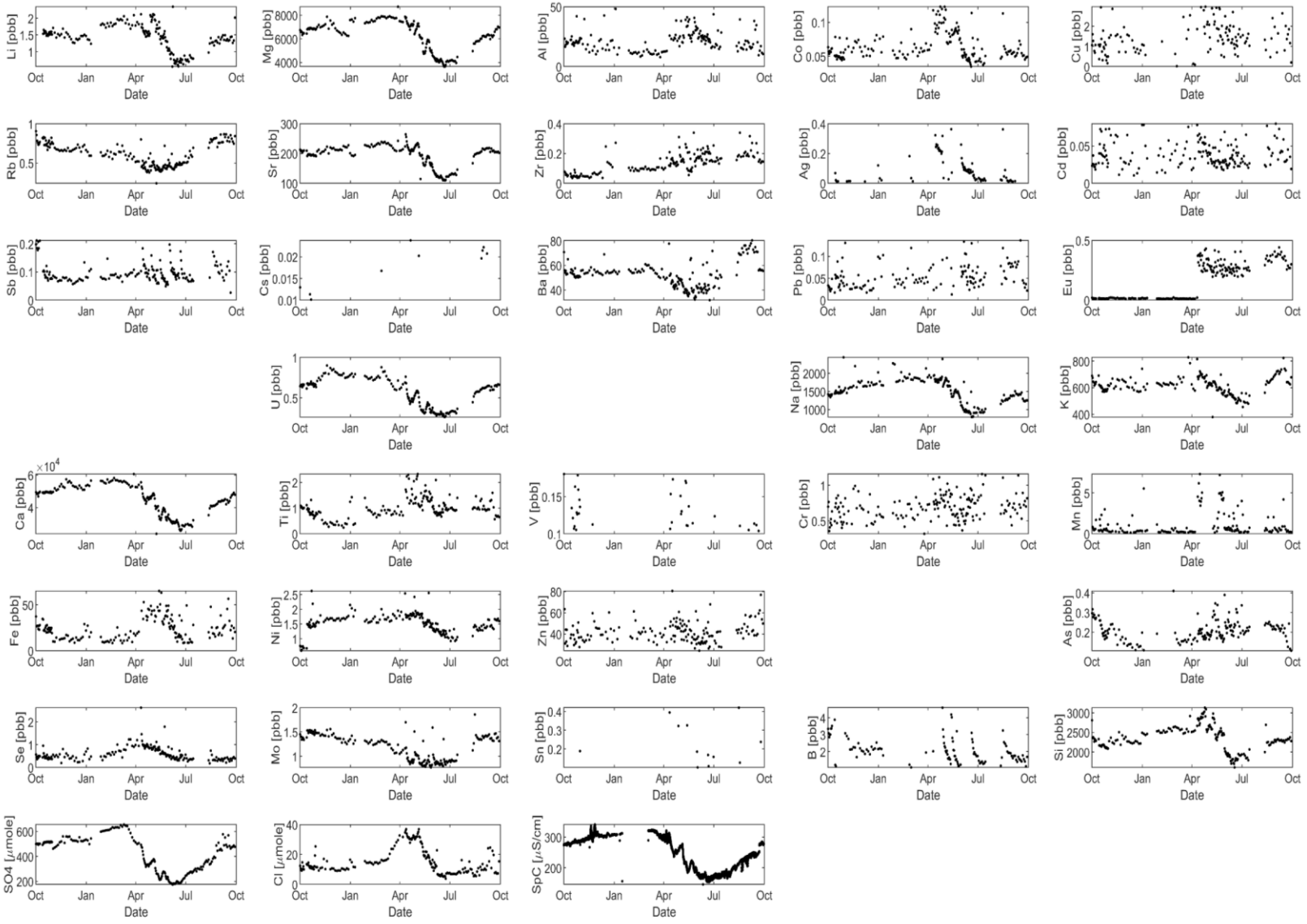

Figure A2. Time series of all solutes analyzed for the 2017 WY

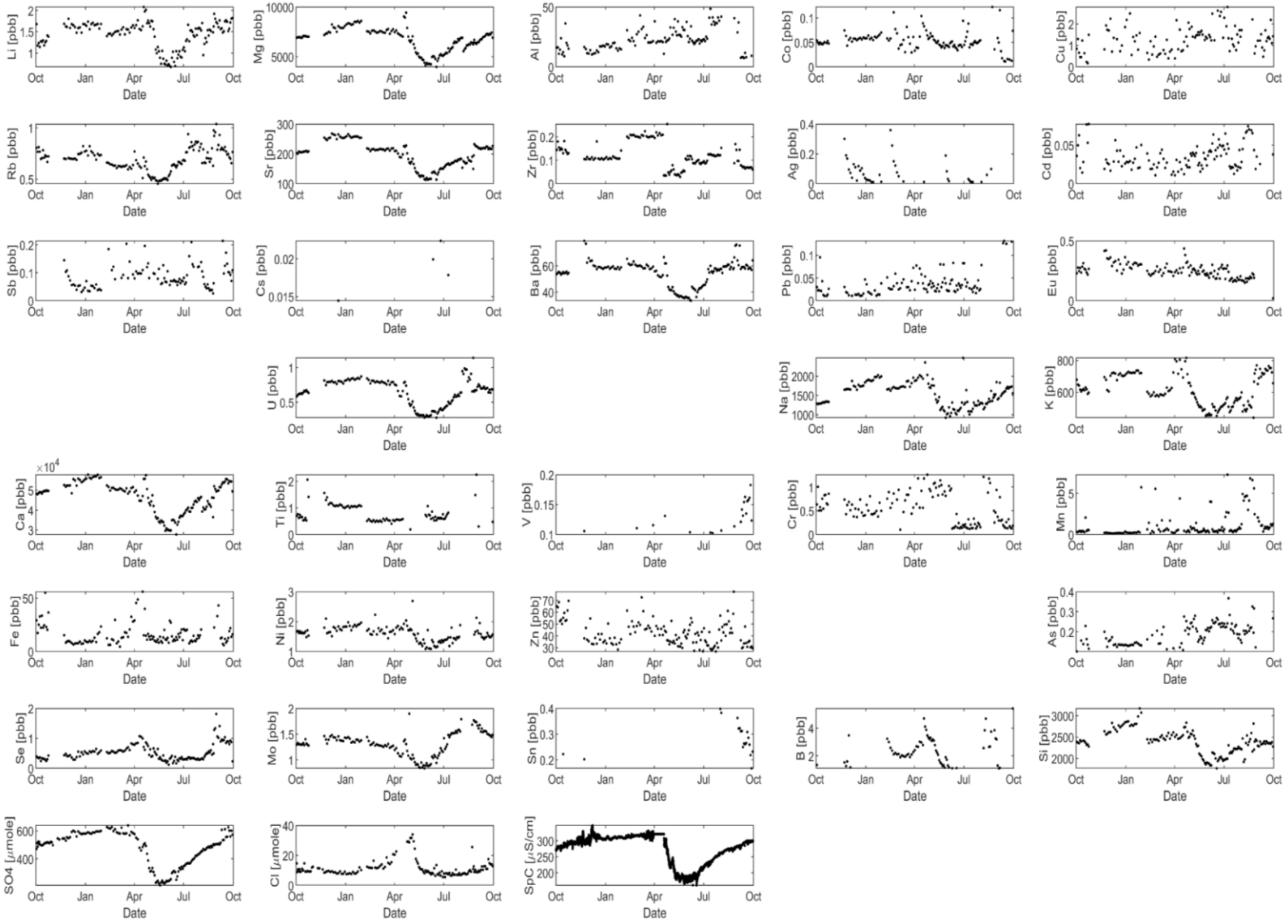

Figure A3. Time series of all solutes analyzed for the 2018 WY

Table A1. Solutes that met flow criteria as defined by Table 1.

	2015-16			2016-17			2017-18		
Solute	Slope	R^2	RMSE	Slope	R^2	RMSE	Slope	R^2	RMSE
Al	Poor	Poor	Poor	Poor	Poor	Poor	Poor	Poor	Poor
As	Poor	Poor	Poor	Poor	Poor	Poor	Poor	Poor	Poor
Be	Poor	Poor	Poor	Poor	Poor	Poor	Poor	Poor	Poor
Ba	Poor	Moderate	Moderate	Poor	Poor	Poor	Moderate	Best	Moderate
Ca	Moderate	Best	Best	Moderate	Best	Best	Poor	Moderate	Moderate
Cd	Best	Poor	Poor	Poor	Poor	Poor	Poor	Poor	Poor
Cl	Poor	Poor	Poor	Poor	Poor	Poor	Poor	Poor	Poor
Co	Poor	Poor	Poor	Poor	Poor	Poor	Poor	Poor	Poor
Cr	Poor	Poor	Poor	Poor	Poor	Poor	Poor	Poor	Poor
Cu	Best	Poor	Poor	Moderate	Poor	Poor	Moderate	Poor	Poor
Eu	Poor	Poor	Poor	Best	Poor	Poor	Poor	Poor	Poor
Fe	Poor	Poor	Poor	Poor	Poor	Poor	Poor	Poor	Poor
K	Poor	Poor	Poor	Poor	Poor	Poor	Poor	Poor	Poor
Li	Moderate	Poor	Poor	Moderate	Poor	Poor	Moderate	Poor	Poor
Mg	Poor	Moderate	Moderate	Poor	Moderate	Poor	Poor	Poor	Poor
Mn	Best	Poor	Poor	Best	Poor	Poor	Poor	Poor	Poor
Mo	Poor	Poor	Moderate	Poor	Moderate	Poor	Poor	Poor	Poor
Na	Poor	Poor	Poor	Poor	Poor	Poor	Poor	Poor	Poor
Ni	Poor	Poor	Poor	Poor	Poor	Poor	Poor	Poor	Poor
Pb	Moderate	Poor	Poor	Poor	Poor	Poor	Poor	Poor	Poor
Rb	Poor	Poor	Poor	Poor	Poor	Poor	Poor	Poor	Poor
Sb	Poor	Poor	Poor	Poor	Poor	Poor	Poor	Poor	Poor
Se	Poor	Poor	Poor	Poor	Poor	Poor	Moderate	Poor	Poor
Si	Poor	Poor	Moderate	Poor	Poor	Poor	Poor	Poor	Poor
SO4	Best	Best	Best	Best	Best	Best	Best	Best	Best
Sr	Moderate	Best	Moderate	Poor	Poor	Moderate	Moderate	Best	Poor
Ti	Poor	Poor	Poor	Poor	Poor	Poor	Poor	Poor	Poor
U	Best	Best	Moderate	Best	Best	Best	Best	Best	Poor
Zn	Poor	Poor	Poor	Poor	Poor	Poor	Poor	Poor	Poor
Zr	Poor	Poor	Poor	Best	Poor	Poor	Best	Poor	Poor
SpC	Poor	Best	Best	Moderate	Best	Best	Moderate	Best	Best

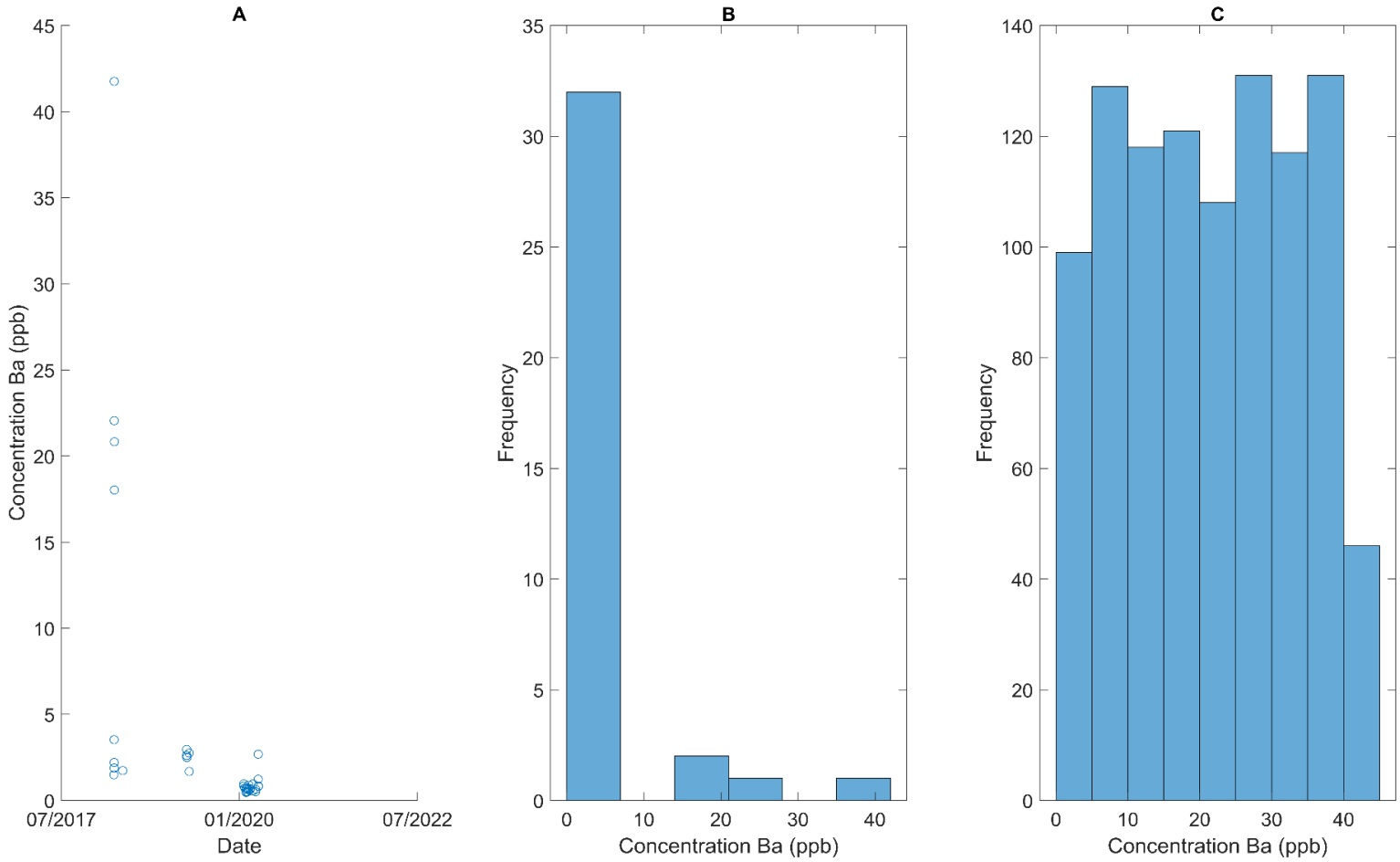

Figure A4. (A) Time series of composite barium snow field samples. (B) Distribution of composite barium snow field samples. (C). Distribution of the 1000 randomly generated samples based on the minimum and max. Plot C represents the sampled distribution for the hydrograph separation using measured end-members

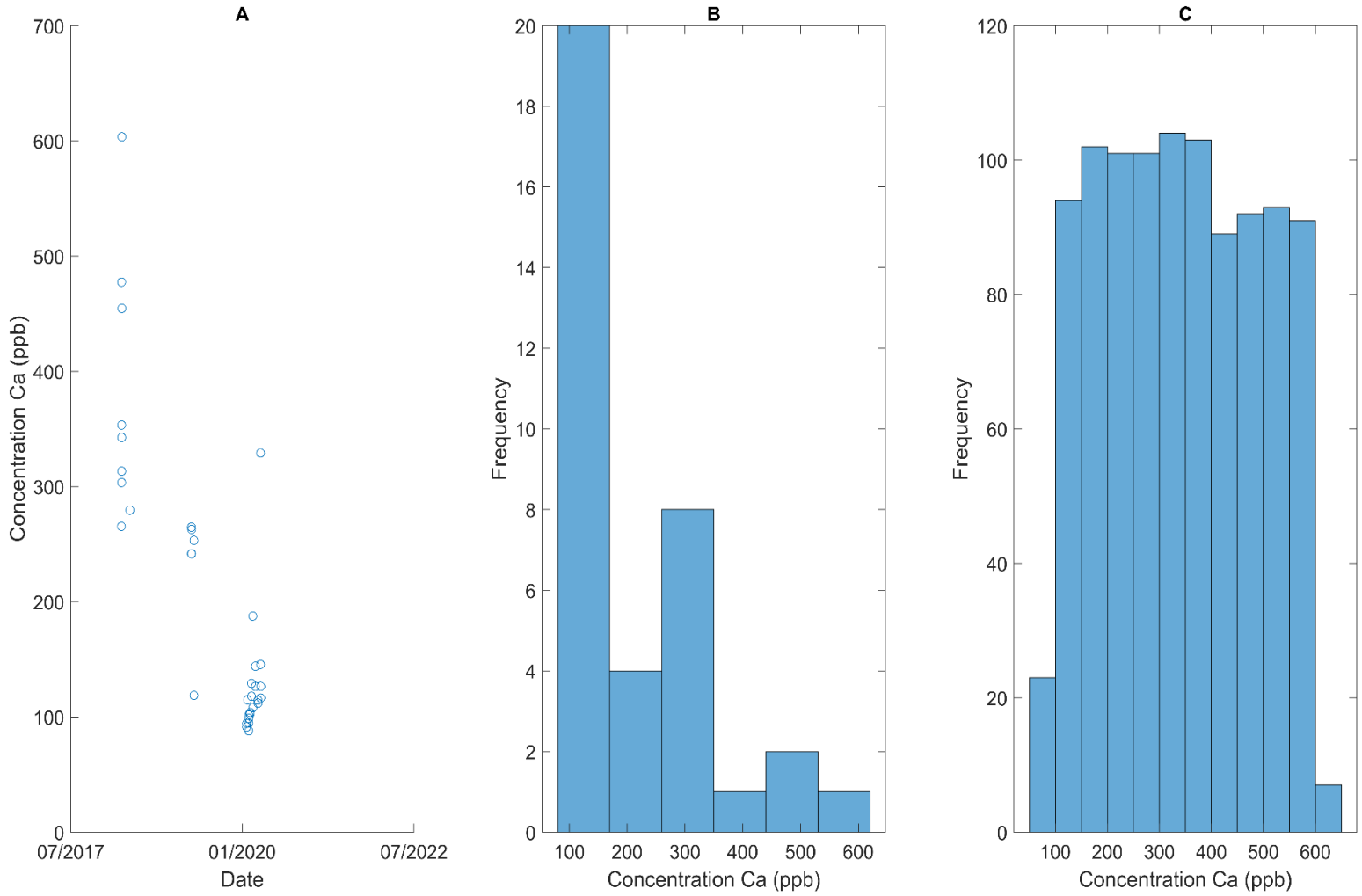

Figure A5. (A) time series of composite calcium snow field samples. (B) Distribution of composite calcium snow field samples. (C). Distribution of the 1000 randomly generated samples based on the minimum and max. Plot C represents the sampled distribution for the hydrograph separation using measured end-members

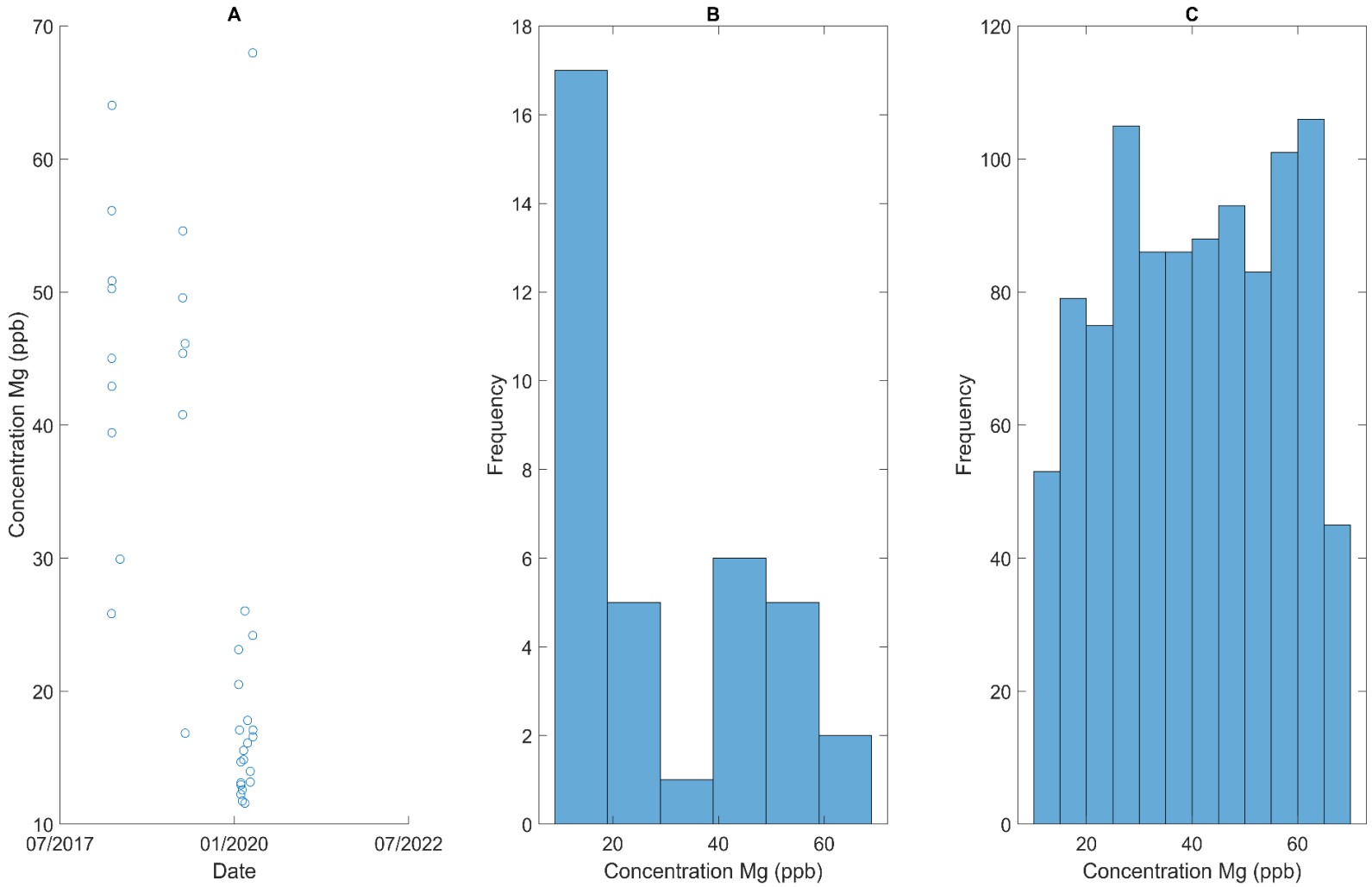

Figure A6. (A) time series of composite magnesium snow field samples. (B) Distribution of composite magnesium snow field samples. (C). Distribution of the 1000 randomly generated samples based on the minimum and max. Plot C represents the sampled distribution for the hydrograph separation using measured end-members

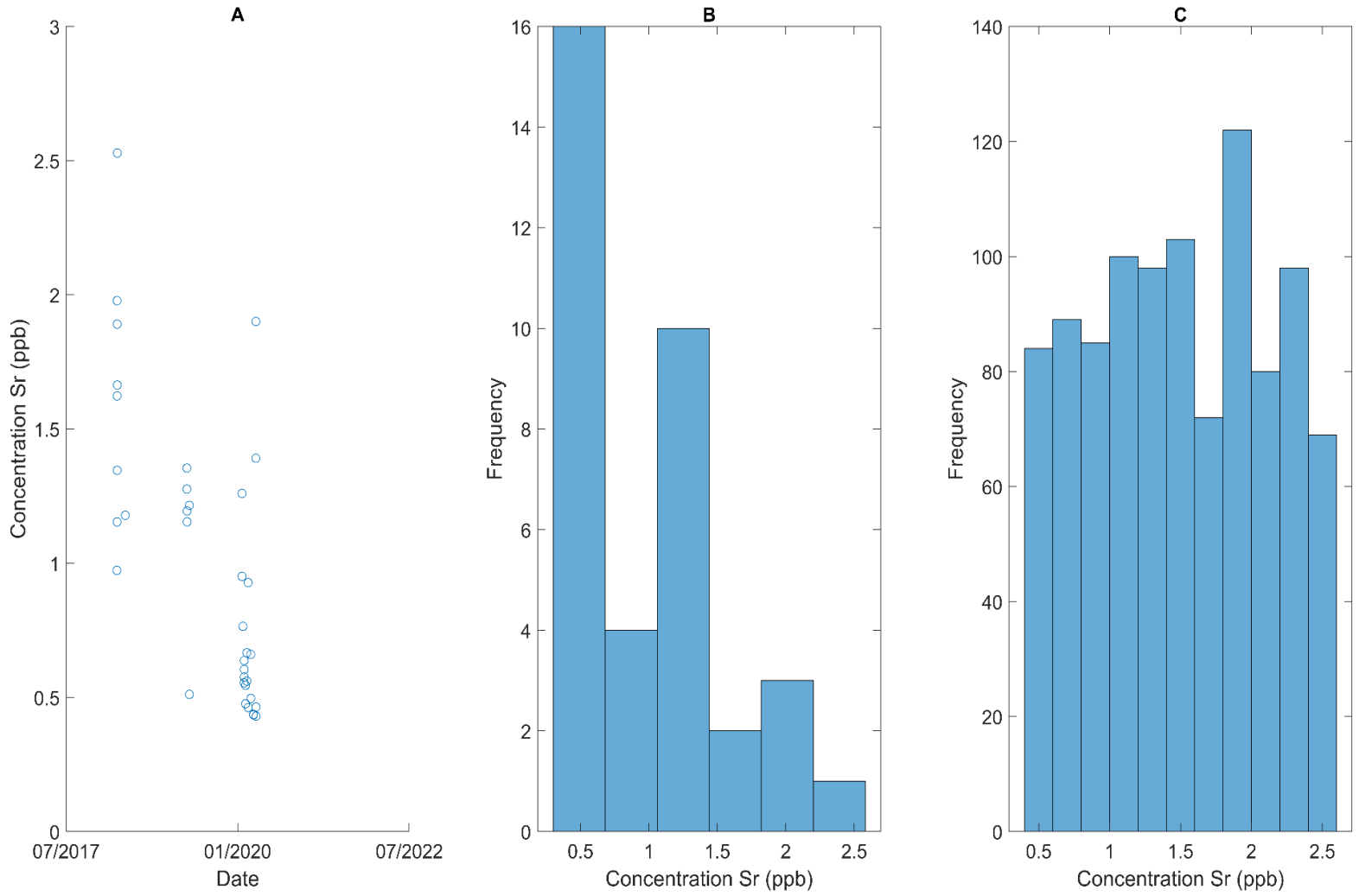

Figure A7. (A) time series of composite strontium snow field samples. (B) Distribution of composite strontium snow field samples. (C). Distribution of the 1000 randomly generated samples based on the minimum and max. Plot C represents the sampled distribution for the hydrograph separation using measured end-members

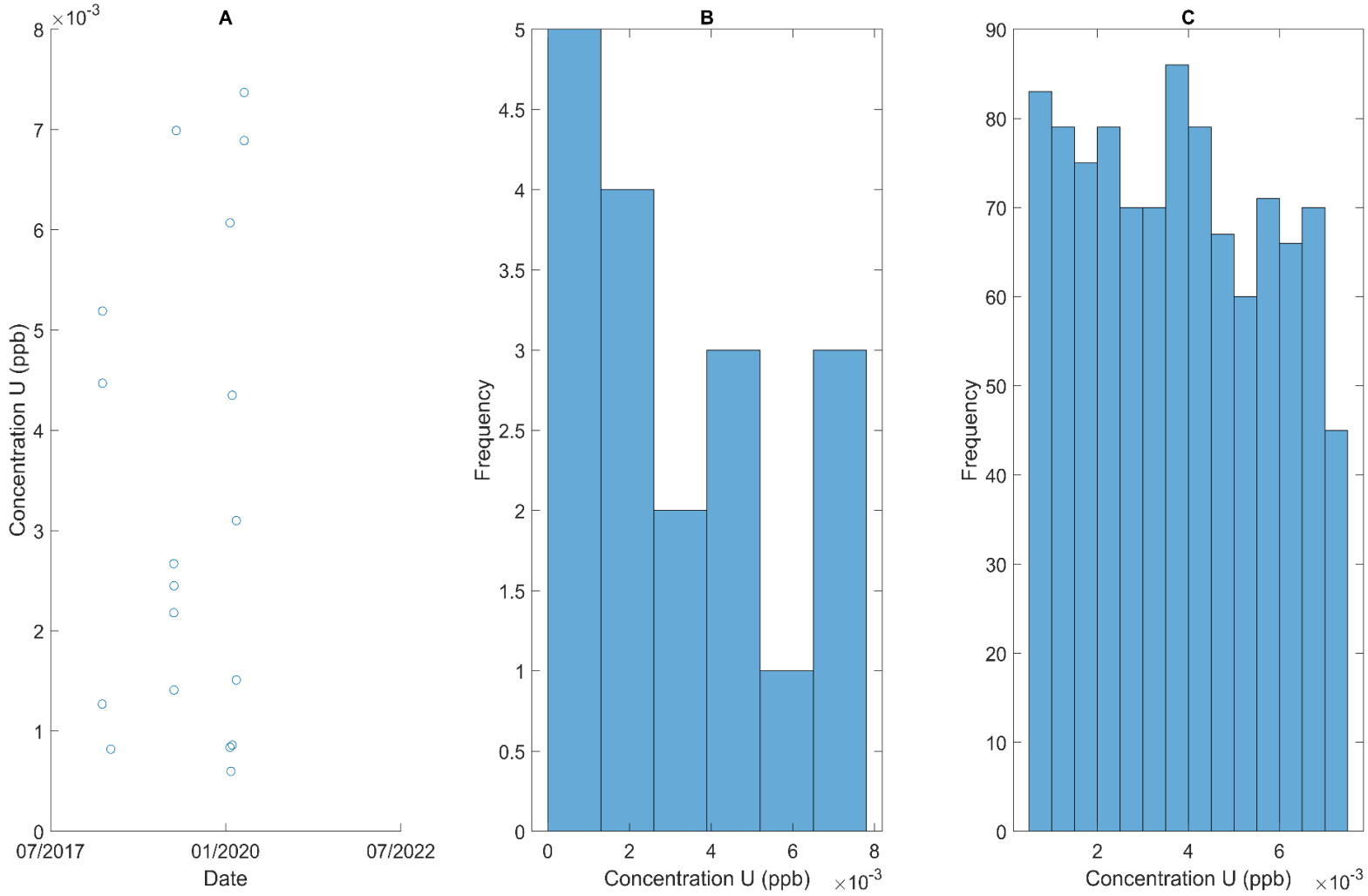

Figure A8. (A) time series of composite uranium snow field samples. (B) Distribution of composite uranium snow field samples. (C). Distribution of 1000 randomly generated samples based on the minimum and max. Plot C represents the sampled distribution for the hydrograph separation using measured end-members

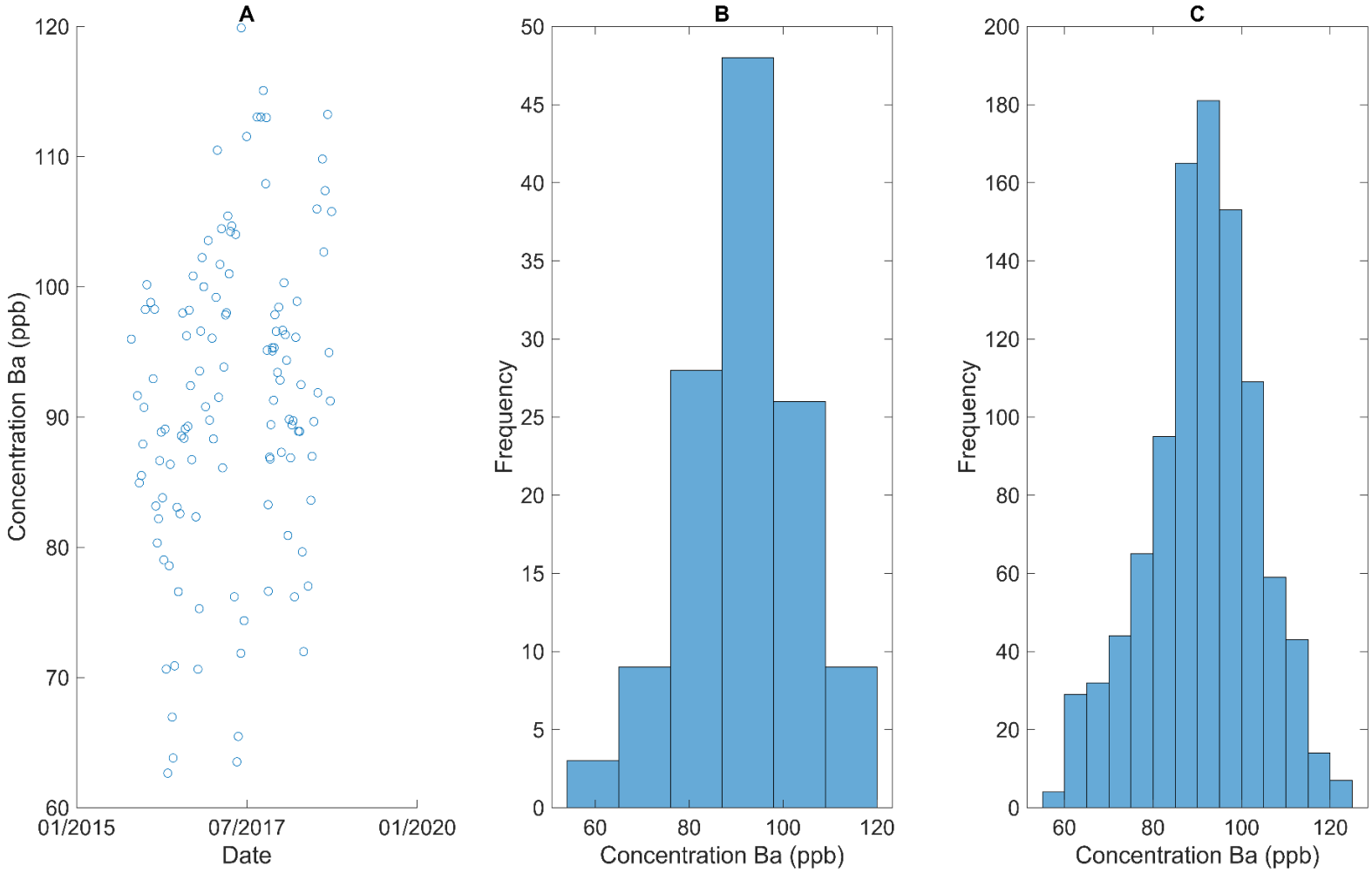

Figure A9. (A) Time series of barium groundwater field samples. (B) Distribution of barium groundwater field samples. (C). Distribution of the 1000 randomly generated samples based on the distribution inherent to the solute set. Plot C represents the sampled distribution for the hydrograph separation using measured end-members

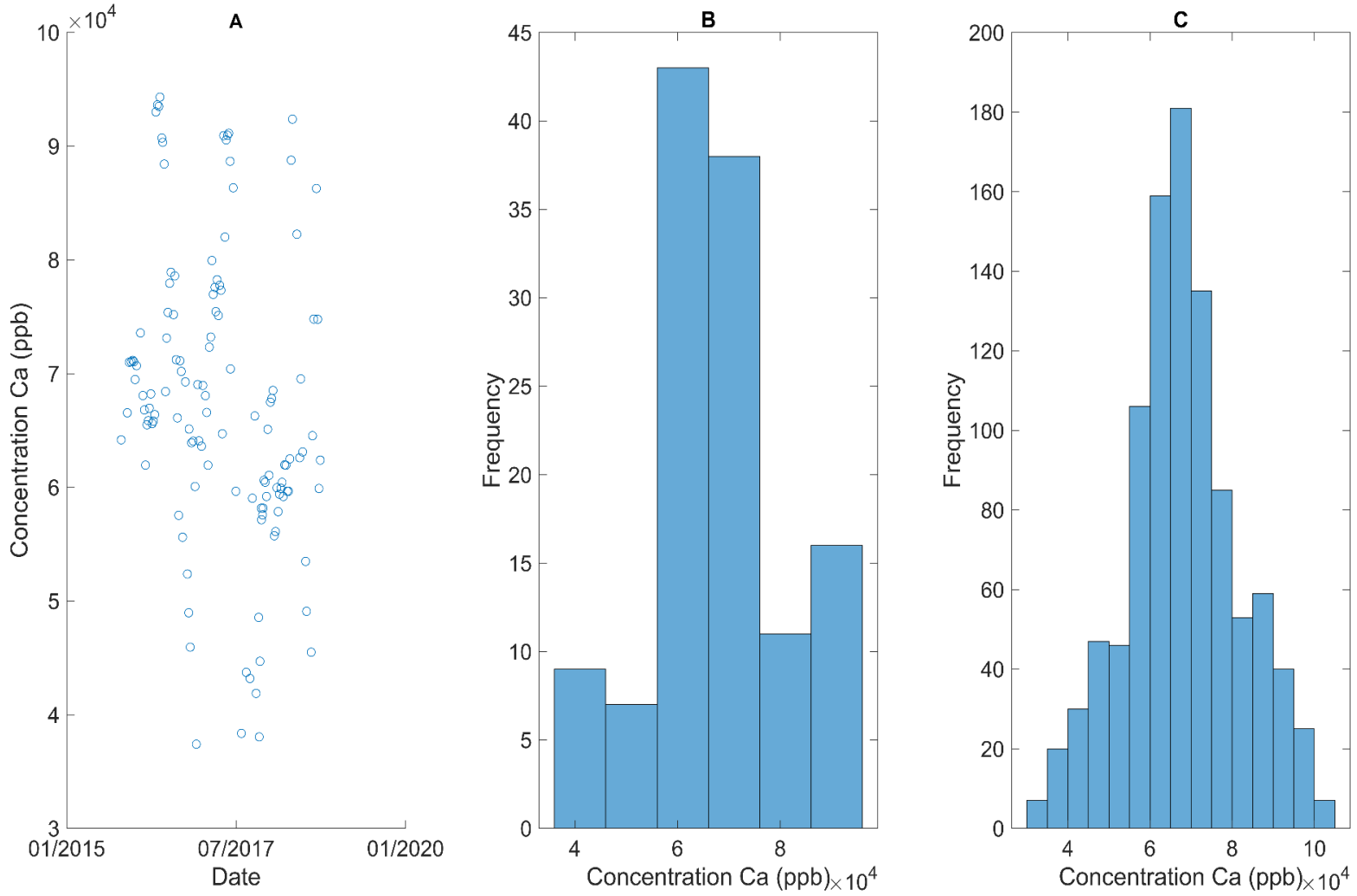

Figure A10. (A) Time series of calcium groundwater field samples. (B) Distribution of calcium groundwater field samples. (C). Distribution of the 1000 randomly generated samples based on the distribution inherent to the solute set. Plot C represents the sampled distribution for the hydrograph separation using measured end-members

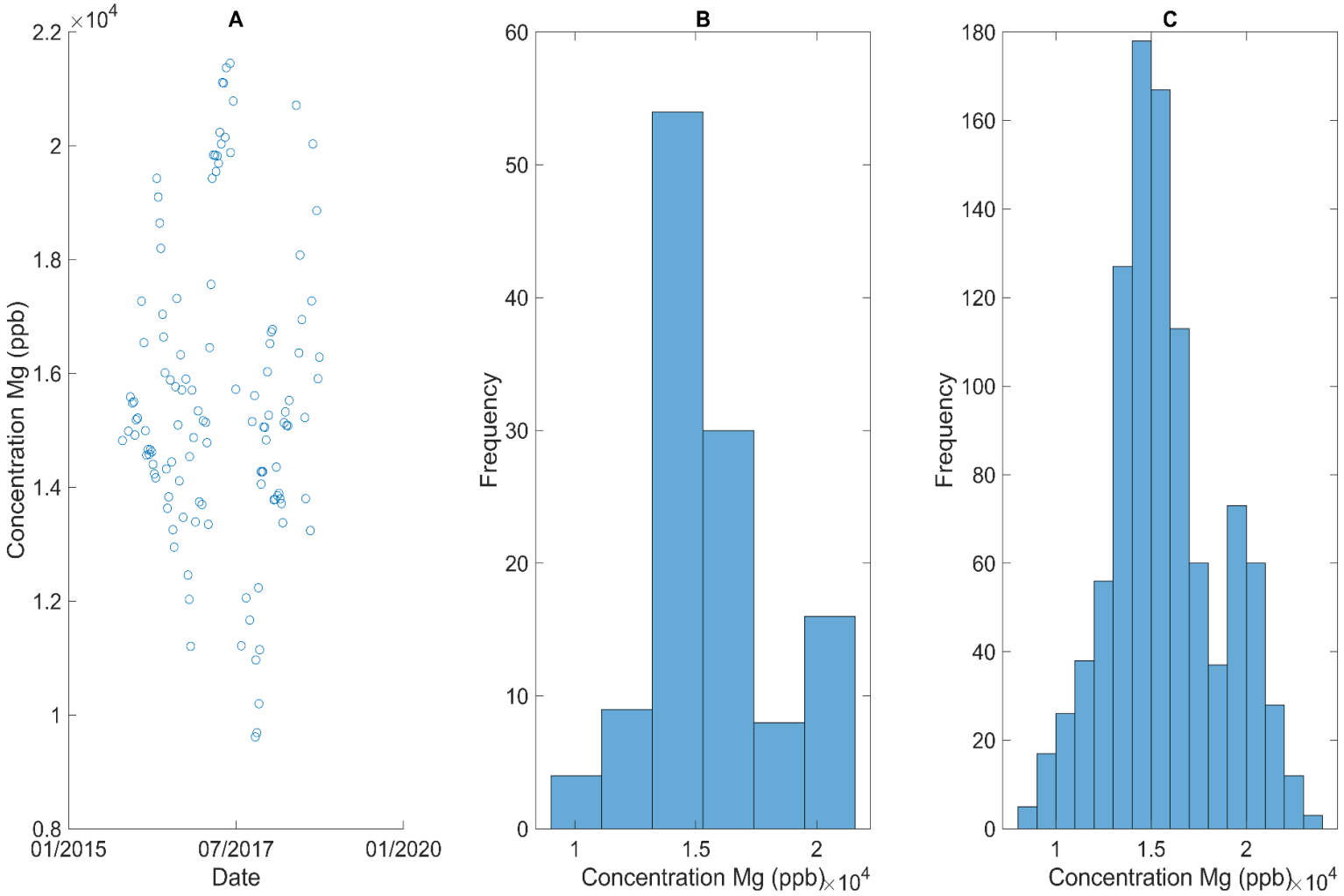

Figure A11. (A) Time series of magnesium groundwater field samples. (B) Distribution of magnesium groundwater field samples. (C). Distribution of the 1000 randomly generated samples based on the distribution inherent to the solute set. Plot C represents the sampled distribution for the hydrograph separation using measured end-members

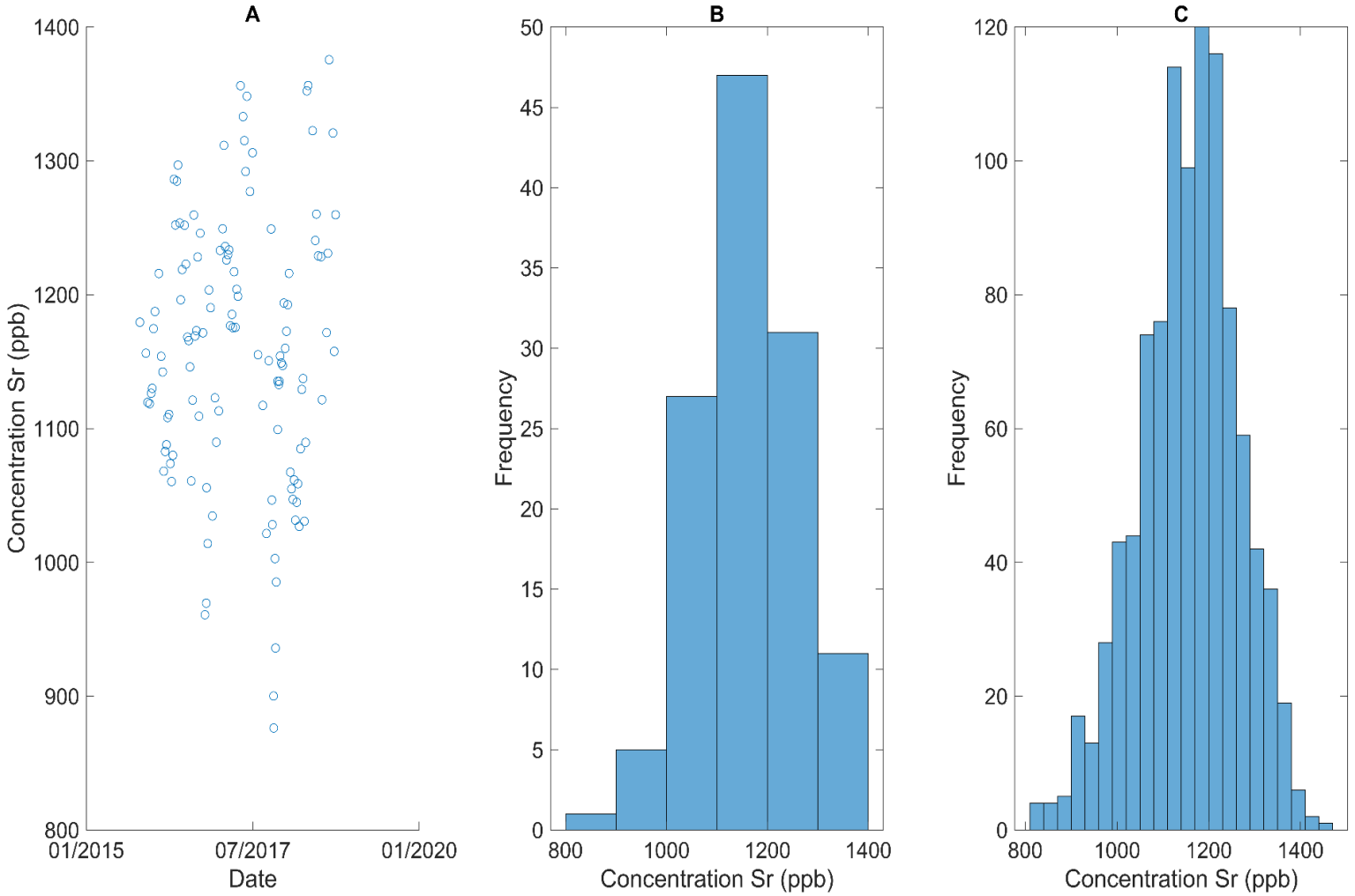

Figure A12. (A) Time series of strontium groundwater field samples. (B) Distribution of strontium groundwater field samples. (C). Distribution of the 1000 randomly generated samples based on the distribution inherent to the solute set. Plot C represents the sampled distribution for the hydrograph separation using measured end-members

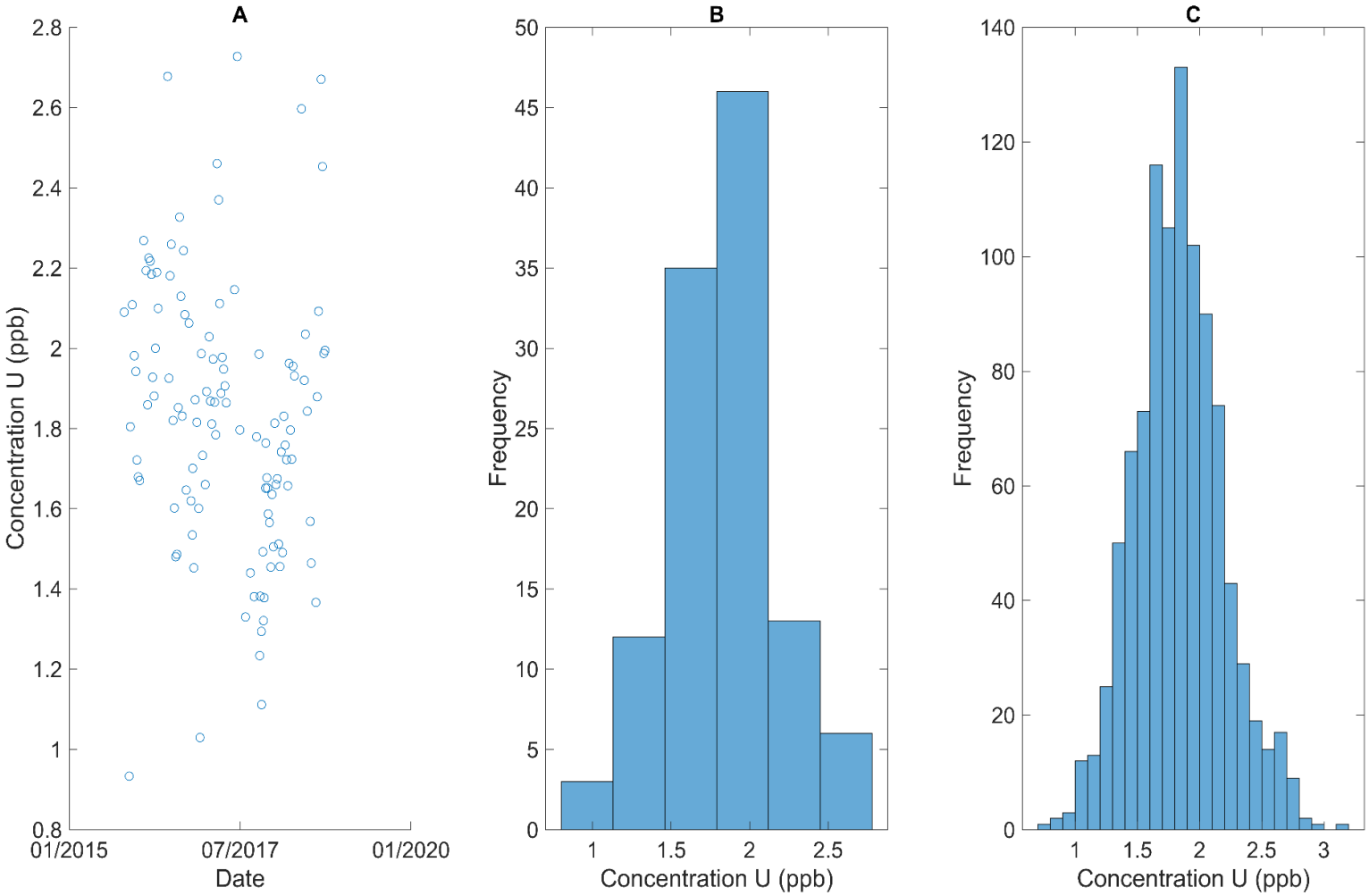

Figure A13. (A) Time series of uranium groundwater field samples. (B) Distribution of uranium groundwater field samples. (C). Distribution of 1000 randomly generated samples based on the distribution inherent to the solute set. Plot C represents the sampled distribution for the hydrograph separation using measured end-members

Equations

To begin the statistically-based method of hydrograph separation, the set of solutes selected from criteria in Table 1 were placed into a *i* x *j* matrix where *i* represents the sample number and *j* represents the solute. The data were standardized by calculating the z-scores as

$$\frac{C_{ij} - \overline{C_j}}{s_j} = x_{ij} \tag{A1}$$

where C_{ij} represents the instream concentration of the i^{th} element of the j^{th} solute, $\overline{C_j}$ represents the average of the j^{th} solute, s_j represents the standard deviation of the j^{th} solute, and x_{ij} represents the standardized i^{th} element of the j^{th} solute. All x_{ij} formed the standardized solute matrix, $\boldsymbol{X}$. Standardization was needed so that the order of magnitude of the data and the units of the data set did not significantly affect the final PCA. However, the scaling of the data due to standardization may have slightly altered the variation of the high-order and low-order of magnitude data (Davis, 2002). The end-members were also standardized to the instream data as

$$\frac{b_{ij}^n - \overline{C_j}}{s_j} = B_{ij}^n \tag{A2}$$

where b_{ij}^n represents the n^{th} end-member concentration of the i^{th} element of the j^{th} solute and B_{ij}^n represents the standardized i^{th} element of the j^{th} solute of the n^{th} end-member. All B_{ij}^n formed the standardized n^{th} end-member matrix, $\boldsymbol{B}^n$.

The correlation matrix, $\boldsymbol{A}$, is then computed from $\boldsymbol{X}$ and the eigenstuff is found by solving

$$\boldsymbol{AV} = \lambda \boldsymbol{V} \tag{A3}$$

where $\boldsymbol{V}$ is the *m* x *j* eigenvector and λ is the matrix of eigenvalues of the matrix, $\boldsymbol{X}$. *m* represents the number of dimensions. Calculating the correlation matrix and solving Equation A3 is quickly and easily done in many coding programs and as a result the details will not be discussed here. All data in matrix $\boldsymbol{A}$ represent data in the solute, *S*, space (Christophersen & Hooper, 1992). This is the higher dimensional space from which the data is projected into a lower dimensional space (referred to as the *U*-space) defined

by the principal components retained. To project data into the *U*-space, see Equations 1. To calculate residuals and determine the number of principal components to retain see Equations 2 & 3.

Once the number of principal components to retain was decided, $\boldsymbol{X}$ was projected into the *U*-space using

$$\boldsymbol{U} = \boldsymbol{X}\boldsymbol{V}' \tag{A4}$$

where $\boldsymbol{U}$ is an *i* x *m* matrix of solutes projected into the principal component space (Christophersen & Hooper, 1992). Similarly, $\boldsymbol{B}^n$ was projected into the *U*-space using

$$\boldsymbol{W}^n = \boldsymbol{B}^n\boldsymbol{V}' \tag{A5}$$

where $\boldsymbol{W}^n$ is the n^{th} end-member projected into the principal component space. A set of linear equations is solved to determine the fraction of instream signal due to each water source (Equation 4).

Table A2. Range of R^2 and RRMSE seen in similar studies for analyzing residuals.

Study	R^2	RRMSE %
Carroll et al. 2018	< 0.04	< 3.3 %
Ali et al. 2010	--	0 - 14 %
Bearup et al. 2014	0.02 – 0.07	2.8 – 7.2 %

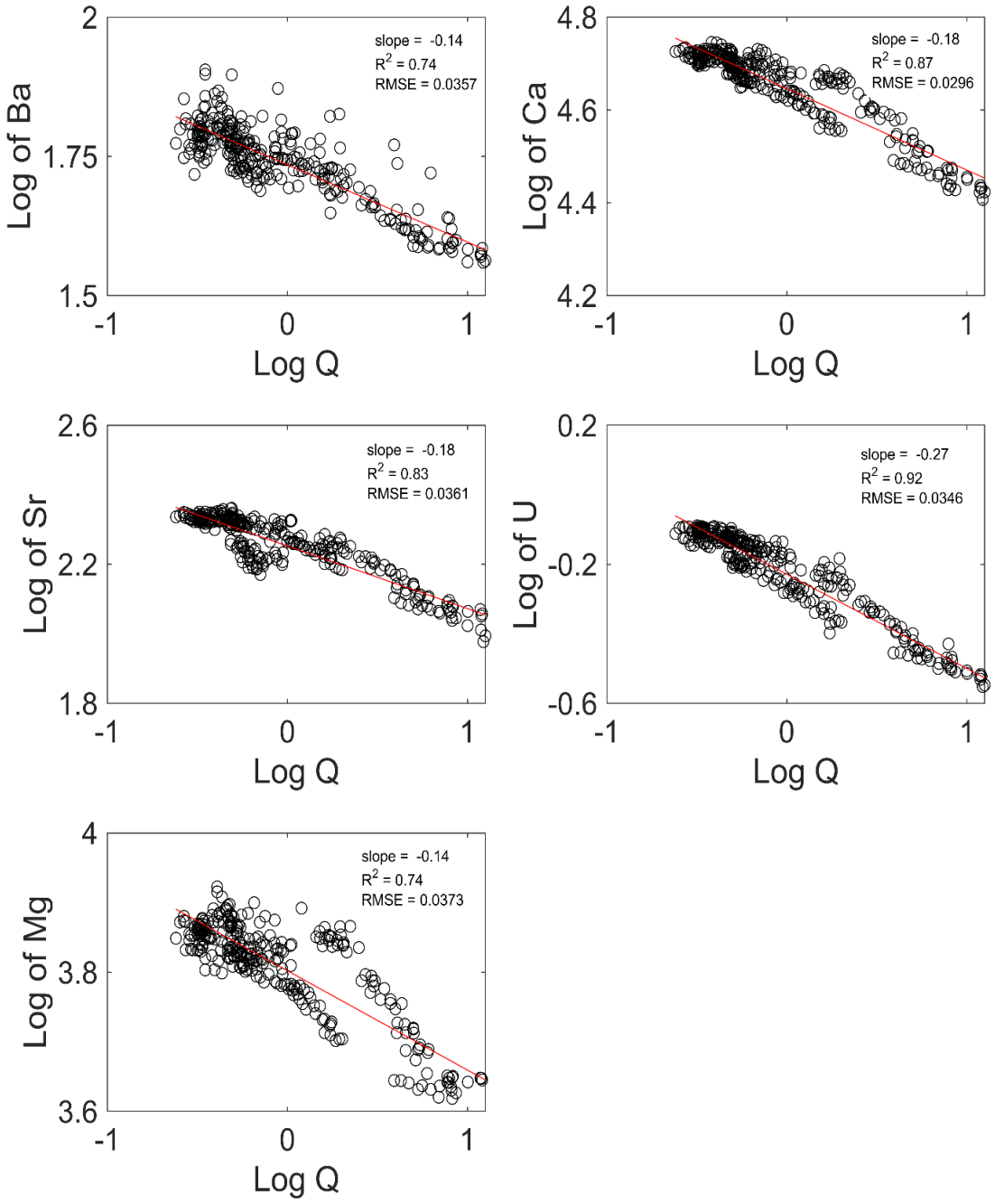

Figure A14. Log-Log Q-C plots for the instream solutes at the pump house for the 2016 water year. Black circles represent measured data points by the LBNL. Red line shows linear trend.

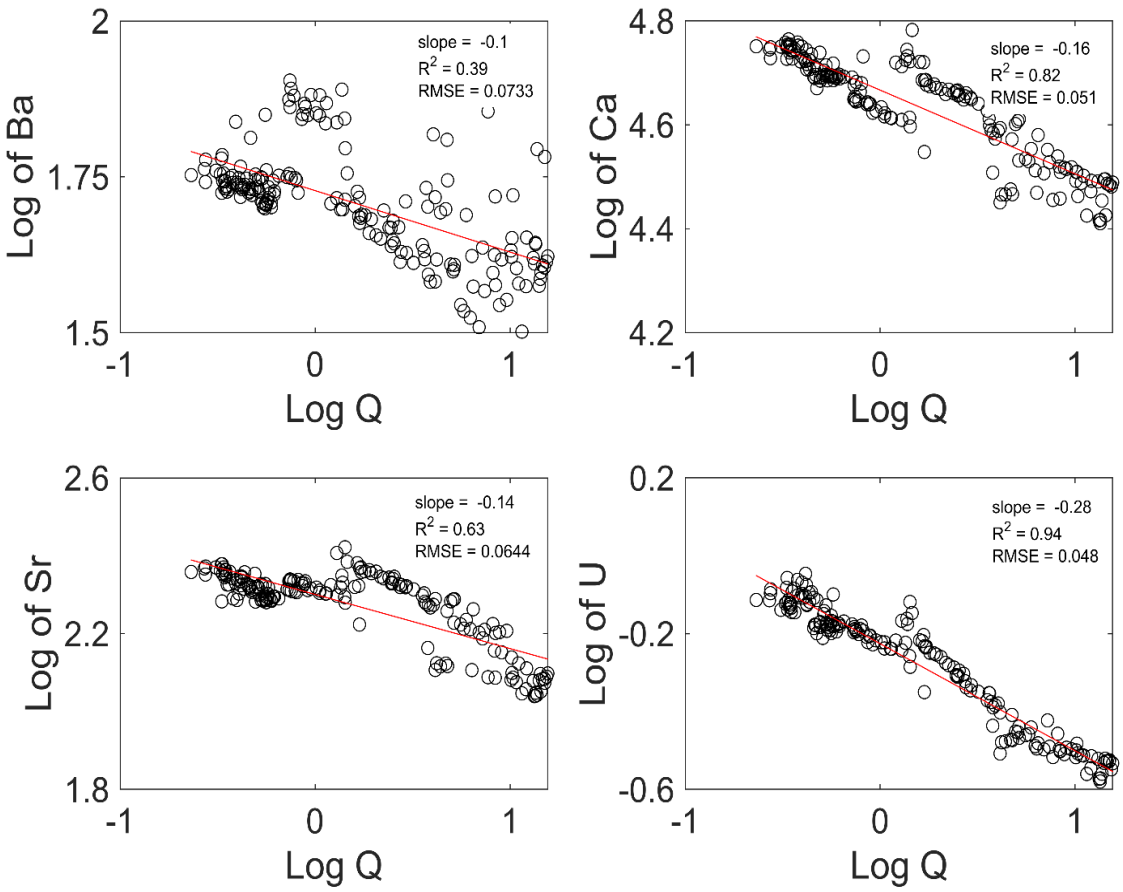

Figure A15. Log-Log Q-C plots for the instream solutes at the pump house for the 2017 water year. Black circles represent measured data points by the LBNL. Red line shows linear trend

.

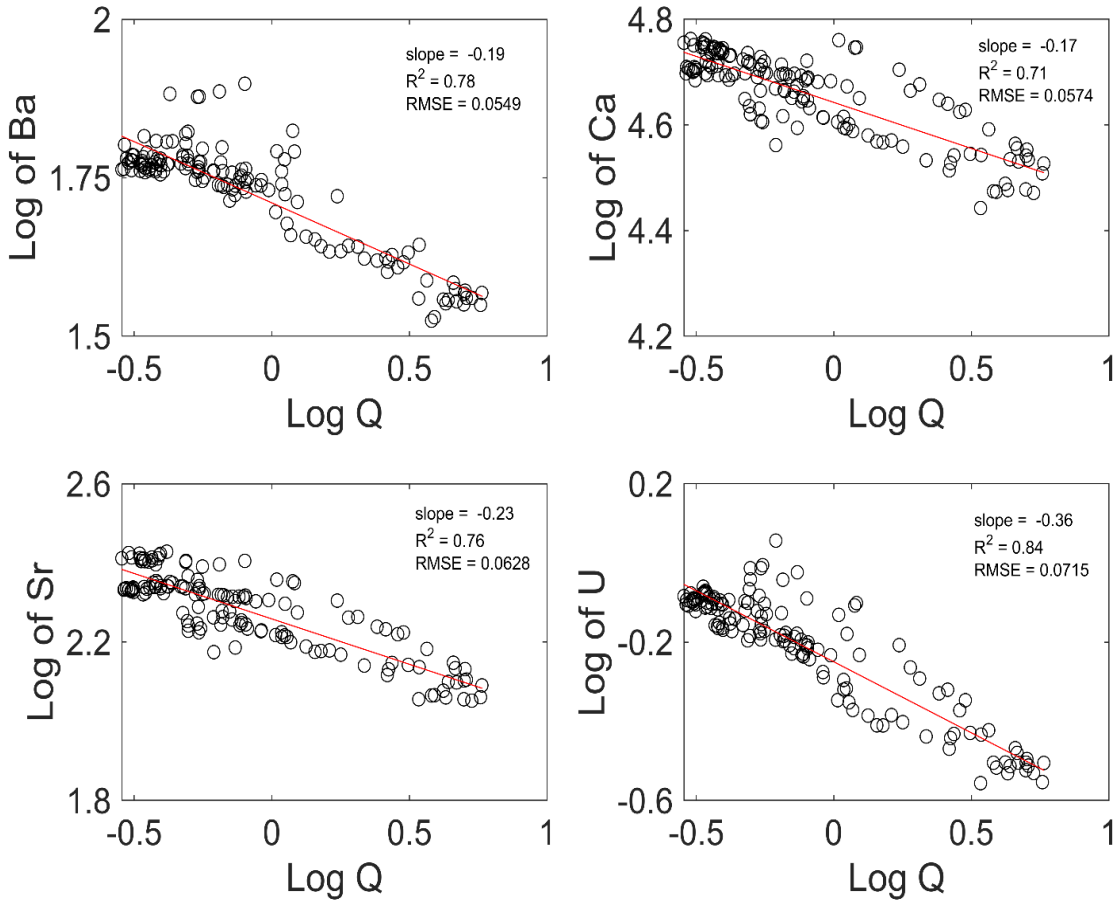

Figure A16. Log-Log Q-C plots for the instream solutes at the pump house for the 2018 water year. Black circles represent measured data points by the LBNL. Red line shows linear trend

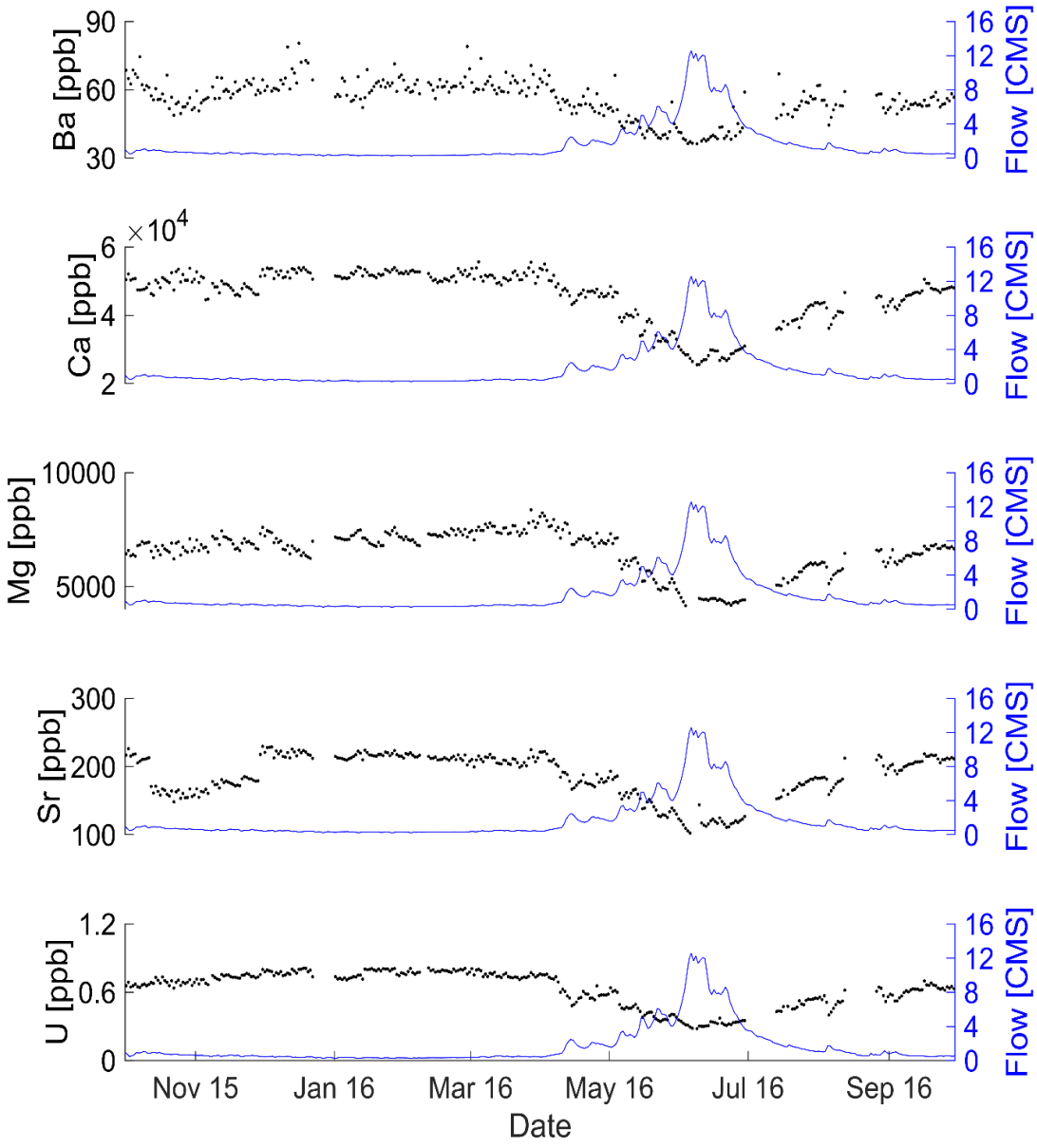

Figure A17. Time series plots for the 2016 water year for samples from the pump house. Black dots indicate solute data points corresponding to the left axis. Blue line shows flow corresponding with the right axis

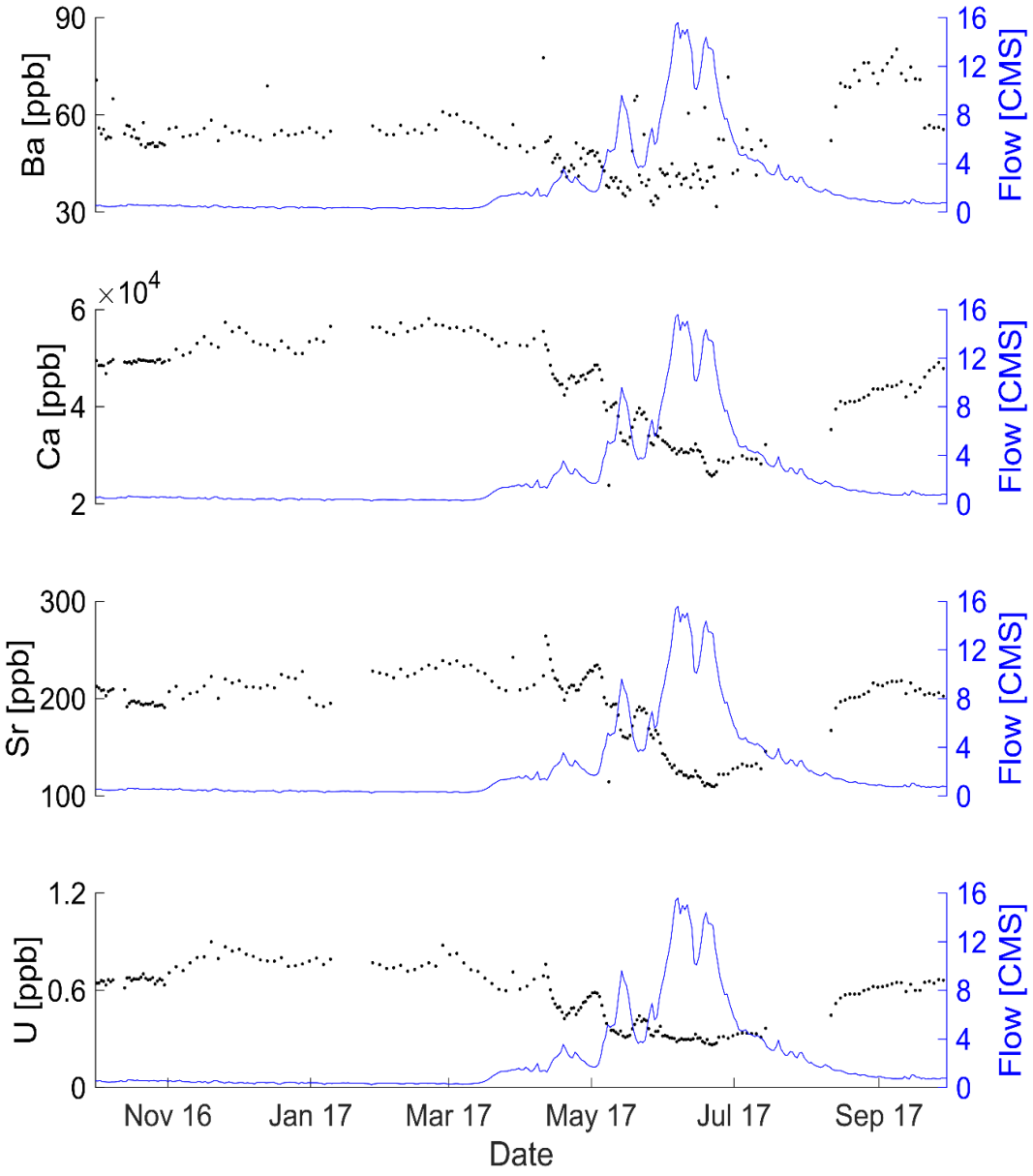

Figure A18. Time series plots for the 2017 water year for samples from the pump house. Black dots indicate solute data points corresponding to the left axis. Blue line shows flow corresponding with the right axis

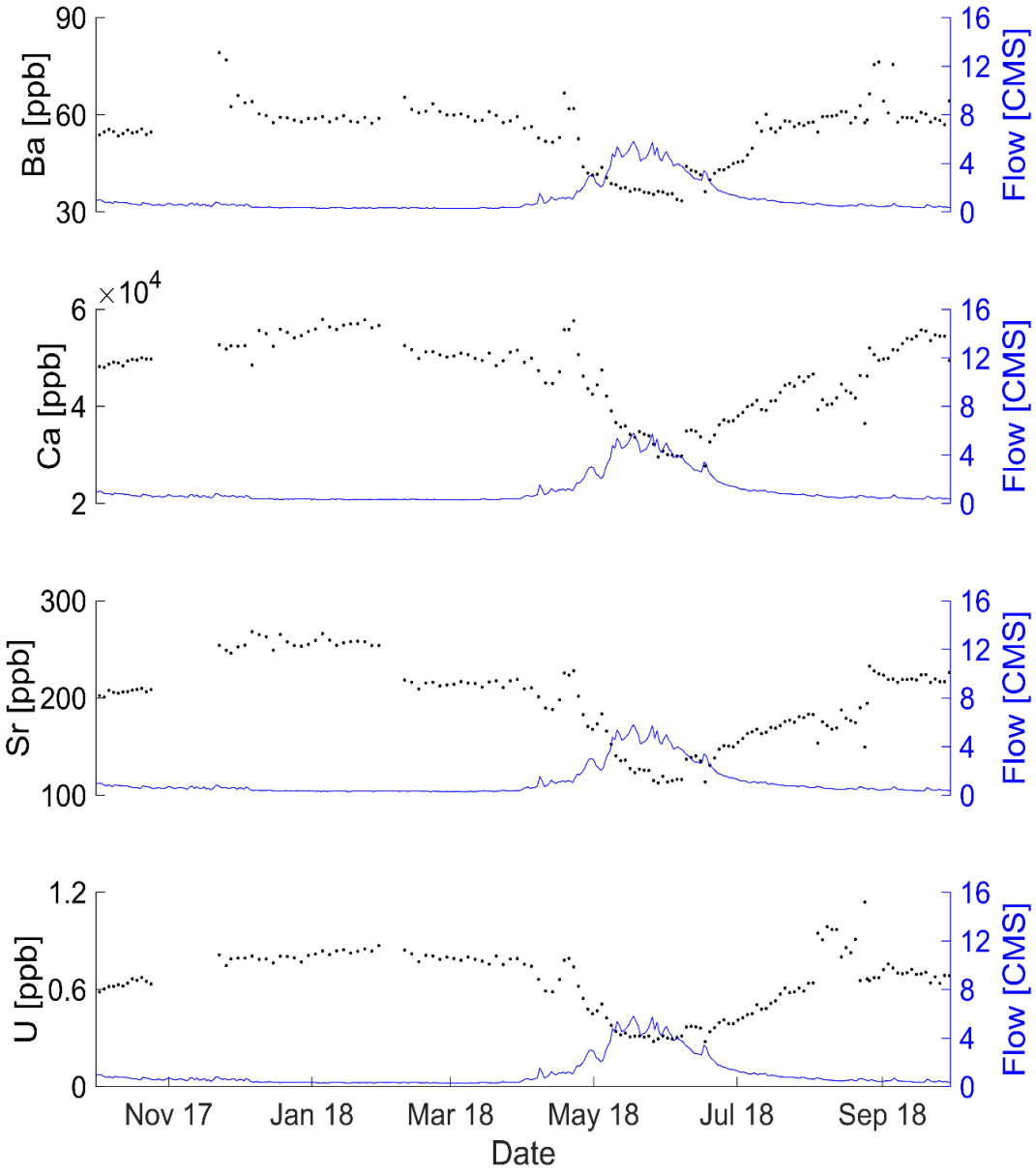

Figure A19. Time series plots for the 2018 water year for samples from the pump house. Black dots indicate solute data points corresponding to the left axis. Blue line shows flow corresponding with the right axis

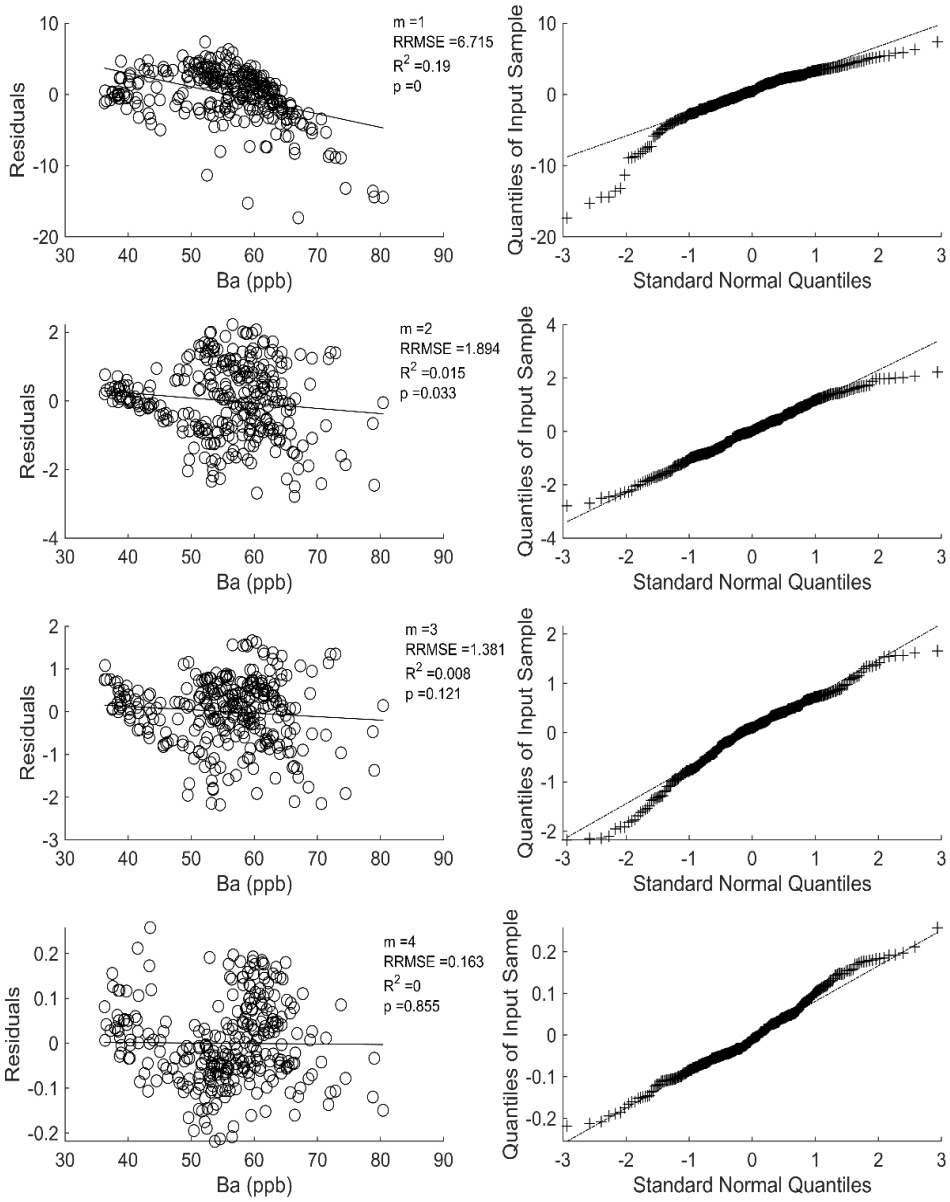

Figure A20. Residuals analysis for the 2015-16 water year for barium. Left hand plots show residuals at different numbers (*m*) of principal component retention and the associated R^2 and RRMSE. Open dots represent data points. Line indicates any linearity. Right hand plots assess normality at each level of retention. Plus signs indicate data. Dashed line represents the theoretical normal distribution the data would follow if it were normally distributed

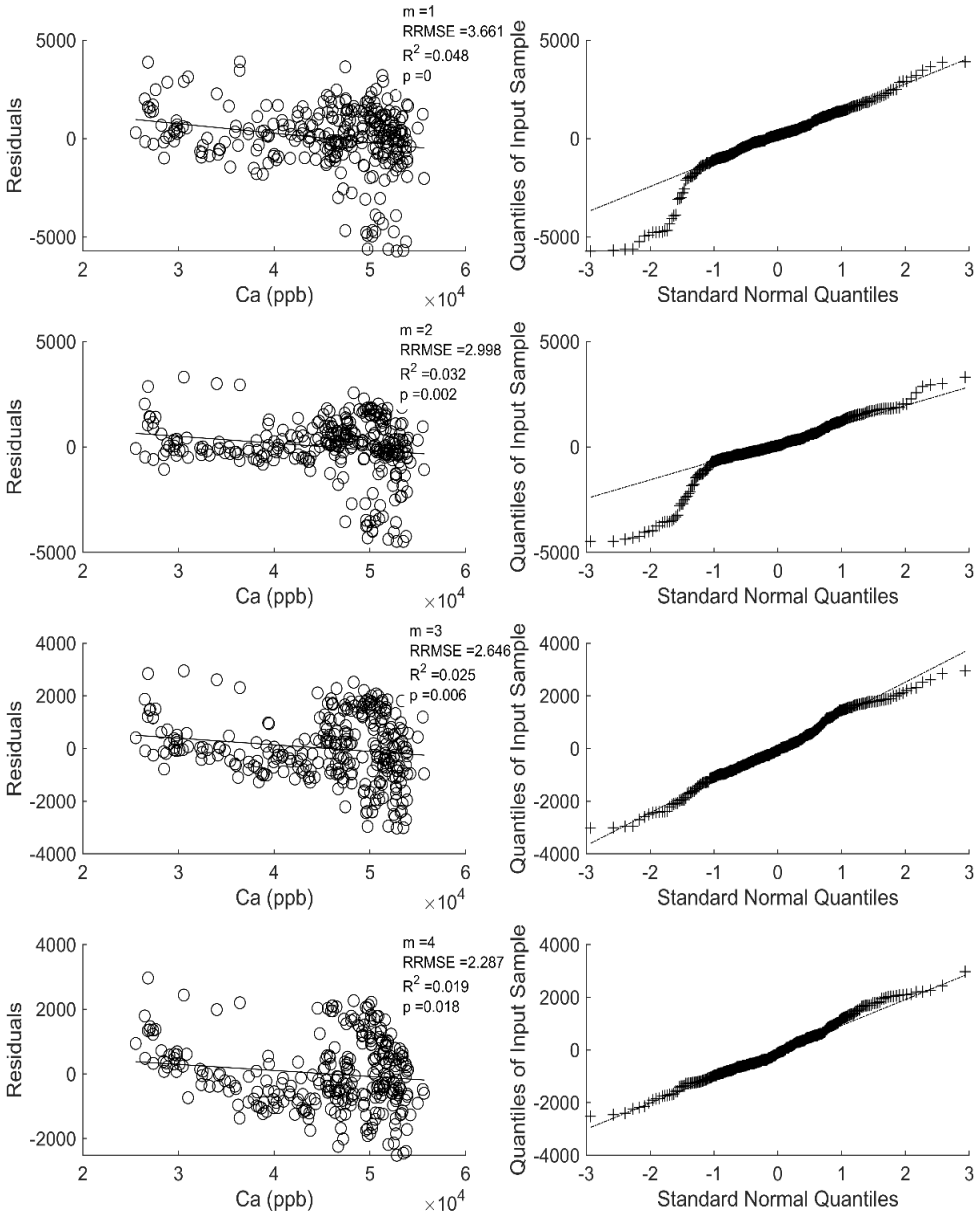

Figure A21. Residuals analysis for the 2015-16 water year for calcium. Left hand plots show residuals at different numbers (*m*) of principal component retention and the associated R^2 and RRMSE. Open dots represent data points. Line indicates any linearity. Right hand plots assess normality at each level of retention. Plus signs indicate data. Dashed line represents the theoretical normal distribution the data would follow if it were normally distributed

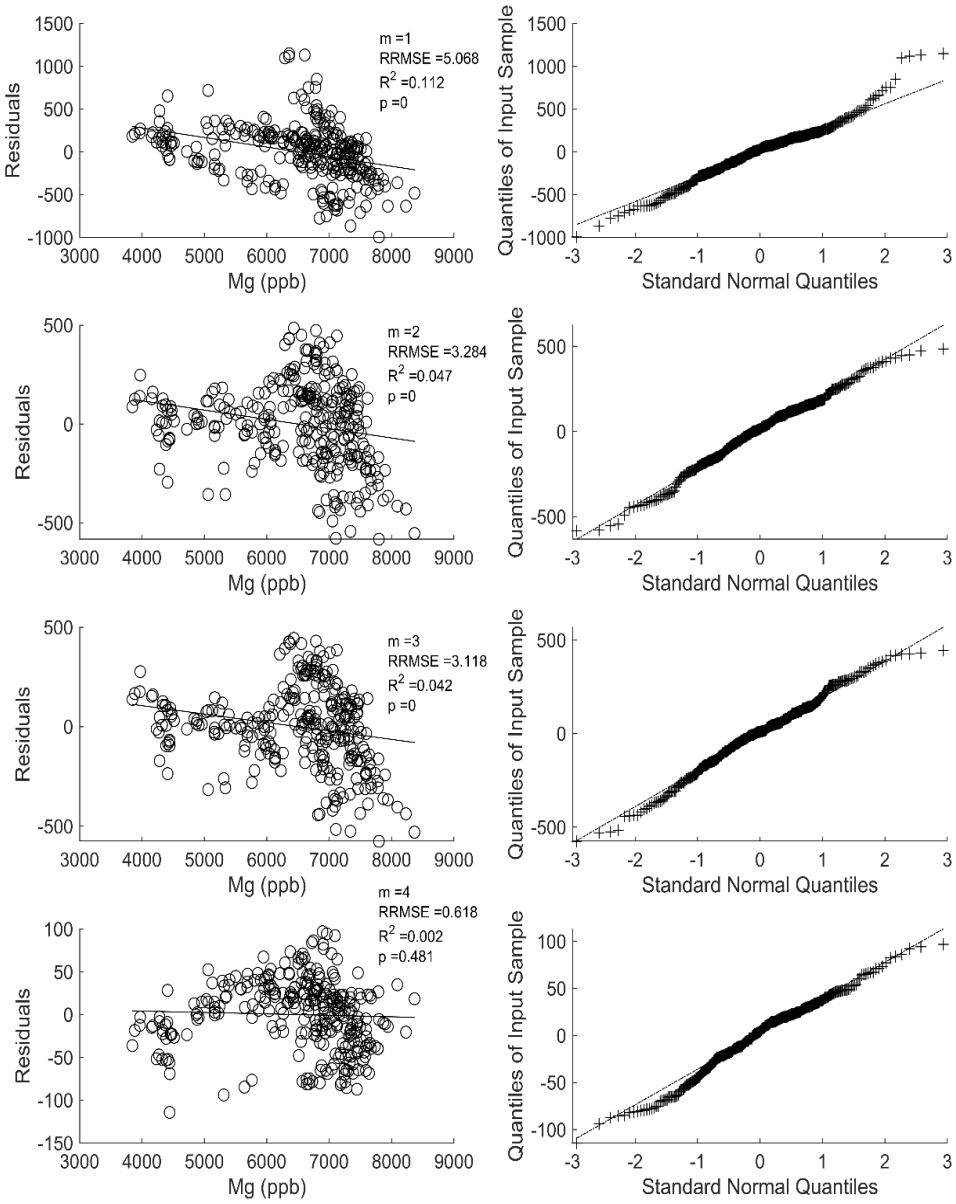

Figure A22. Residuals analysis for the 2015-16 water year for magnesium. Left hand plots show residuals at different numbers (*m*) of principal component retention and the associated R^2 and RRMSE. Open dots represent data points. Line indicates any linearity. Right hand plots assess normality at each level of retention. Plus signs indicate data. Dashed line represents the theoretical normal distribution the data would follow if it were normally distributed

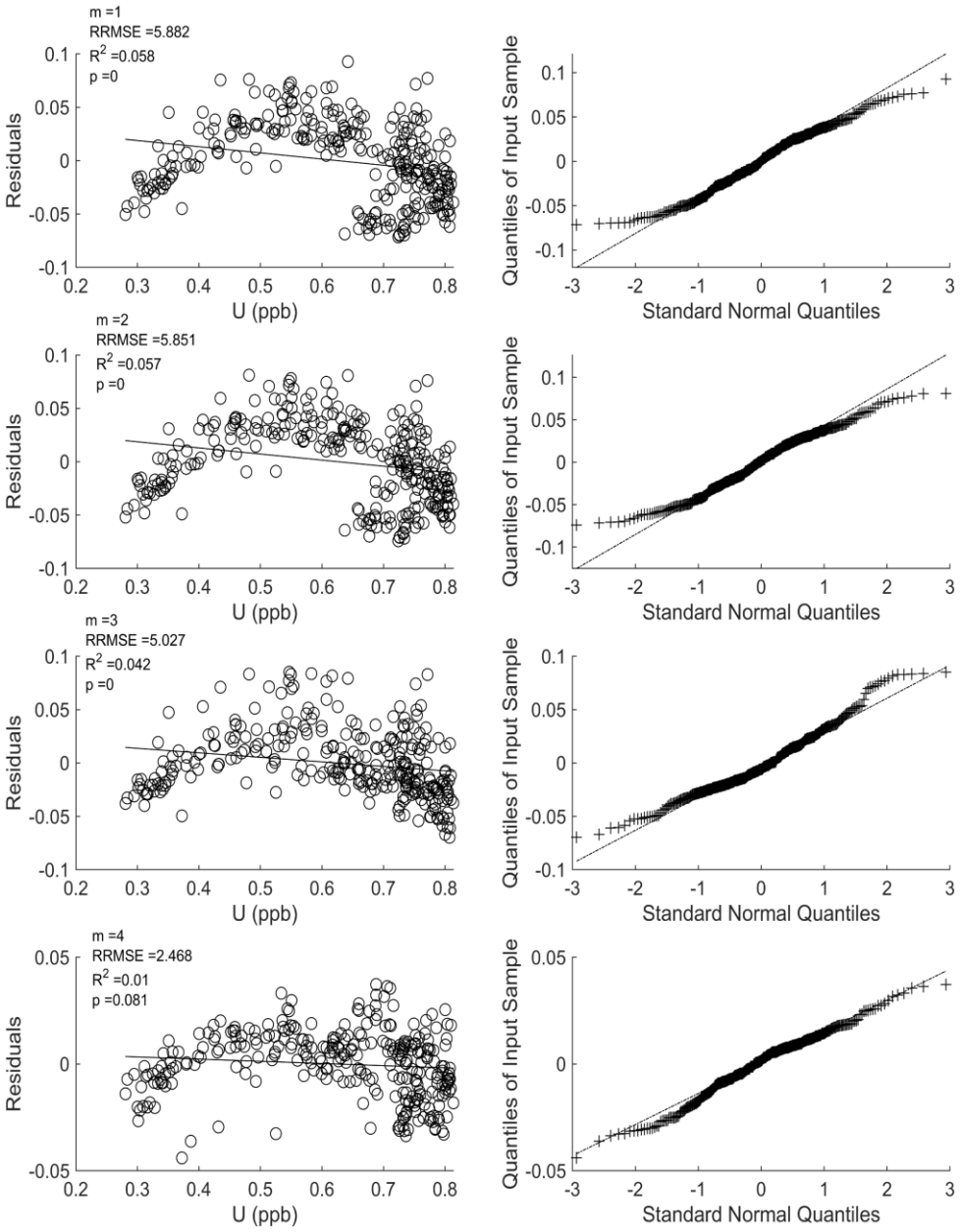

Figure A23. Residuals analysis for the 2015-16 water year for uranium. Left hand plots show residuals at different numbers (*m*) of principal component retention and the associated R^2 and RRMSE. Open dots represent data points. Line indicates any linearity. Right hand plots assess normality at each level of retention. Plus signs indicate data. Dashed line represents the theoretical normal distribution the data would follow if it were normally distributed

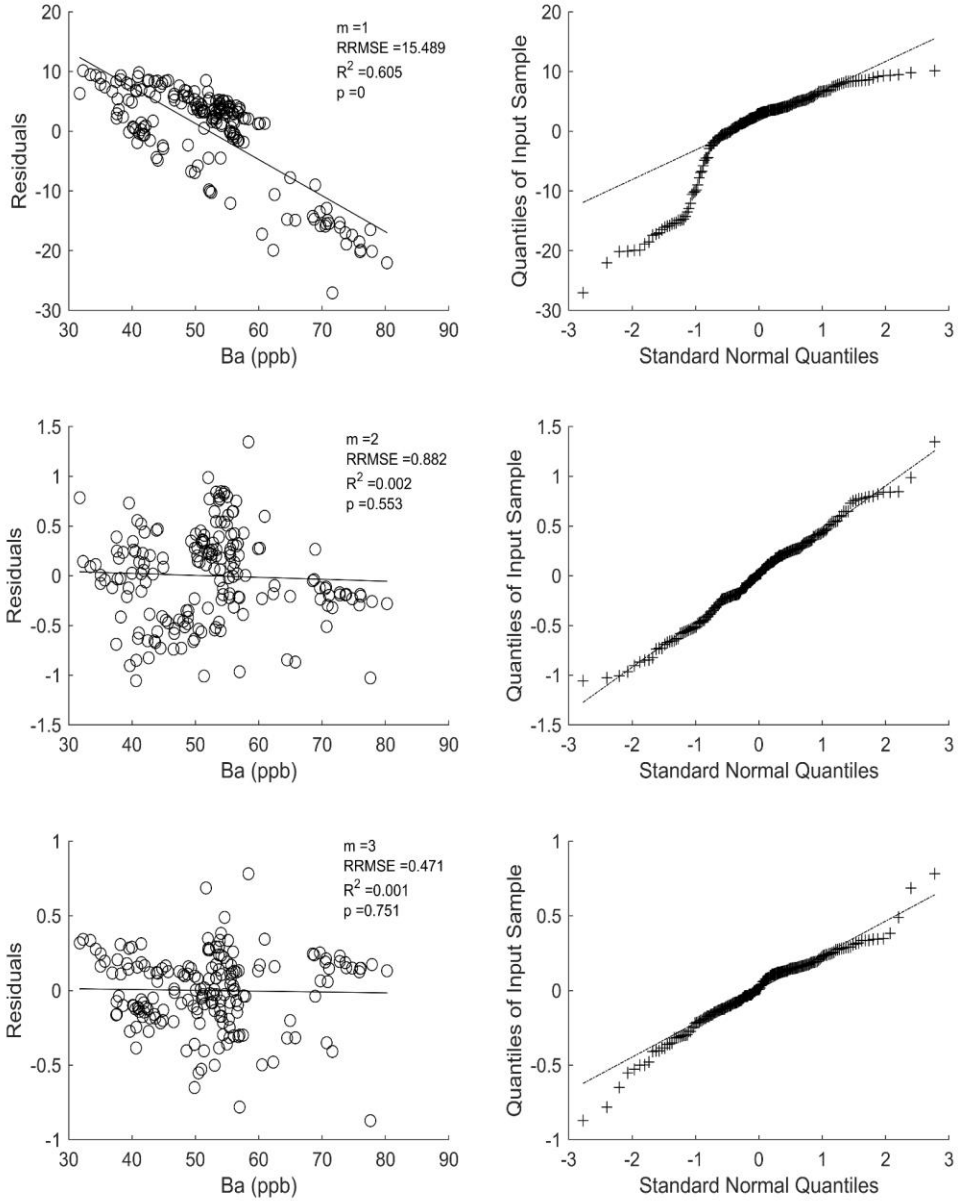

Figure A24. Residuals analysis for the 2016-17 water year for barium. Left hand plots show residuals at different numbers (*m*) of principal component retention and the associated R^2 and RRMSE. Open dots represent data points. Line indicates any linearity. Right hand plots assess normality at each level of retention. Plus signs indicate data. Dashed line represents the theoretical normal distribution the data would follow if it were normally distributed

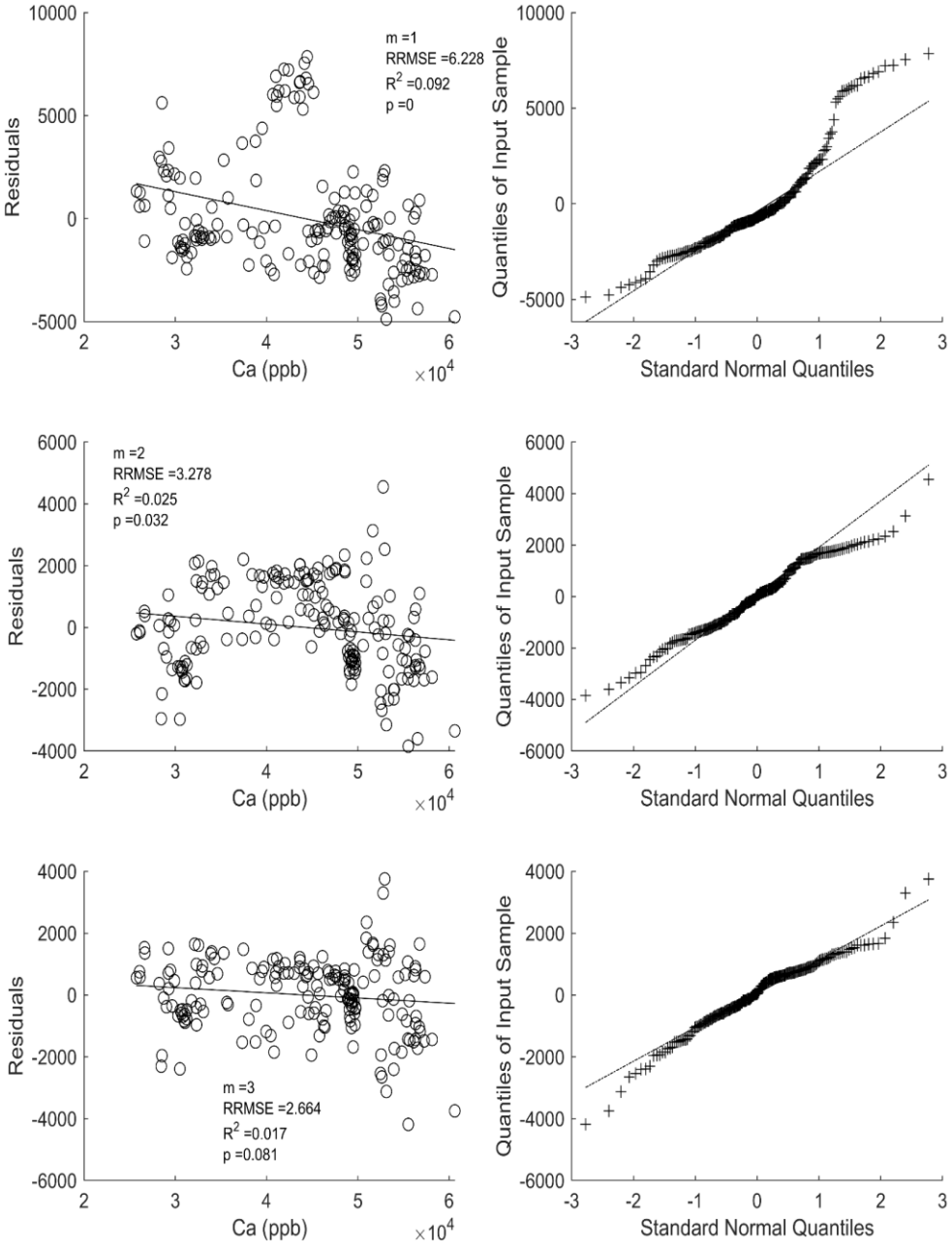

Figure A25. Residuals analysis for the 2016-17 water year for calcium. Left hand plots show residuals at different numbers (*m*) of principal component retention and the associated R^2 and RRMSE. Open dots represent data points. Line indicates any linearity. Right hand plots assess normality at each level of retention. Plus signs indicate data. Dashed line represents the theoretical normal distribution the data would follow if it were normally distributed

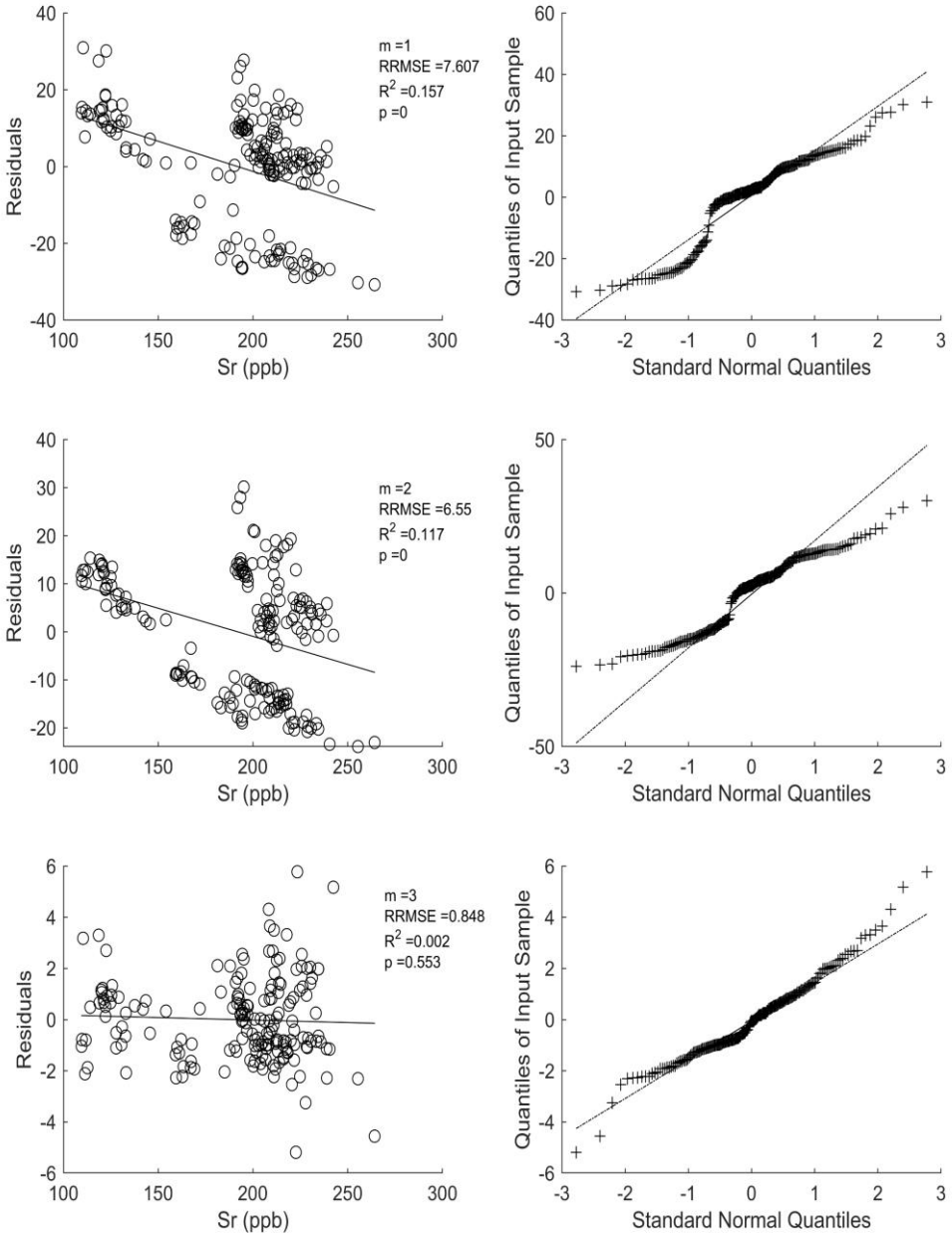

Figure A26. Residuals analysis for the 2016-17 water year for strontium. Left hand plots show residuals at different numbers (*m*) of principal component retention and the associated R^2 and RRMSE. Open dots represent data points. Line indicates any linearity. Right hand plots assess normality at each level of retention. Plus signs indicate data. Dashed line represents the theoretical normal distribution the data would follow if it were normally distributed

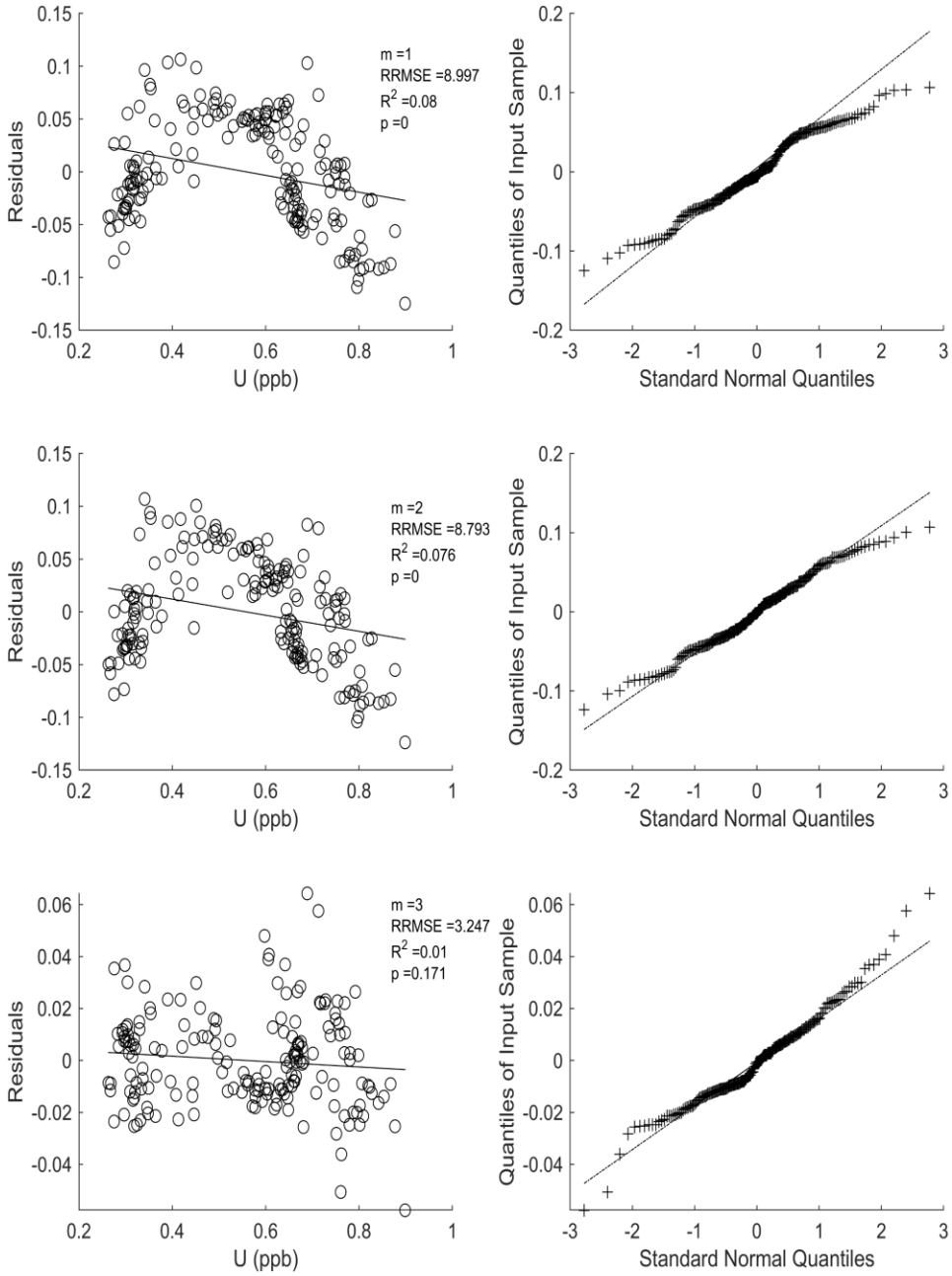

Figure A27. Residuals analysis for the 2016-17 water year for uranium. Left hand plots show residuals at different numbers (*m*) of principal component retention and the associated R^2 and RRMSE. Open dots represent data points. Line indicates any linearity. Right hand plots assess normality at each level of retention. Plus signs indicate data. Dashed line represents the theoretical normal distribution the data would follow if it were normally distributed

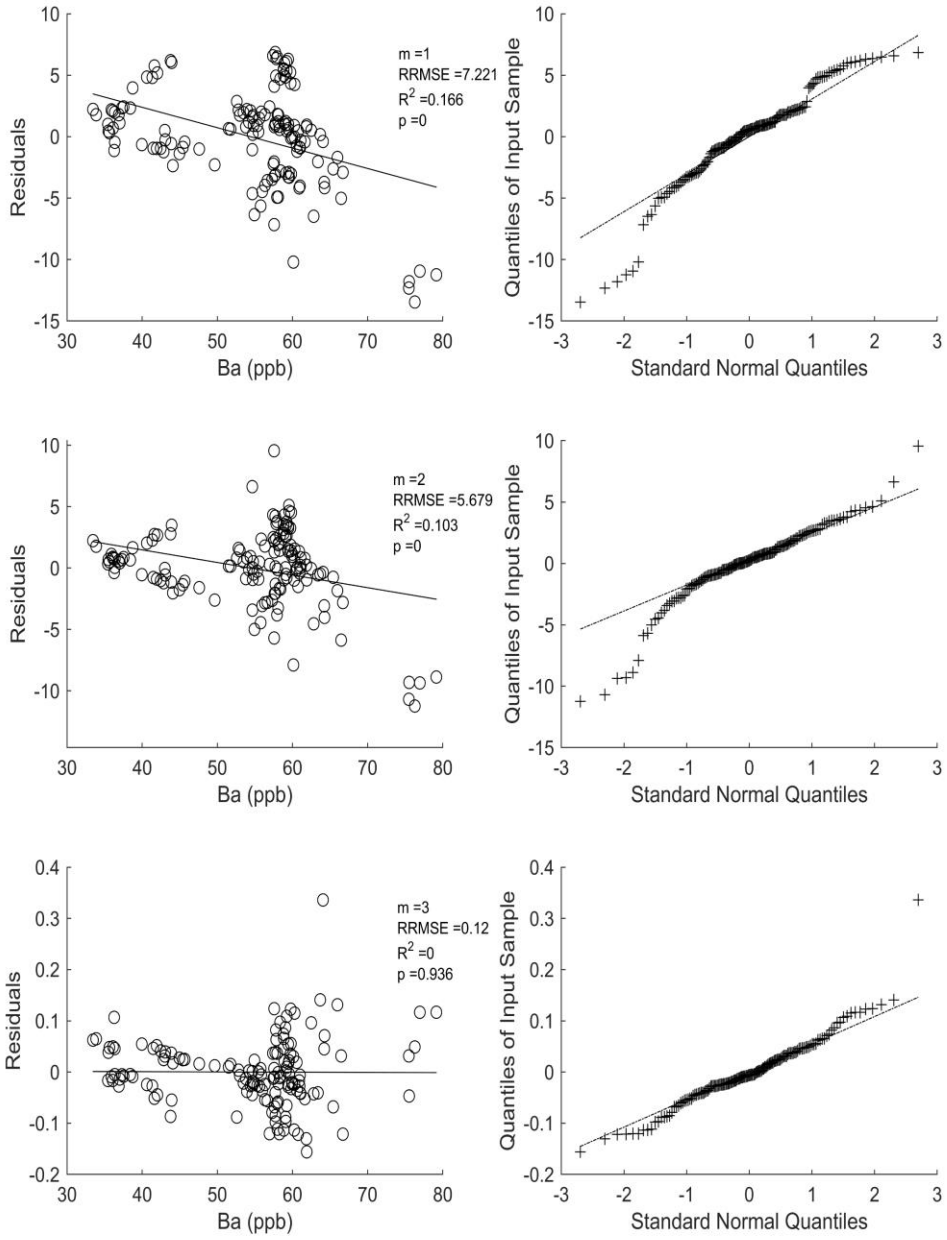

Figure A28. Residuals analysis for the 2017-18 water year for barium. Left hand plots show residuals at different numbers (*m*) of principal component retention and the associated R^2 and RRMSE. Open dots represent data points. Line indicates any linearity. Right hand plots assess normality at each level of retention. Plus signs indicate data. Dashed line represents the theoretical normal distribution the data would follow if it were normally distributed

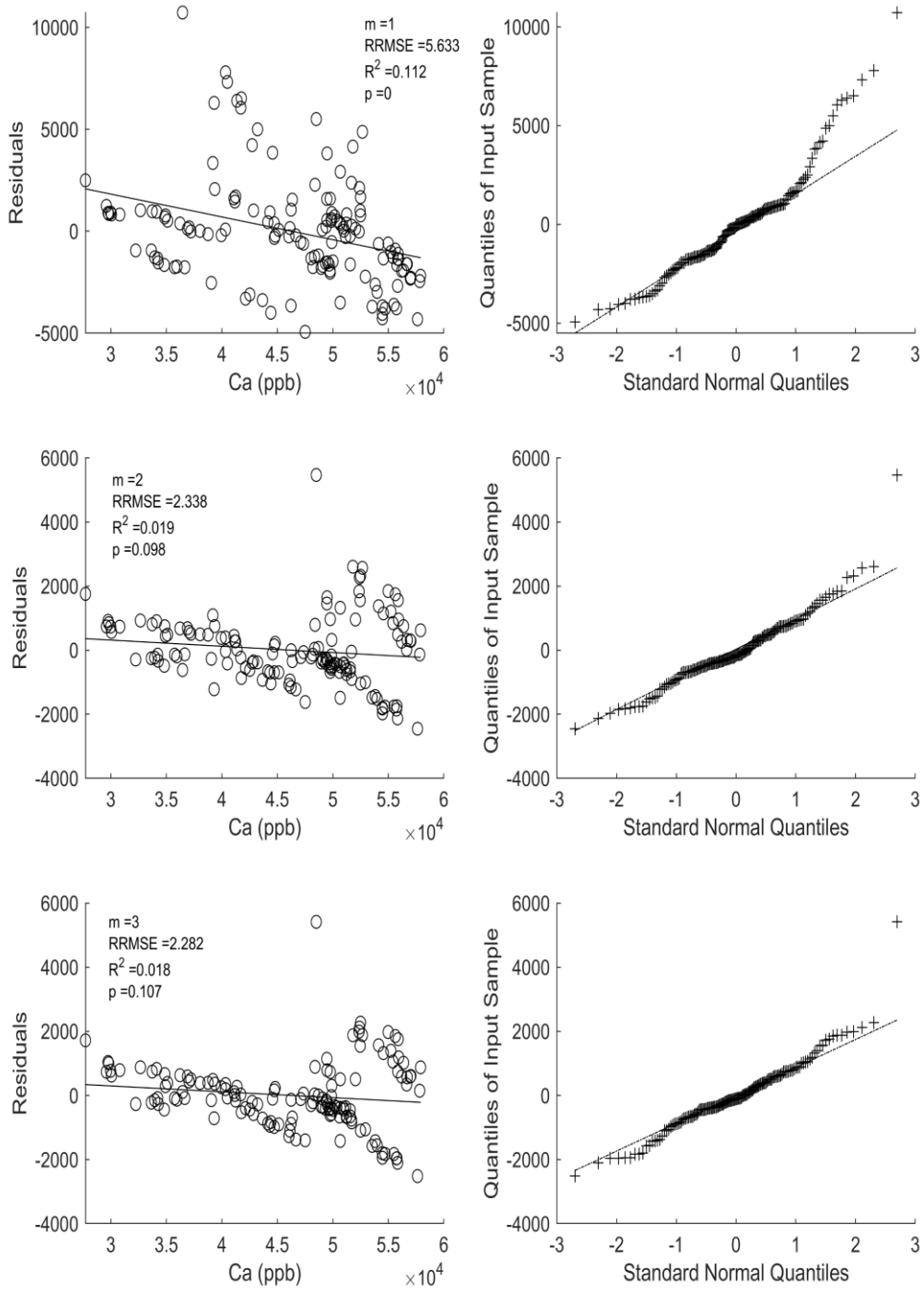

Figure A29. Residuals analysis for the 2017-18 water year for calcium. Left hand plots show residuals at different numbers (*m*) of principal component retention and the associated R^2 and RRMSE. Open dots represent data points. Line indicates any linearity. Right hand plots assess normality at each level of retention. Plus signs indicate data. Dashed line represents the theoretical normal distribution the data would follow if it were normally distributed

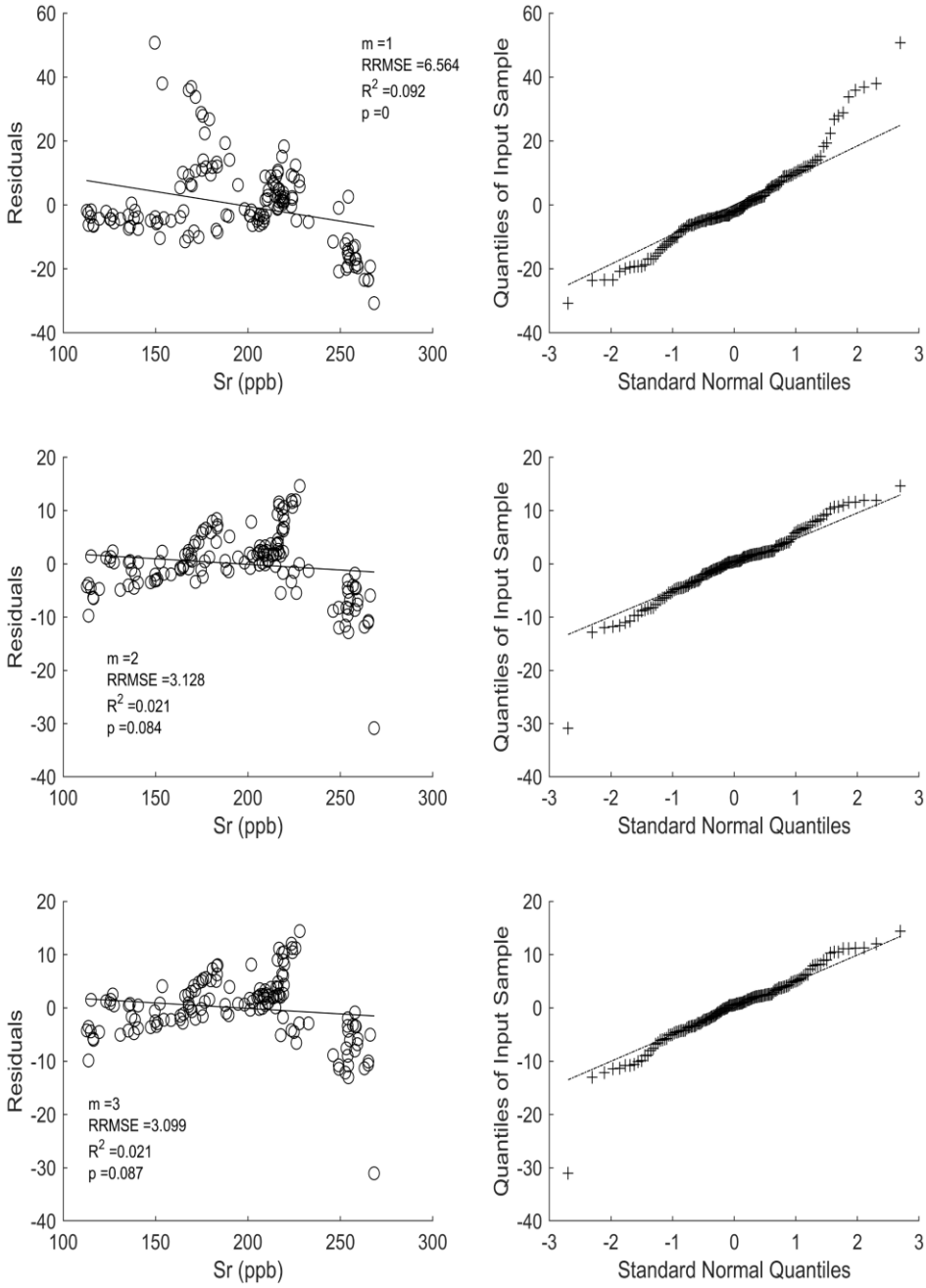

Figure A30. Residuals analysis for the 2017-18 water year for strontium. Left hand plots show residuals at different numbers (*m*) of principal component retention and the associated R^2 and RRMSE. Open dots represent data points. Line indicates any linearity. Right hand plots assess normality at each level of retention. Plus signs indicate data. Dashed line represents the theoretical normal distribution the data would follow if it were normally distributed

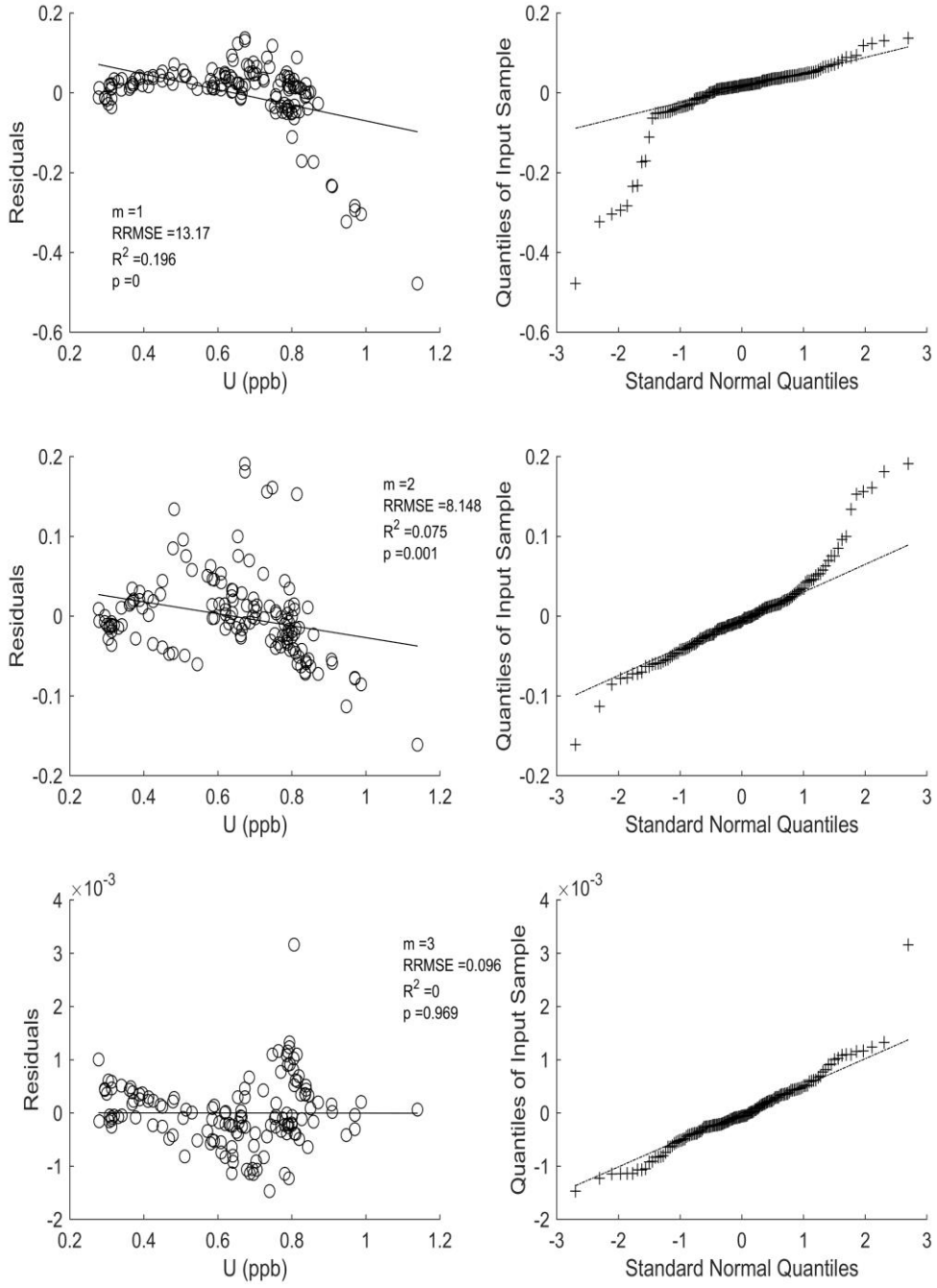

Figure A31. Residuals analysis for the 2017-18 water year for uranium. Left hand plots show residuals at different numbers (*m*) of principal component retention and the associated R^2 and RRMSE. Open dots represent data points. Line indicates any linearity. Right hand plots assess normality at each level of retention. Plus signs indicate data. Dashed line represents the theoretical normal distribution the data would follow if it were normally distributed

Table A3. Residuals results for the 2016 water year. The mean values for m = 2, 3, and 4 are all reasonable for the ranges defined by Table A2.

	RRMSE (%)					Mean
m	U	Sr	Mg	Ca	Ba	RRMSE (%)
1	5.883	6.569	5.068	3.661	6.715	5.579
2	5.851	6.566	3.284	2.998	1.894	4.119
3	5.027	0.384	3.118	2.646	1.381	2.511
4	2.468	0.130	0.618	2.287	0.163	1.133
	R^2					Mean
m	U	Sr	Mg	Ca	Ba	R^2
1	0.058	0.135	0.112	0.048	0.190	0.109
2	0.057	0.135	0.047	0.032	0.015	0.057
3	0.042	0.000	0.042	0.025	0.008	0.024
4	0.010	0.000	0.002	0.019	0.000	0.006
	p					# of Solutes
m	U	Sr	Mg	Ca	Ba	$p < 0.05$
1	0	0	0	0	0	5
2	0	0	0	0.002	0.033	5
3	0	0.711	0	0.006	0.121	3
4	0.081	0.900	0.481	0.018	0.855	1

Table A4. Residuals results for the 2017 water year. The average values for m = 2 and 3 are reasonable for the ranges defined by Table A2.

	RRMSE (%)				Mean
m	U	Sr	Ca	Ba	RRMSE (%)
1	8.997	7.607	6.228	15.490	9.581
2	8.793	6.550	3.278	0.882	4.876
3	3.247	0.848	2.664	0.471	1.807
	R^2				Mean
m	U	Sr	Ca	Ba	R^2
1	0.080	0.157	0.092	0.605	0.233
2	0.076	0.117	0.025	0.002	0.055
3	0.010	0.002	0.017	0.001	0.007
	p				# of Solutes
m	U	Sr	Ca	Ba	$p < 0.05$
1	0	0	0	0	4
2	0	0	0.032	0.553	3
3	0.171	0.553	0.081	0.751	0

Table A5. Residuals results for the 2018 water year. The average values for m = 2 and 3 are reasonable for the ranges defined by Table A2.

	RRMSE (%)				Mean
m	U	Sr	Ca	Ba	RRMSE (%)
1	13.170	6.564	5.633	7.221	8.147
2	8.148	3.128	2.338	5.679	4.823
3	0.096	3.099	2.282	0.120	1.399
	R^2				Mean
m	U	Sr	Ca	Ba	R^2
1	0.196	0.092	0.112	0.166	0.141
2	0.075	0.021	0.019	0.102	0.054
3	0.000	0.021	0.018	0.000	0.010
	p				# of Solutes
m	U	Sr	Ca	Ba	$p < 0.05$
1	0	0	0	0	4
2	0.001	0.084	0.098	0	2
3	0.969	0.087	0.107	0.936	0

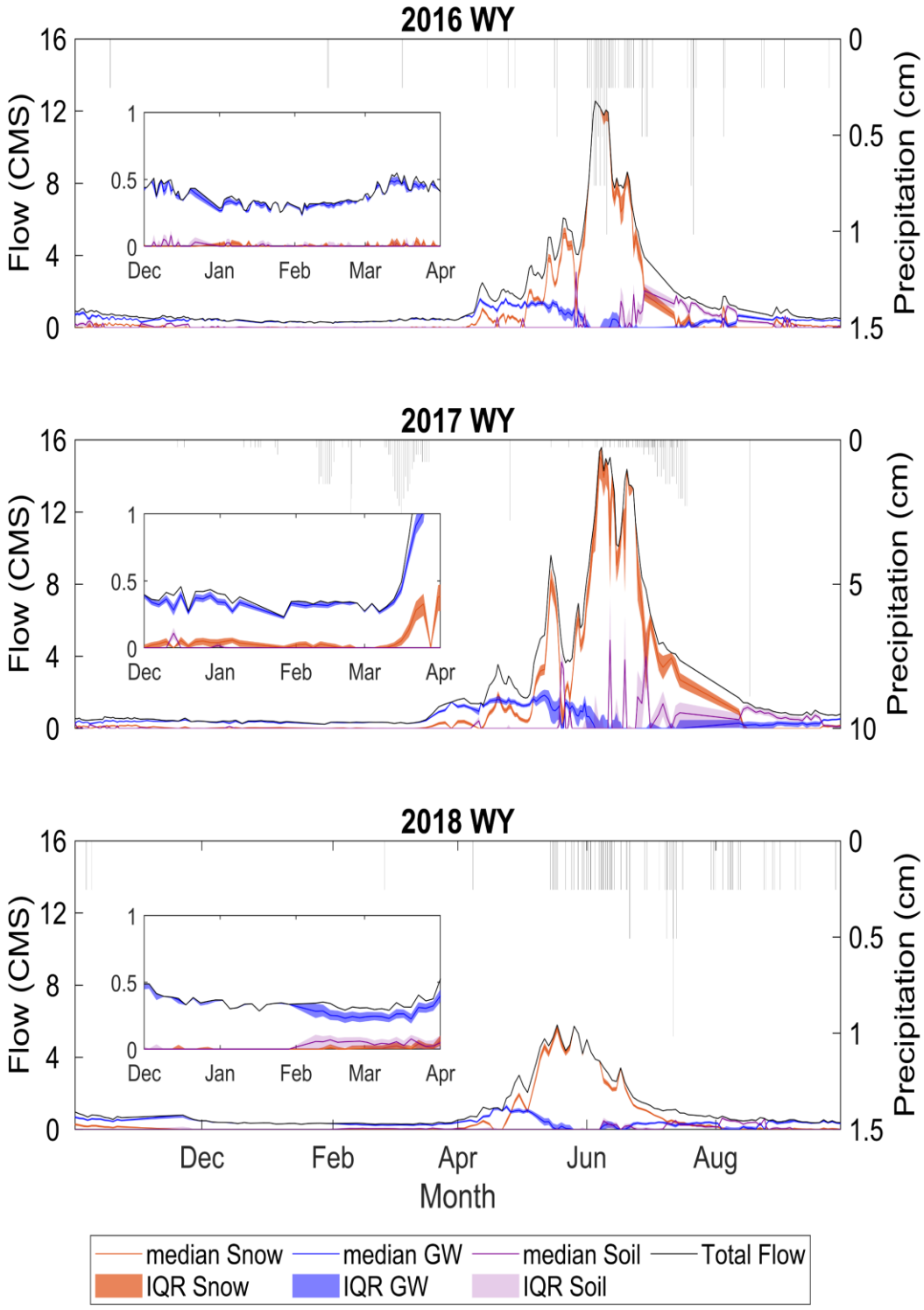

Figure A32. Separation with three hydrologically rationalized end-members using statistically-based methods plotting on the left axis. Precipitation plotting on the right

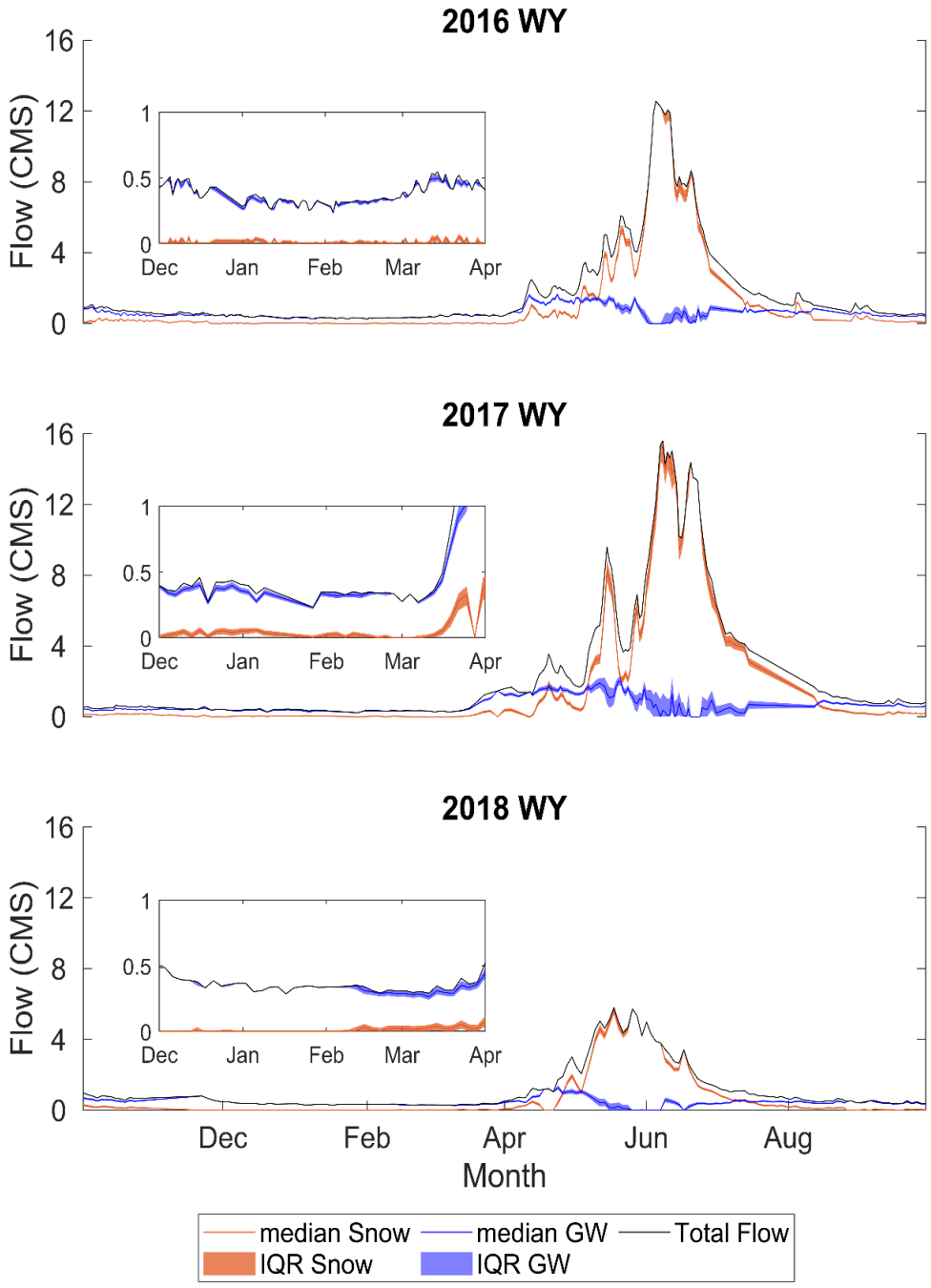

Figure A33. Hydrograph separation of two end-members with hydrologically rationalized concentrations (2 H-EM) using the statistically-based method of separation. Lines indicate median response from 1000 samplings around the mean and standard deviation of the end-member concentrations. The interquartile range (IQR) shaded around the median represents the lower 25th to upper 75th quantiles.

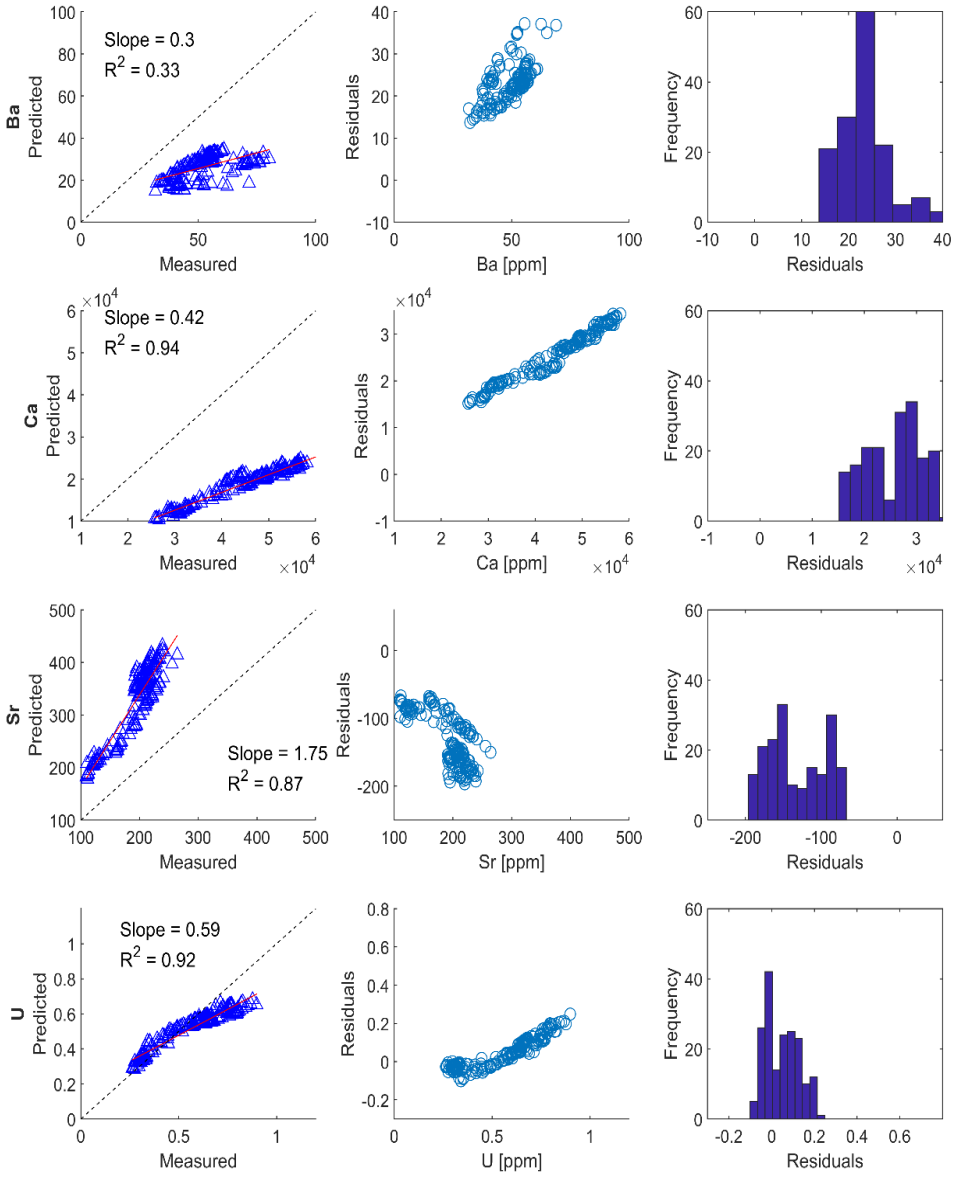

Figure A34. Plots on the left show predicted versus measured concentrations of the instream using two end-members characterized by measurements in the 2017 WY. Trends indicated by red line. Dashed lined shows the theoretical perfect predicition of instream concentrations. Middle plots show residuals between predicted and measured instream concentration data. Histogram on the right show the distribution of residuals

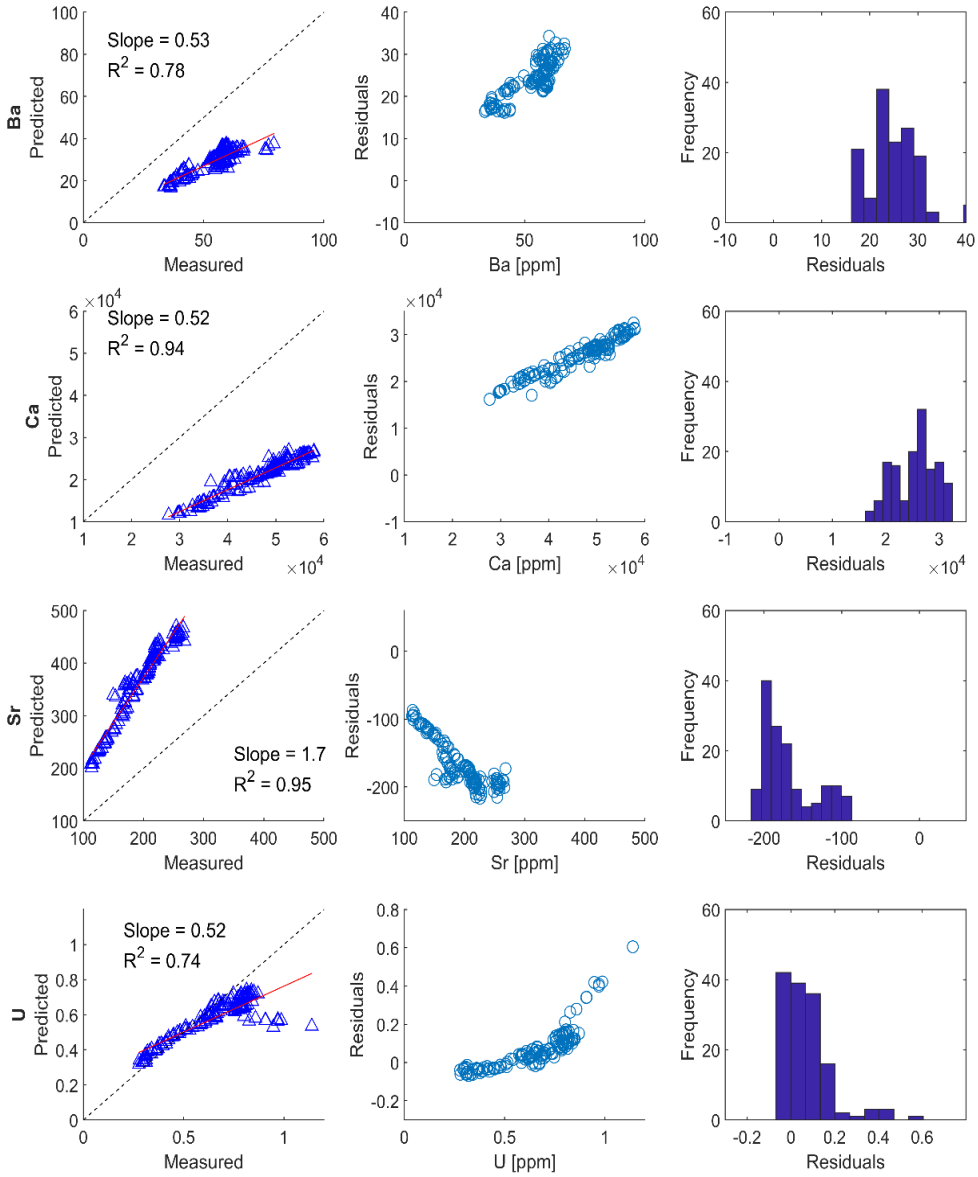

Figure A35. Plots on the left show predicted versus measured concentrations of the instream using two end-members characterized by measurements in the 2018 WY. Trends indicated by red line. Dashed lined shows the theoretical perfect predicition of instream concentrations. Middle plots show residuals between predicted and measured instream concentration data. Histogram on the right show the distribution of residuals

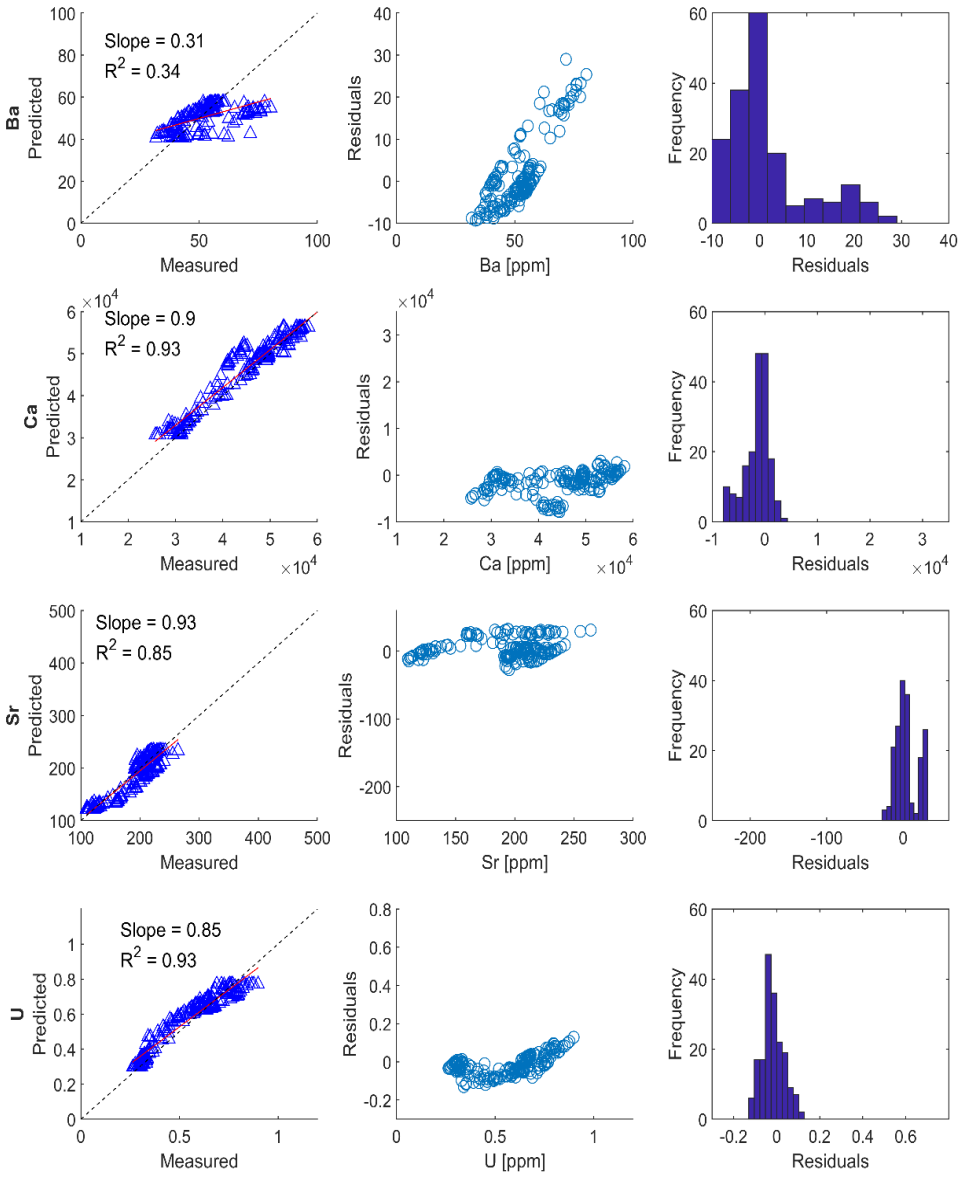

Figure A36. Plots on the left show predicted versus measured concentrations of the instream using two end-members characterized by hydrologic rationalization in the 2017 WY. Trends indicated by red line. Dashed lined shows the theoretical perfect predicition of instream concentrations. Middle plots show residuals between predicted and measured instream concentration data. Histogram on the right show the distribution of residuals

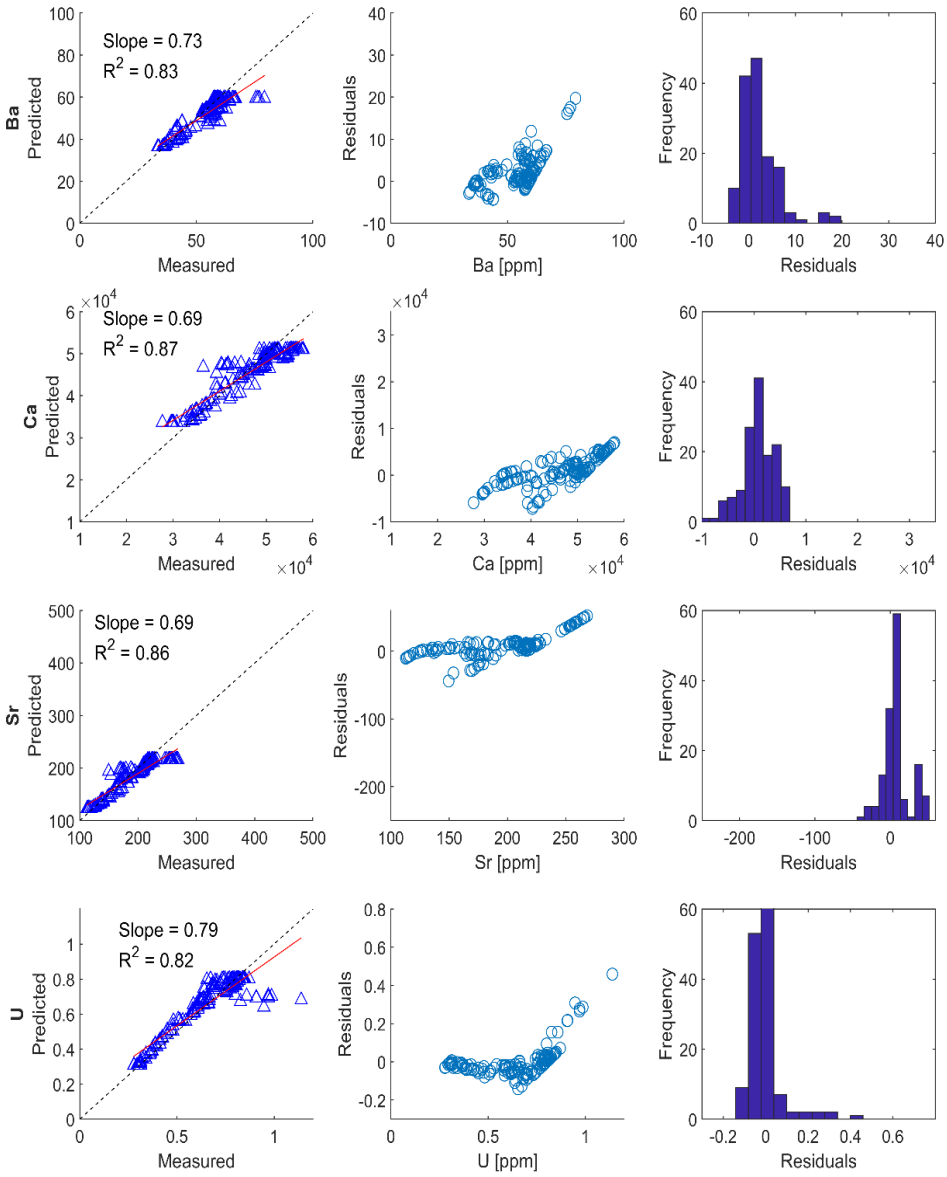

Figure A37. Plots on the left show predicted versus measured concentrations of the instream using two end-members characterized by hydrologic rationalization in the 2018 WY. Trends indicated by red line. Dashed lined shows the theoretical perfect predicition of instream concentrations. Middle plots show residuals between predicted and measured instream concentration data. Histogram on the right show the distribution of residuals

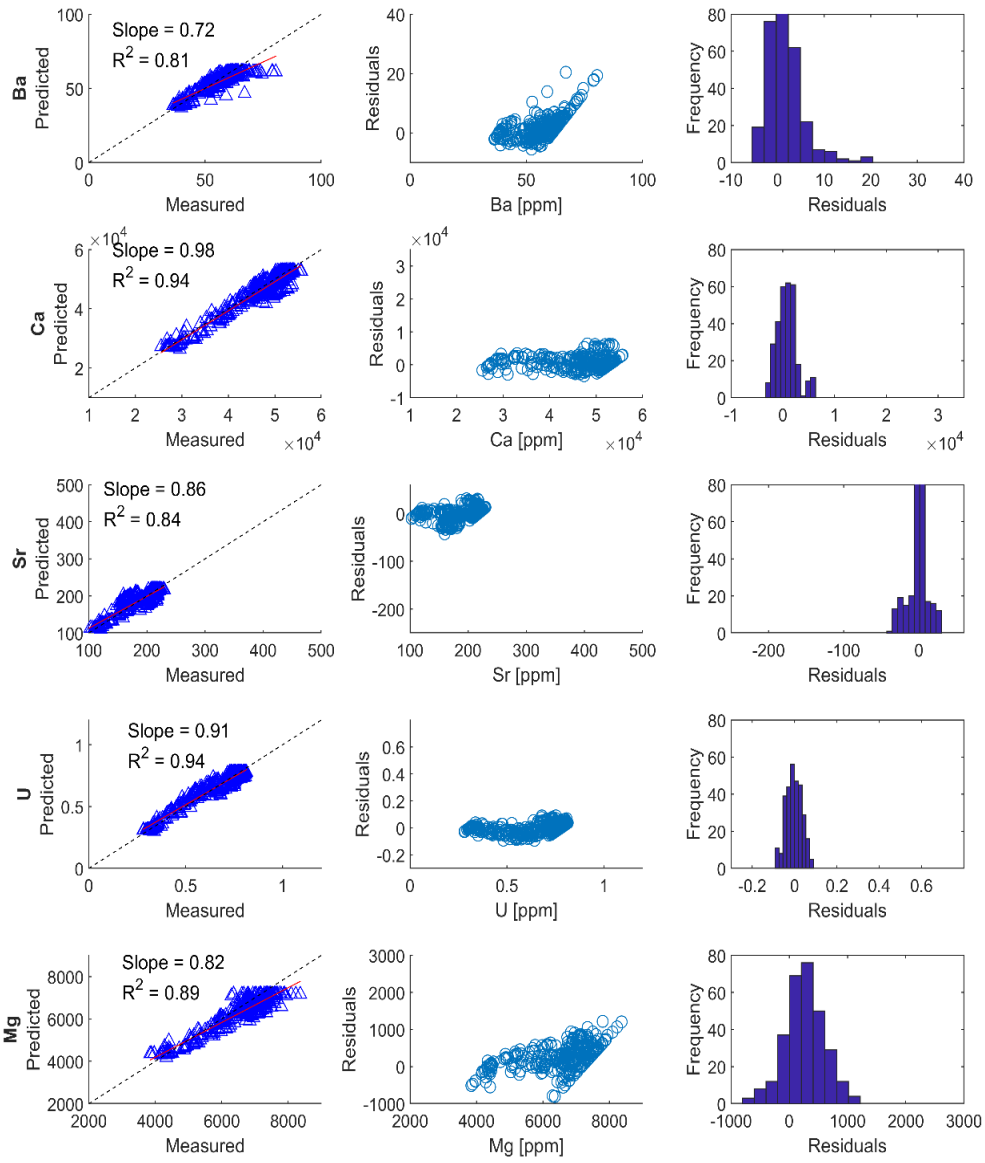

Figure A38. Plots on the left show predicted versus measured concentrations of the instream using three end-members characterized by hydrologic rationalization in the 2016 WY. Trends indicated by red line. Dashed lined shows the theoretical perfect predicition of instream concentrations. Middle plots show residuals between predicted and measured instream concentration data. Histogram on the right show the distribution of residuals

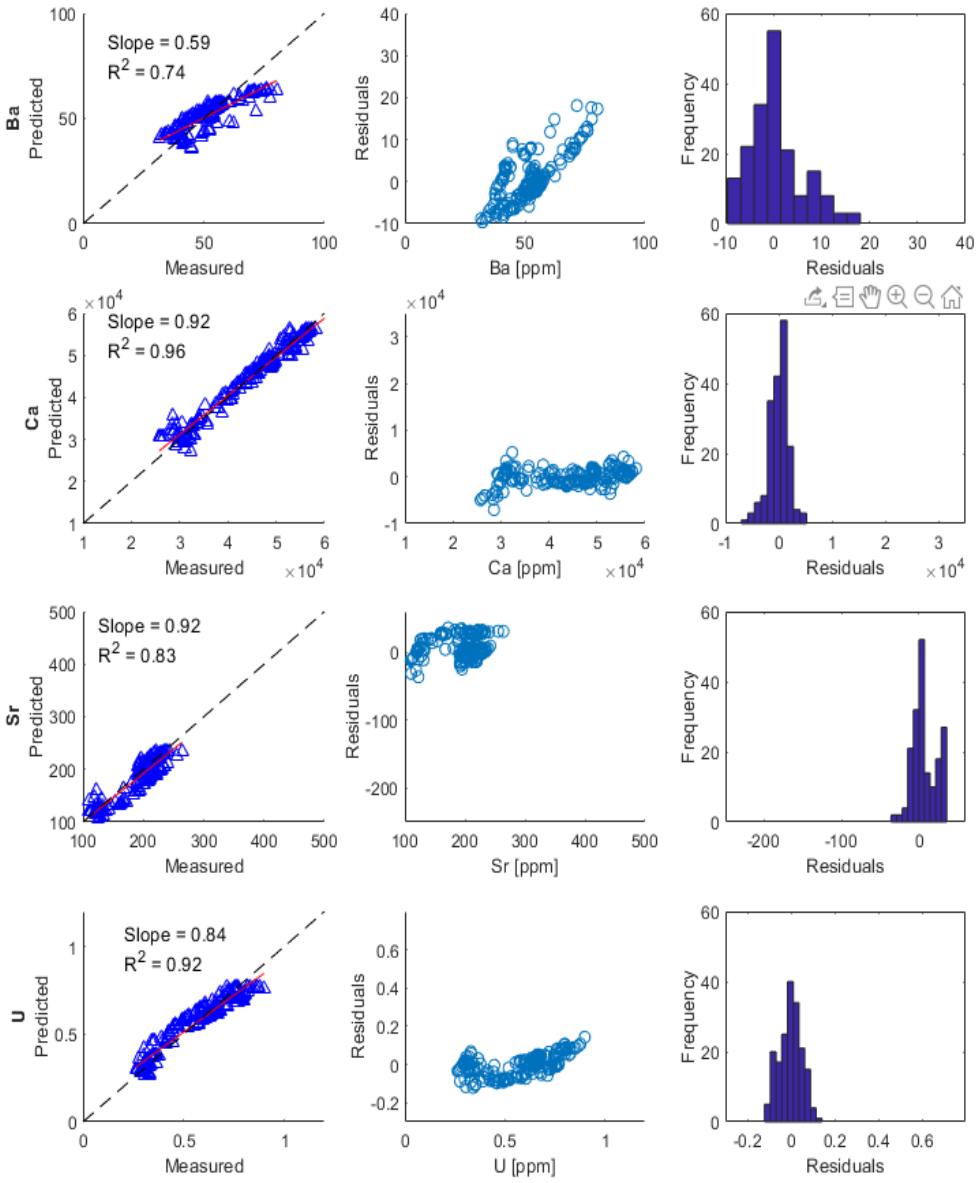

Figure A39. Plots on the left show predicted versus measured concentrations of the instream using three end-members characterized by hydrologic rationalization in the 2017 WY. Trends indicated by red line. Dashed lined shows the theoretical perfect predicition of instream concentrations. Middle plots show residuals between predicted and measured instream concentration data. Histogram on the right show the distribution of residuals

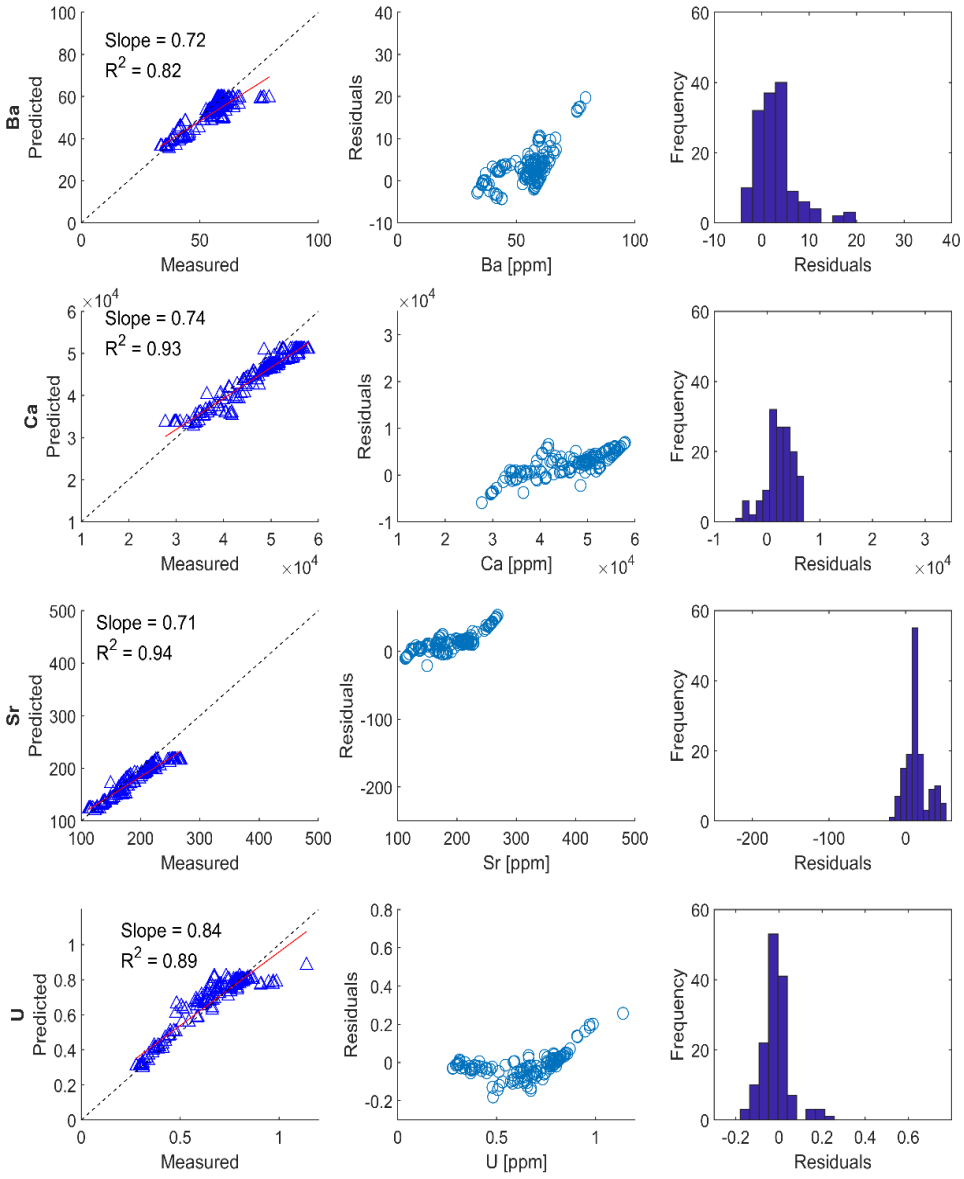

Figure A40. Plots on the left show predicted versus measured concentrations of the instream using three end-members characterized by hydrologic rationalization in the 2018 WY. Trends indicated by red line. Dashed lined shows the theoretical perfect predicition of instream concentrations. Middle plots show residuals between predicted and measured instream concentration data. Histogram on the right show the distribution of residuals

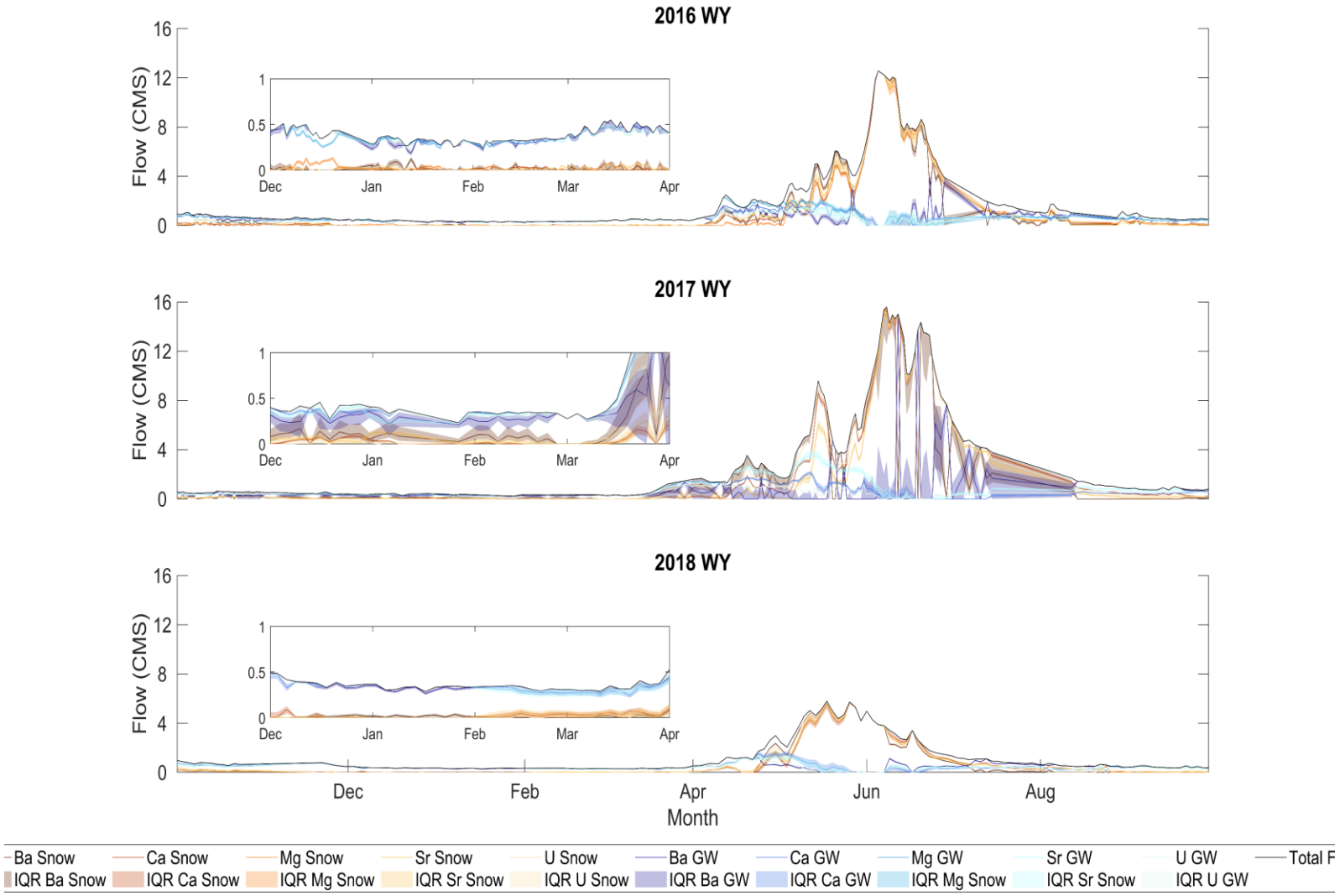

Figure A41. Hydrograph separation of two end-members with hydrologically rationalized concentrations (2 H-EM) shown by solute using the mass-based method of separation. Lines indicate median response from all solutes where each end-member concentration for each solute was sampled 1000 times. The interquartile range (IQR) shaded around the median represents the lower 25th to upper 75th quantiles.

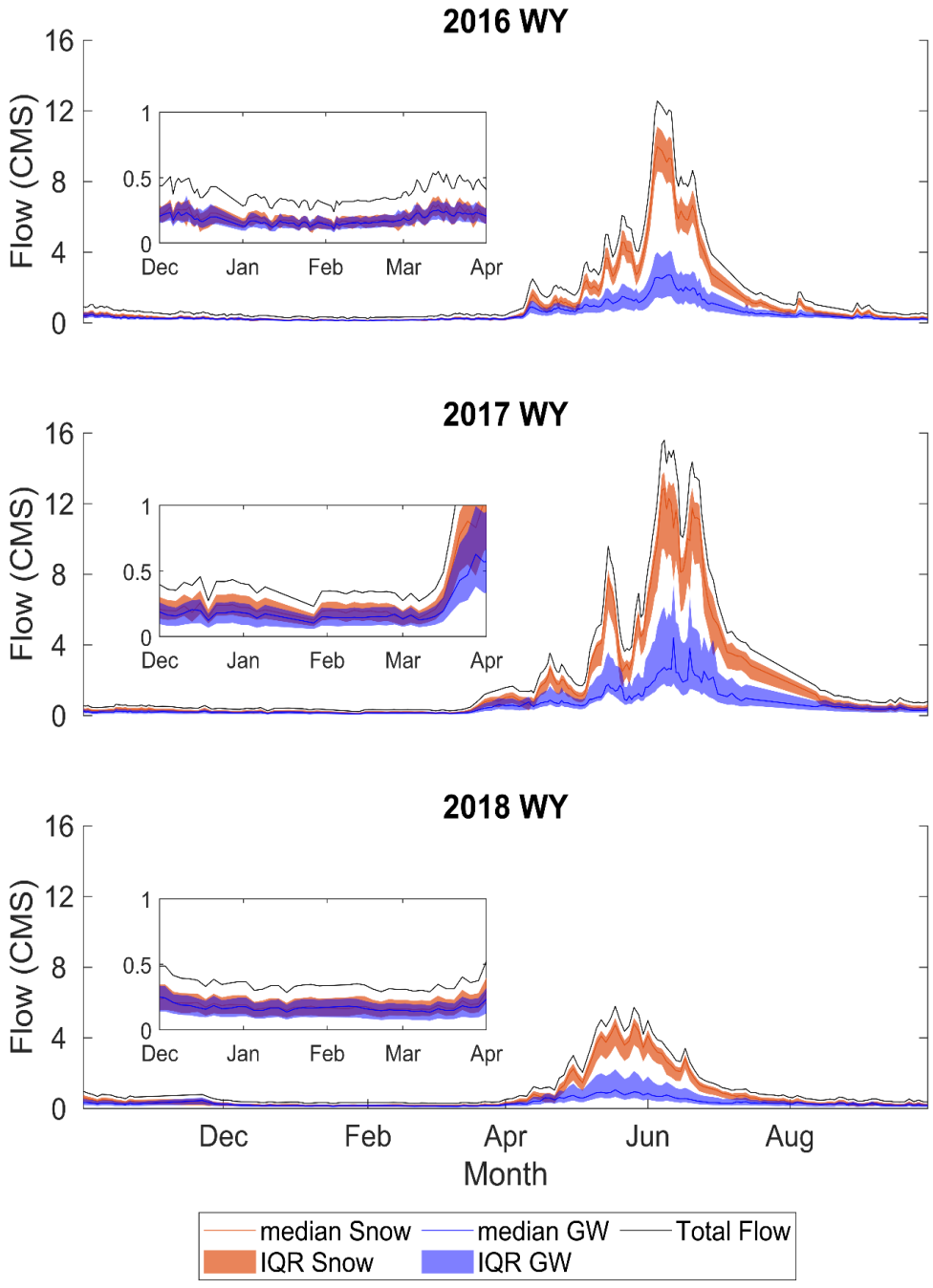

Figure A42. Hydrograph separation of two end-members with measured concentrations (2 M-EM) using the mass-based method of separation. Lines indicate median response from all solutes where each end-member concentration for each solute was sampled 1000 times. The interquartile range (IQR) shaded around the median represents the lower 25th to upper 75th quantiles

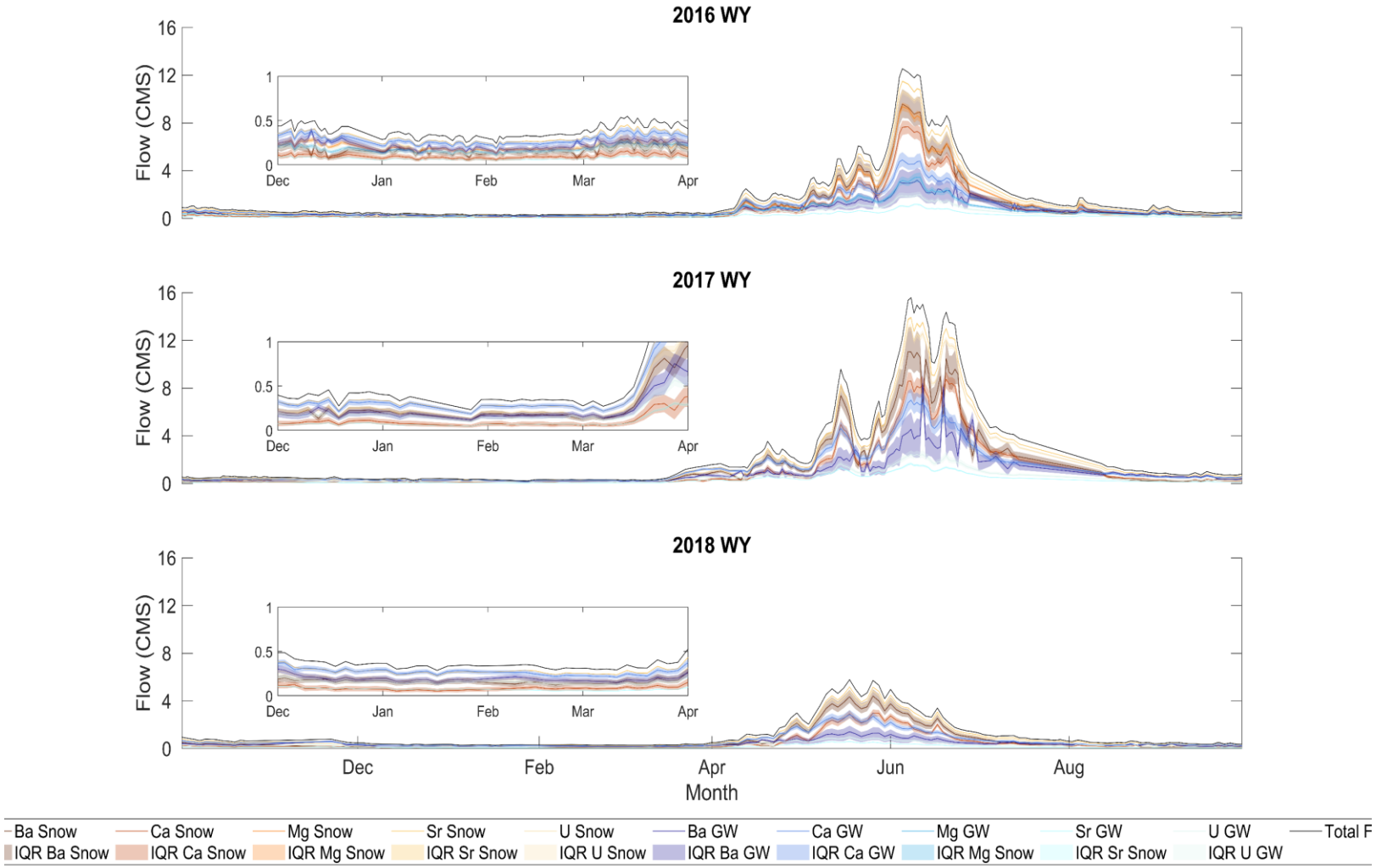

Figure A43. Hydrograph separation of two end-members with measured concentrations (2 M-EM) shown by solute using the mass-based method of separation. Lines indicate median response from all solutes where each end-member concentration for each solute was sampled 1000 times. The interquartile range (IQR) shaded around the median represents the lower 25th to upper 75th quantiles

.

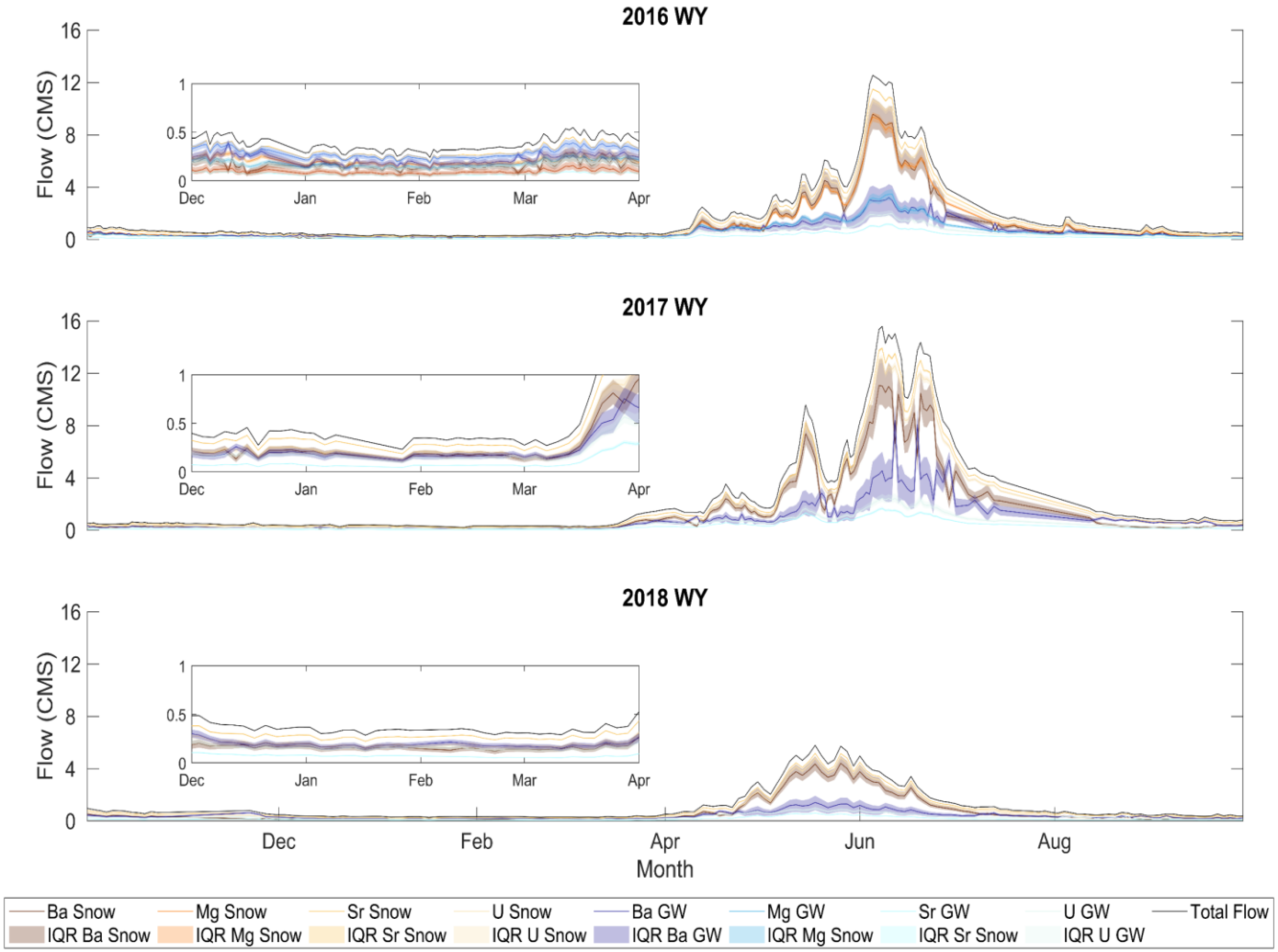

Figure A44. Hydrograph separation of two end-members with measured concentrations (2 M-EM) shown by solute using the mass-based method of separation. Lines indicate median response from all solutes except calcium where each end-member concentration for each solute was sampled 1000 times. The interquartile range (IQR) shaded around the median represents the lower 25th to upper 75th quantiles.

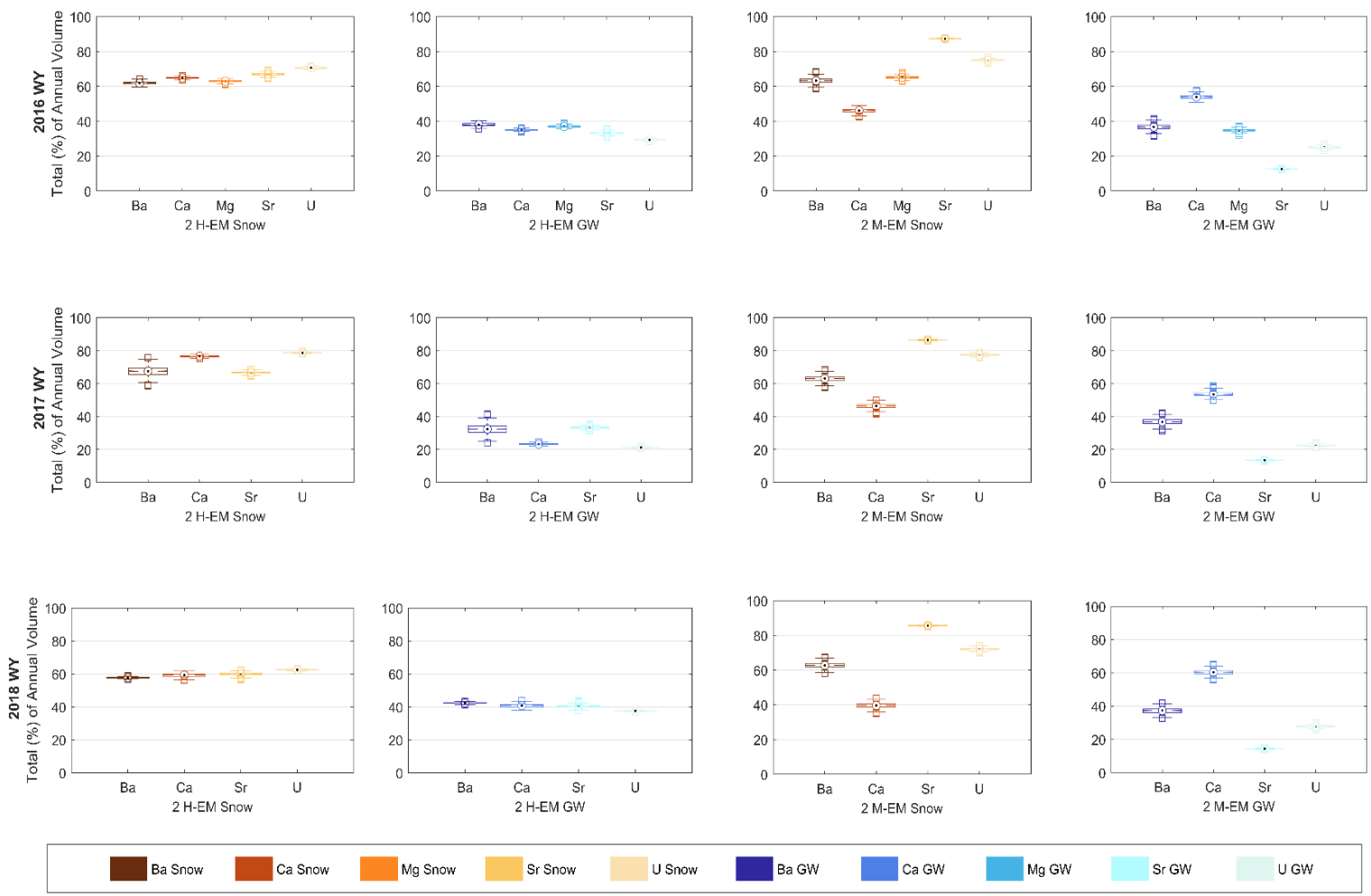

Figure A45. Total percent of the annual volume of water leaving the catchment coming from each end-member – groundwater (GW) or snowmelt (snow) via the mass-based method of separation with hydrologically rationalized end-member concentration (H-EM) and measured end-member concentrations (M-EM). Targets represent the median, boxes represent the interquartile range (IQR) spanning the 25^{th} to 75^{th} quantiles with error bars representing the minimum and maximum, and boxes representing outliers (1.5IQR). The snow end-member is represented in orange, groundwater in blue. H-EMs show n = 1000 for all years while M-EMs show n = 4000 (n = 5000 for 2016WY only).